Qualification of metalworking fluids by Tapping Torque Tests and related Acoustic Emission-based classifications

Von der Fakultät für Ingenieurwissenschaften,
Abteilung Maschinenbau und Verfahrenstechnik der

Universität Duisburg-Essen

zur Erlangung des akademischen Grades

einer

Doktorin der Ingenieurwissenschaften

Dr.-Ing.

genehmigte Dissertation

von

Anna Lena Demmerling
aus
Mönchengladbach, Deutschland

Gutachter:
Univ.-Prof. Dr.-Ing. Dirk Söffker
Univ.-Prof. Dr.-Ing. Hans-Christian Möhring

Tag der mündlichen Prüfung: 06.07.2023

Danksagung

Diese Dissertation entstand in der Zeit von 2016 bis 2023 am Lehrstuhl Steuerung, Regelung und Systemdynamik an der Universität Duisburg-Essen neben meiner Tätigkeit als Entwicklungsingenieurin für Kühlschmierstoffe bei der Rhenus Lub GmbH & Co KG. Ich danke meiner Arbeitgeberin für die Möglichkeit der berufsbegleitenden Promotion und ganz besonders meinem damaligen Vorgesetzten, Herrn Dr. Hans-Jürgen Schlindwein, der sich von meiner Idee begeistern ließ und mich stets in meinem Vorhaben unterstützte.
Meinem Erstgutachter, Herrn Univ.-Prof. Dr.-Ing. Dirk Söffker, der seiner Rolle als Doktorvater in jeglicher Hinsicht gerecht wurde, gilt besonderer Dank. Hierbei sind sein unermüdlicher Einsatz, die fachliche Führung und Diskussionen, die mein Denken und meine Arbeit geprägt haben, hervorzuheben. Er verstand es, mich als junge Erwachsene individuell fachlich zu fordern, meine Stärken zu fördern und meine Persönlichkeit (mit) zu formen. "Am Ende Ihrer Promotion werden Sie ein anderer Mensch sein." Ja, in der Tat und ich blicke positiv und mit anderen Augen auf diesen Prozess zurück.
Weiterhin bedanke ich mich herzlich bei meinem Zweitgutachter, Herrn Univ.-Prof. Dr.-Ing. Hans-Christian Möhring, für seine wertvollen Kommentare und Anregungen. Ich freue mich schon auf weiteren Austausch in den kommenden Jahren.
Außerdem möchte ich meinen Kolleg:innen bei Rhenus Lub und meinen Mitdoktorand:innen am Lehrstuhl SRS für die gute Zusprache und die fachlichen Diskussionen danken. Schließlich möchte ich auch meinem Ehemann David für seine (jahrelange) Geduld danken. Aufzugeben, war auch für mich nie eine Option - qui nihil audet, nihil proficit!

Mönchengladbach im Juli 2023

Anna Lena Demmerling

Kurzfassung

An den Bearbeitungsprozess angepasste Kühlschmierstoffe sind wichtig für eine verlässliche und effiziente Zerspanung. Schmieraktive Substanzen lagern sich an der Oberfläche an, verringern Reibung und Temperatur in der Kontaktfläche zwischen den Reibpartnern und können so den Verschleiss mindern. Die Einordnung der Schmierleistung ist von grosser Bedeutung. Aufgrund des breiten Spektrums an Anwendungen eignet sich nicht jeder Kühlschmierstoff für alle Einsatzfälle. Um verlässliche Empfehlungen für einen Kühlschmierstoff auszusprechen, müssen die Anforderungen des Anwenders bekannt sein. Die Schmierwirkung ist dabei nur eine von vielen weiteren typischen Anforderungen an Kühlschmierstoffe. Die Leistung von wassergemischten Kühlschmierstoffen und Bearbeitungsölen wird im Kühlschmierstofflabor anhand verschiedener standardisierter Testmethoden bewertet und eingeordnet.

Der Tapping Torque Test (TTT), auch Drehmomenttest genannt, ist ein standardisierter Test, um die Schmierwirkung von Kühlschmierstoffen zu bestimmen. Bei der Herstellung von Innengewinden wird das benötigte Drehmoment als Kriterium für die Kühlschmierstoff-Qualifizierung herangezogen. Ein niedriges Drehmoment zeigt dabei eine gute Schmierwirkung des Testfluids an. Die Möglichkeit viele verschiedene Werkstoffpaarungen miteinander testen zu können, macht diesen Test als praxisnahen Schmierstofftest besonders interessant. Die Anwendung der aktuellen Norm für den TTT, ASTM D8288-19, ermöglicht jedoch nicht immer eine Unterscheidung der Kühlschmierstoffe, insbesondere nicht, wenn sich die Kühlschmierstoffe chemisch nur gering unterscheiden. Es ist das Ziel der vorliegenden Arbeit, die Grundlagen und Möglichkeiten neuer Testverfahren zur Differenzierung von Kühlschmierstoffen in spanlosen Bearbeitungsprozessen zu schaffen.

Bei dem Versuch die Differenzierbarkeit der Kühlschmierstoffe im TTT zu verbessern, wird neben dem Drehmoment als zweite Messgrösse der Körperschall eingeführt. Während der Gewindeherstellung finden elastische und plastische Verformungen statt, die im Werkstoff durch die Verschiebung von Korngrenzen Schallwellen außerhalb des wahrnehmbaren Bereichs des Menschens erzeugen. Die Emission im Ultraschallbereich wird in dieser Arbeit als Acoustic Emission (AE) bezeichnet. Die AE-Signale werden zusätzlich für die Klassifikation der Kühlschmierstoffe verwendet. Es werden Vorteile, Möglichkeiten und Grenzen des Einsatzes von AE-Signalen für den Zweck der Kühlschmierstoffbewertung aufgezeigt. Dafür werden die AE-Signale sowohl als Rohdaten als auch als weiterverarbeitete/transformierte Daten in unterschiedlichen Klassifikationsverfahren genutzt.

Die Experimente werden in dem Prozess des Gewindeformens durchgeführt. Dabei werden verschiedene Kühlschmierstoffe als Testfluide eingesetzt. Zunächst wird der Testablauf nach ASTM vorgestellt und kritisch begutachtet. Ein veränderter

Testablauf, der die während der Versuche neu entdeckten und als signifikant bewerteten Nebeneffekte berücksichtigt, wird vorgeschlagen. Für die Mittelwerte der Drehmomente wird eine neue Berechnungsmethode entwickelt, die die Differenzierbarkeit der Testfluide bereits verbessert. In den Kernexperimenten dieser Arbeit werden dann auch die AE-Signale aufgenommen. Da das Drehmoment nicht immer eine Unterscheidung der Kühlschmierstoffkomponenten erlaubt, werden AE-Signale zur Klassifikation genutzt. Hierzu werden Klassifikationsmethoden wie k-means clustering oder konvolutionale neuronale Netzwerke, eine Methode des maschinellen Lernens, angewendet.

Die Ergebnisse zeigen, dass grössere Unterschiede in der Kühlschmierstoffzusammensetzung schon mithilfe der Drehmomentmittelwerte erkannt werden können. Bei sehr viel kleineren Unterschieden, die bis auf die chemische Ebene der Additivmoleküle gehen, übertreffen die neuen Methoden mit der Bewertung der AE-Signale den klassischen TTT. Die höchsten Klassifikationsgenauigkeiten werden mit einem konvolutionalen neuronalen Netzwerk erreicht, bei dem die transformierten AE-Signale als Eingangsdaten verwendet werden. Sogar der Ansatz des Transferlernens zwischen zwei Datensätzen erreicht zufriedenstellende Ergebnisse. Mithilfe dieses Verfahrens ist es sogar möglich, zwischen unterschiedlichen Molekülkettenlängen oder Elementgehalten der Kühlschmierstoffzusätze zu differenzieren. Das Verfahren liefert jedoch keine direkte Aussage über die Schmierwirkung des Testfluids.

Diese Ergebnisse könnten eine grosse Rolle bei der Online-Zustandsüberwachung von Kühlschmierstoffen spielen. Während des Zerspanprozesses könnte zukünftig die Eignung des Kühlschmierstoffes für die aktuell vorliegende tribologische Paarung bewertet und eventuell die Zusammensetzung automatisch angepasst werden. Dieses kontinuierliche Fluidmanagement könnte die Zuverlässigkeit und Produktivität von Zerspanprozessen erhöhen.

Abstract

Well-suited metalworking fluids (MWFs) are important for reliable and efficient machining processes. Lubricants adhere on the surfaces, reduce friction and temperature in the contact zone of the tribological pair, and can reduce wear. The classification of lubricant's performance is important. Due to the wide range of applications, not every MWF can be successfully used for all applications. For a reliable recommendation, quality requirements of the user have to be known. Lubricity is only one of multiple typical requirements. For evaluation of fluid performance, diverse standardized test methods are available to qualify lubricating oils and water-mixed MWFs.

Tapping Torque Test (TTT) is a standardized evaluation approach to determine the lubricity of MWFs. During internal threading, tapping torque is used as a feature for fluid qualification. A low tapping torque indicates a good lubricity of the test fluid. The large amount of possible tribological pairs is a great advantage of TTTs and enables a evaluation by conduction of very near-to-practice tests. Chemically different fluids measured according to the relevant standard ASTM D8288-19 often cannot be distinguished. It is the aim of this thesis to establish fundamentals and possibilities of new test methods for the differentiation of MWFs in machining processes.

Trying to enhance the distinguishability of TTTs, Acoustic Emission (AE) is introduced as a second measure to the tapping torque measurement. During threading, elastic and plastic deformations take place which generate acoustic waves in the material outside the human audible range due to the displacement of grain boundaries. The emission in the ultrasonic range is called AE in this work. These AE signals are additionally used for MWF classification. Advantages, possibilities, and limits of AE signals for evaluation of MWFs are shown. For this purpose, AE signals are used as raw data as well as processed data after wavelet transformation in different classification approaches.

Different MWFs are tested in thread forming experiments. The test procedure according to ASTM is critically reviewed. A changed, new test procedure is proposed considering important side effects recently found out during the research. A new evaluation approach for tapping torque means is developed to enhance the distinguishability of test fluids. During the main experiments of this work, AE signals are additionally recorded. While tapping torque means do not always allow the distinction of MWFs' additives, AE signals are used to classify MWFs. Here, k-means clustering and Convolutional Neural Networks, a method of machine learning, are applied as classification approaches.

The results show that larger differences in test fluids' compositions can already be detected by tapping torque means. For smaller differences on the chemical level of the used additives, the new approaches evaluating AE signals outperform classical

TTT. The classification accuracies of Convolutional Neural Network based methods using transformed AE signals as inputs are the highest. Even Transfer Learning between two datasets obtain satisfying results. Furthermore by looking at the chemical structure of MWF's additives, it is possible to distinguish between different chain lengths of molecules or different contents of special elements. However, the method does not provide any direct information about the lubricating effect of the test fluid.

These results indicate the importance of this work for online fluid condition monitoring during machining processes. In the future, the suitability of MWFs could be evaluated for the current tribological pair and possibly be automatically adapted. This could increase reliability and productivity of machining processes by continuous fluid management suited on the current situation.

Contents

Abbreviations

AE	Acoustic Emission
AW	Anti wear
bnorm	Batch normalization
CNN	Convolutional neural network
conv	Convolutional
CWT	Continuous Wavelet Transformation
drop	Dropout
EP	Extreme pressure
fc	Fully connected
FC	False clustered
MWF	Metalworking fluid
mpool	Max pooling
relu	Rectified linear unit
softmax	Softmax
STFT	Short Time Fourier Transformation
TC	True clustered
TL	Transfer Learning
TTT	Tapping Torque Test

1 Introduction

The use of metalworking fluids (MWFs) in industrial machining processes is widely spread. The fluids cool and lubricate the contact zone between tool and workpiece to prevent tool wear and to ensure manufacturing of required geometries and surface qualities. Digitization can be used as tool for quality management for early failure recognition in machining. Condition monitoring and structural health monitoring is not only applied in moving machine parts but also for manufacturing. Reliable process automation and monitoring becomes more important in regard to application of digital twins and artificial intelligence.

Artificial intelligence is already used for tool condition monitoring. During machining, one of the worst failures is tool breakage. A broken tool can damage the workpiece irreparably. This could mean expensive rework or a total dismiss of the workpiece. Dependent on the complexity and sensitivity of the workpiece, a no-failure-strategy is predefined. In most monitoring techniques, tool condition is highlighted. Proceeding tool wear is monitored to predict the risk of failures and the end of tool life. Indirectly, friction between tool and workpiece is measured. The higher the friction, the faster can proceed the process of tool wear. Concluding, tool wear can be positively influenced by reducing friction during machining. Lubrication reduces friction between tool and workpiece and can increase surface quality and tool life time. A general statement is not possible and the machining result depends on the effects of the fluid's contents. The type of lubricant and its contents/additives mainly affect tool wear and surface roughness or make higher machining speeds possible to decrease manufacturing time and increase the output. A monitoring of MWFs in regard to quality of workpieces or efficiency of machining is not realized in common monitoring techniques.

In practice, one MWF is used in the same machining center for various workpieces. Before starting the machining process of a newly developed workpiece, usually, no check of the lubrication condition is conducted. Metalworking fluid and its concentration are kept the same. When the first tools were severely damaged or broken and the machine operator has tried to change all possible machining parameters, then the lubrication condition will be considered. Metalworking fluids are mainly viewed as auxiliary tool. Recently, they are more and more recognized as liquid tool with an higher influence than expected. Environmental aspects raised the interest in efficient lubricating concepts in the last years. Developing efficient lubrication means monitoring, analyzing, and understanding of tribological contacts.

Lubricant manufacturers use empirical data of similar applications as well as results from standard laboratory wear tests to recommend the best suitable MWF for each machining process. Standardized wear test such as Reichert and Brugger test or cutting force tests e.g. Tapping Torque Test (TTT) are used to qualify their products. Lubrication can increase surface quality and tool life time by reducing

friction between tool and workpiece. The functionality depends on the effects of the fluid's additives mainly affecting tool wear and surface roughness. By improving friction and cooling properties, higher machining speeds could be possible and manufacturing time could be decreased.

1.1 Motivation and research questions

The goal of this work is to show techniques to monitor and classify lubrication states during thread forming. Real-time evaluation of lubrication during machining could be an important step towards fully automated production processes including MWF condition monitoring. For changing workpiece materials – meaning for changing tribo-pairs – the MWF could be adapted in short term by automatically dosage of needed additives or concentrate. Application of artificial intelligence could enable the control system to adapt the MWF by previously learnt events. The prediction of maintenance tasks would make timely intervention possible. This could reduce the needed resources to keep the MWF stable and efficient. A more reliable machining process of the future could be the result.

The present dissertation contributes a small part to the goal of monitoring lubrication during machining. Different MWFs are investigated in thread forming processes. In threading, workpiece material is elastically and plastically deformed by the forming lobes of the tap. The contact condition between tap and workpiece is monitored indirectly by measuring tapping torque and Acoustic Emission (AE) signals. The focus of this work is to show the possibility of MWF qualification and distinction by these measures. The first part of this research is more or less a feasibility study. In the second part, the limits of different evaluation approaches applied on a more demanding dataset are investigated. Thus, two different datasets are used in this work. Classification approaches are developed including statistical analysis, unsupervised partitioning methods, and machine learning methods such as neural networks. The performance of these approaches is evaluated using two different datasets. In both cases, the qualification of MWFs by classification of tapping torque or AE signals is focused. The research questions are formulated as follows

- Is the conduction of TTTs efficient for the distinction of MWFs?
- Are tapping torque or AE signals generally suitable to reflect changes in MWFs?
- Which features and which approaches can help to differentiate MWFs?
- Is a detection of quite large differences in MWFs like between lubricating oils and emulsions possible by AE signals?
- Are even chemical differences such as chain lengths of additives in MWFs detectable?
- Can neural networks improve the classification result or make a classification even possible when other approaches fail?

1.2 Organization of the dissertation

In Chapter 2, the use of MWFs including lubricating mechanisms, functions of MWF additives, and laboratory tests for fluid qualification are detailed. A literature review about TTTs to differentiate MWFs is included. Chapter 2 consists further of literature reviews about AE techniques used for tool condition monitoring in machining processes. Directly after this, machine learning methods used in manufacturing processes are reviewed and some basic machine learning methods are surveyed. The second chapter is closed by summarizing the research gaps and describing the scientific goals of this dissertation.

In Chapter 3, the experimental setup of the newly developed extended TTT is illustrated and test fluids and test parameters are described for two datasets. The chemical structures of the used lubricating additives are illustrated in detail.

In Chapter 4, the evaluation approaches for analyzing tapping torque and AE signals are introduced. Conduction and evaluation of TTTs are introduced. Problems with the relevant standard test method are highlighted. At the same time, important and so far unnoticed facts to the current test method are revealed and improvements are suggested. Furthermore, basics about AE signal transformation methods and clustering approaches are briefly described. For the approaches using Convolutional Neural Networks (CNNs), the models applied on the two datasets are presented. Used prefilters are described and CNN architectures are shown.

In Chapter 5, results for both datasets applying the previously introduced approaches are presented. The results are shown in order to the datasets. If required for scientific aspects, small specific changes in the models are mentioned at appropriate place. After presentation of all results for one dataset, results are summarized in a table. The chapter is closed with a discussion.

In Chapter 6, the whole thesis is summarized and suggestions for future work are given.

2 Literature review and theoretical background

In times of rising interest in Industry 4.0, applications for process monitoring are focused by industrial and scientific researchers. Monitoring of machining processes has become an important part for increasing process stability and reliability. Real-time monitoring techniques are developed to prevent machine malfunctions [1]. The operation of unmanned machines and the need for reliable sensory have already been discussed 40 years ago [2]. Reliable automated monitoring techniques to enhance process stability are still in focus of industrial research [3, 4, 5, 6, 7].

This chapter includes

1. theoretical background about lubrication strategies in machining, requirements and characteristics of MWFs,
2. overview about lubricating mechanisms and effect of lubricating additives,
3. introduction to general laboratory tests for MWF qualification,
4. basics about tapping and literature review about application of TTT,
5. basics and review about AE measurement,
6. review for tool condition monitoring in different machining processes with focus on AE techniques,
7. review about different machine learning approaches used for machining processes, and
8. theoretical background about CNN used in this work.

In this chapter, parts of own publications [8, 9, 10, 11, 12] have been taken over.

2.1 Metalworking fluids in machining

The importance of lubricants for machining processes has been shown for example in [13, 14, 4]. The performance of different lubricants has been evaluated in punching and blanking in [15]. Application in journal bearings and gears is typical for lubricants such as gear oils or greases. A recent review about the performance of non-water miscible lubricants is given by [16]. Investigations concerning tribological contact, wear development, condition monitoring, and predictive maintenance of these systems are diverse and widely spread [17, 18, 19, 20, 21, 22, 23].

In regard to their two main tasks, MWFs are also called coolants or lubricants. They cool and lubricate the contact zone between tool and workpiece. In addition to thermal, chemical, and tribological tasks, MWFs have the task of transporting chips out of the machining zone. Worse chip transportation can mainly affect machining qualities when chips get stuck in the machining zone and damage surfaces irreversibly. Furthermore, chip formation is influenced by jet pressures of MWF. High jet forces cause the chip to twist and break off [24]. In the present work, the chemical composition of MWFs influencing the lubricating performance is focused.

2.1.1 Lubrication strategies

During many machining processes the contact zone between tool and workpiece is splashed with a MWF. The MWF influences the development of wear and can increase tool life time [25]. Several lubrication concepts and application ways can be applied: Exterior or interior cooling with flooding or minimum quantity lubrication, air or cryogenic cooling. The choice of lubrication concept depends on the machining task, existing machine periphery, and individual requirements of the end user. Different lubrication concepts, twist angles of the drilling tool, and feed rates have been tested in drilling carbon fibre reinforced plastics by [26]. It was found that the lubrication concept had the highest impact on the workpiece quality with a contribution ratio at 52.88 % [26].

In minimum quantity lubrication, typically 50 ml/h oil volume is used in average [27]. MWF is sprayed as an aerosol onto the contact zone. Minimum quantity lubrication is a loss lubrication; the used MWF is not reused. Heat reduction or chip removal cannot be realized as reliably as with flooding lubrication. Less machine periphery and less control and care are necessary when using minimum quantity lubrication. In terms of waste reduction, this technique is handled as being more sustainable than flooding lubrication. Recent research deals with the topic of sustainable minimum quantity lubricants e.g. [28, 29, 30, 31, 32]. Furthermore, minimum quantity lubrication can be combined with cryogenic cooling so that the cooling effect is improved e.g. with carbon dioxide [28, 31, 33], nitrogen [34, 33], or argon [34].

In the present work, MWFs typically used in flooding lubrication are focused because this concept is still wide spread and the conventional way of MWF application. In various application cases, it can provide better performance compared to minimum quantity lubrication that has for example been shown in [35]. During grinding of VP50IM steels, the conventional flooding lubrication provided better performance than the applied minimum quantity lubricant [35]. By flooding, chips and heat can be well removed out of the machining zone.

If a MWF is used in flooding lubrication, it is circulated and reused for months and sometimes even years. It is continuously filtered after usage to separate chips and machining dust from the fluid. A local storage tank next to a single machine includes at minimum 300 l and in most cases more than 1000 l of the MWF. In regard to the fluid's reuse, regular monitoring and caring of the fluid is required.

2.1.2 Requirements

In Germany, the application of MWFs is ruled by standards for example of the German Statutory accident insurance. In standard BGR/GUV-R 143, requirements for risk assessment, protective measures, control and care, and disposal are described to protect human health and ensure safety [36]. Furthermore, machining industry set additional requirements concerning improvements of the machining process. An overview of important requirements are mentioned in Figure 2.1.

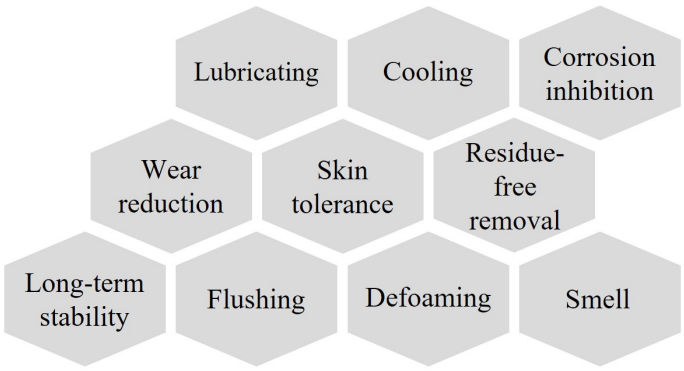

Figure 2.1: Important requirements of MWFs

On the basis of standardized laboratory fluid tests and empirical earned experiences, special fluids are proposed for each application. The condition of the MWF is very important for performance and reliability of the machining process. A degraded fluid is not able to save the tool from wear or the workpiece from corrosion as a well-conditioned fluid. Therefore, it can occur for example that corrosion problems arise at first after several months of successful application. It is possible that corrosion inhibiting substances are carried out over time by workpieces and chips. Choosing

a suitable MWF and ensuring its steadily good condition are fundamental for an economical and harmless application.

2.1.3 Characteristics

Two main groups of MWFs can be distinguished: Non-water mixable and water mixable MWFs. Both types of MWF can be used in flooding lubrication. Advantages of non-water mixable fluids (oils) are for example a very high lubrication, no bacteria and fungi problems due to the lack of water, and the resulting long service life. The disadvantages of higher initial filling costs, less cooling effect, and sometimes special fire protection requirements often lead to the application of water mixable fluids. Water mixable MWFs are divided into in water soluble and in water emulsifiable concentrates. For application, these concentrates are mixed with water typically in a ratio from 1:20 to 1:10. For water containing fluids, monitoring is more complex than for pure oils. Typical values to be checked are concentration, nitride content, pH value, and water hardness. In regard to evaporation, the filling level of the MWF must be constantly checked and filled up. Soluble MWFs are mainly used for processes with undefined cutting edge such as grinding or for easier-to-work materials such as wrought aluminum alloys. Recently, for difficult-to-cut materials such as Inconel 718, titanium alloys or nickel based steel alloys, emulsions are increasingly being used.

In MWFs, a lot of different ingredients are used. These so called additives are used to adjust certain functions of the lubricants and to meet requirements of certain applications. In this work, mainly mineral oil containing emulsions are focused and investigated. An overview of typically used constituents in emulsifiable MWF concentrates is given in Table 2.1. Water and oil are two of the main components of emulsifiable MWF concentrates. Emulsifier has to be used additionally for dispersing oil in water. Due to corrosion inhibition properties and for prevention of bacteria growth, the pH value of water-mixed MWF is generally stabilized in the alkaline range. Functional additives are used for corrosion protection, extreme pressure (EP) applications, or anti wear (AW) tasks and are partly described and explained in the following section.

In literature, the effect of different MWFs has partly been studied. Five different vegetable oils were applied for 45 steel milling and the result shown that cottonseed and palm oils performed better than castor, soybean, and peanut oils by measuring temperature [37].

Modified vegetable oils were employed for turning and drilling of AA 6061 aluminum and AISI 304L stainless steel and their machinability and rheological properties were investigated [38]. Yeast-based MWF was used for milling process of Ti6Al4V titanium alloy and the results showed that it performed similar or better comparing with a mineral oil based reference fluid [39].

Table 2.1: Typical constituents in emulsifiable MWF concentrates

Constituent	**Typical content** [%]
Mineral or ester oil	10 – 40
Water	5 – 50
Emulsifier	10 – 30
Stabilizer of pH value	5 – 20
Functional additives	0 – 20
Conservatives	0 – 5
Defoamer	0 – 1

In the process of tapping, the surfactant structure influence on film forming ability of emulsion was studied [40]. A novel developed biodegradable MWF was designed and its performance was measured during turning of AISI 420 material [41]. In thread forming processes when threads are formed by taps into pilot holes, the MWF prevent the tool from welding with the workpiece material by reducing friction and temperature at the forming lobes. Types and different characteristics of MWFs effect thread quality [42] and tool wear [43].

2.1.4 Lubricating mechanisms

The basics of lubricating mechanisms are well researched but not completely understood. In [44], two different models are proposed for the effect of lubricant additives: adsorption through dipoles and chemical reaction through the input of energy. In [45], lubricating mechanisms of disulfides were investigated by analyzing the worn surfaces using X-ray Photoelectron Spectroscopy. In [46], the tribofilm formation of dialkylpentasulfide was studied using X-ray Absorption Near Edge Structure Spectroscopy and Energy Dispersive Spectroscopy. In [30], the adsorption of two different ionic liquids was simulated. For ionic liquids, lubrication mechanisms were proposed in [47]. The interaction of additives with metallic surfaces was investigated by different authors in [48, 49, 50, 51, 52, 53].

Dependent on the tribofilm thickness, four lubrication regimes are defined: i) boundary, ii) mixed, iii) elastohydrodynamic, and iv) hydrodynamic lubrication [54]. The lubrication regimes are related to the Stribeck curve as shown in Figure 2.2. The Stribeck curve starts at a high friction coefficient in the boundary lubrication regime and decreases in mixed lubrication regime by growing film thickness. In elastohydrodynamic and hydrodynamic lubrication, the friction coefficient increases due to the parameters of fluid friction.

Schemes of boundary and elastohydrodynamic regimes are depicted in Figure 2.3. In boundary lubrication, the surfaces get in contact with each other. By friction, adsorption and reaction layers of the metallic surface are removed and afterward

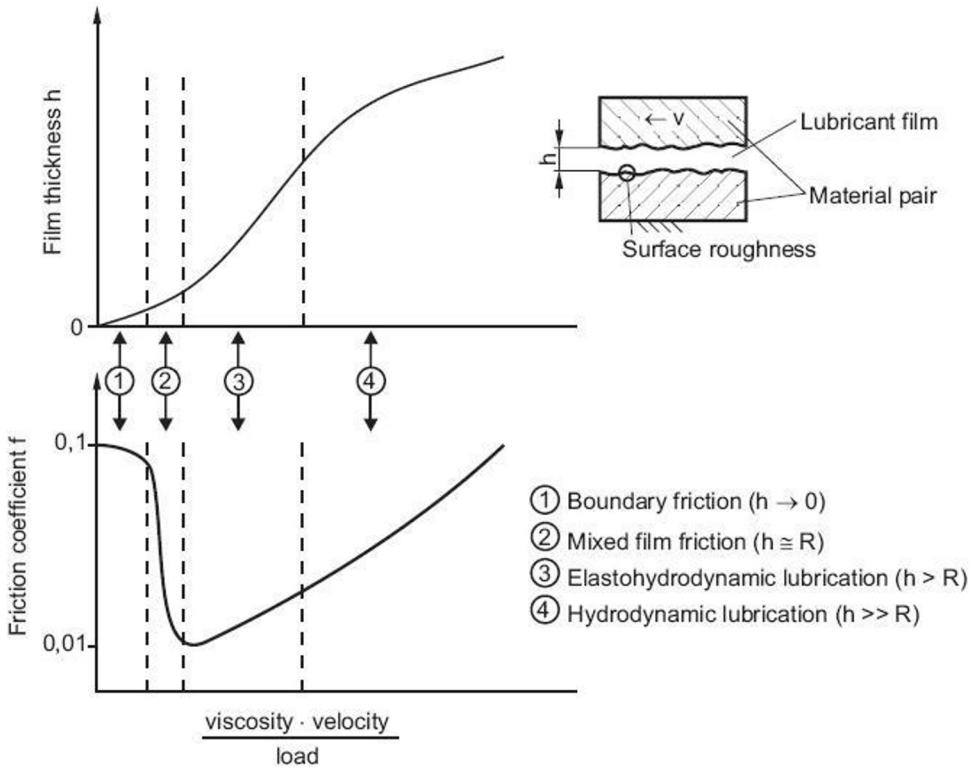

Figure 2.2: Stribeck curve and related lubrication regimes [54]

re-formed. In mixed lubrication, the presence of a lubricant partly prevents direct contact of the friction partners. Where the lubrication film is not thick enough, surface asperities lead to metal-on-metal contact. In hydrodynamic lubrication, the lubricant achieves a nearly complete separation of the friction partners by forming a sufficiently thick liquid separation layer.

For a sufficient lubricity, the lubricant has to be able to carry pressure applied on the friction partners. For a good load-carrying capacity, EP additives are used in lubricants. According to [56], mild EP additives are called AW additives and are organic compounds which are primarily adsorbed on the metal surface by physical forces as Van-der-Waals-force. From a chemical point of view, these additives have at minimum one polar group and thus a high dipole. Example for AW additives are saturated and unsaturated fatty acids, natural or synthetic fatty acid esters, or primary and secondary alcohols [56]. For adsorption, not only polarity is important. The polar group must be able to go into a hydrogen-bonding with the oxygen of the surface [57]. The polar head, for example a carboxyl-group, adsorbs on the oxidized metal surface and the unpolar rest of the molecule, for example alkyl-rest, builds the tribofilm (Figure 2.4a).

In case of sulfur molecules as depicted in Figure 2.4b, the negative dipole of the sulfur molecule interacts with the iron and with hydrogen in the oxidized metal

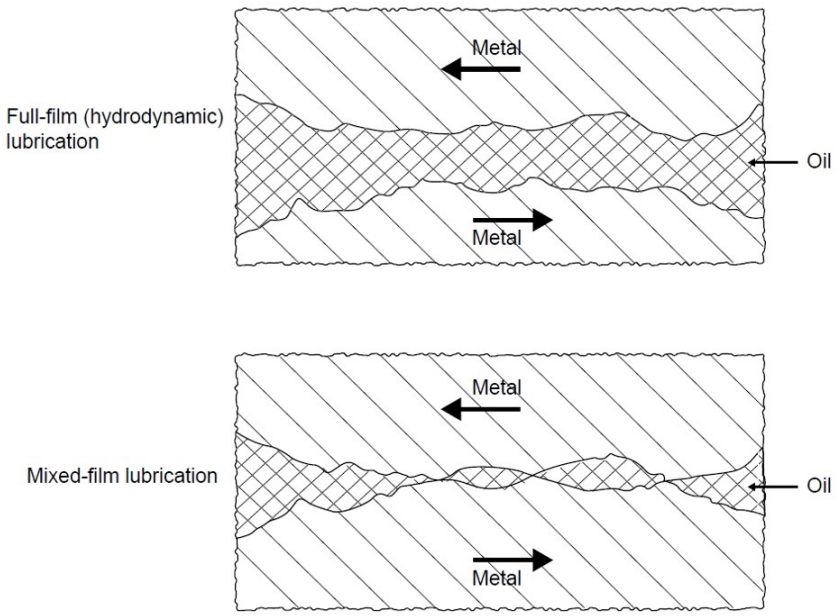

Figure 2.3: Schemes of mixed and hydrodynamic lubrication [55]

surface due to their negative dipoles. For an overbased sodiumsulfonate, an ionic interaction is assumed between the positive sodium atom and the negative oxygen atom on the oxidized metal surface [52]. For native and synthetic esters, two polar oxygen atoms are located between the acid groups and the ester group. These can go into a covalent bonding with neighboring carbon atoms [44]. Phosphorus additives work under the same principle regardless their composition. Phosphorus is brought into contact with the metal surface and can be adsorbed [55]. Highly-efficient EP additives build stable surface layers by chemical reaction [56]. These layers adhere well and are easy to shear.

Tribochemical processes are influenced by the following factors [56]

1. the surface mechanically activated by the friction process,
2. the frictional work as one of the energy suppliers for the reaction,
3. the very short reaction time, and
4. the presence of oxygen.

Furthermore, the reaction intensity of some additives is temperature related. In [58], the function of the additive zincdithiophosphate mainly was explained: It operates in the mixed lubrication regime as AW agent. The film thickness and composition of the tribofilm is temperature related. At low temperatures, zincdithiophosphate is reversibly absorbed onto the metal surface. For rising temperature, zincdithiophosphate is decomposed to dialkyldithiophosphoryl disulfide and disulfide absorbed

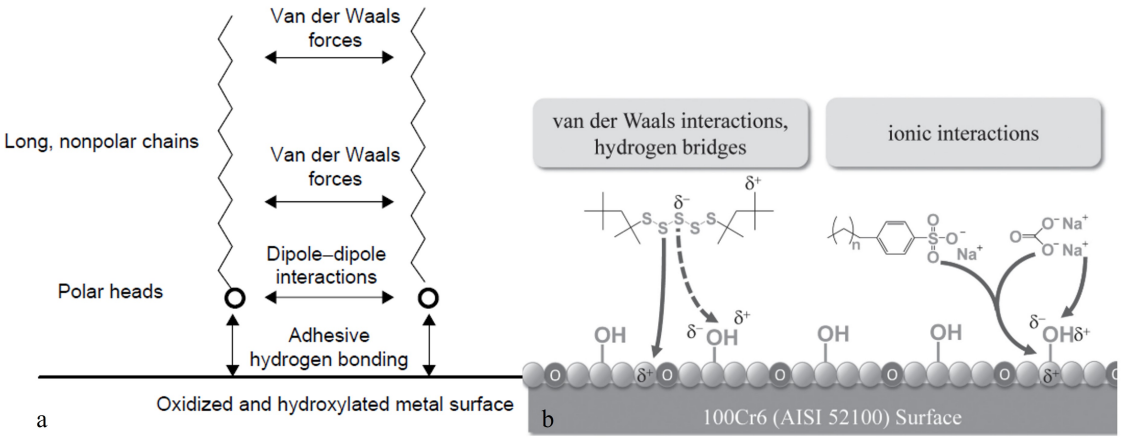

Figure 2.4: a: Polar head adheres to hydrogen of the oxidized metal surface. [57]
b: Negative dipole of sulfur interacts with positive dipole of iron and hydrogen on the oxidized metal surface. [52]

onto the metal surface [58]. This reaction might only occur during processes with longer reaction time, for example in bearings or engines, but it may not occur during machining where material is removed and new surfaces are steadily built. For machining tasks, different additives are used in MWFs but the principle of protecting the surface through adsorption of certain molecules on the surface of tool and/or workpiece is the same. The temperature dependency was also reported for other sulfur containing compounds for example in [59].

2.1.5 Influence of different additives

Additives are used to adjust certain functions of lubricants and to meet requirements of certain MWF applications. In industry and research, it was found that additives may significantly affect the functionality.

A lot of recent research has been carried out on the influence of nanoparticles in lubricants. These particles may contribute to less friction by entering the tribological contact zone and by improving the stability of the tribofilm. In [60], it was discovered that the mixing procedure of boron nitride nanoparticles, oleic acid, and polyalphaolefin has significant impact on the lubricity. The best mixture with 0.5 wt% for nanoparticles and 1 wt% for oleic acid achieved a reduction of coefficient of friction from 0.096 to 0.060 and a reduction of wear rate by 95 %. [60] Similar results could be reached for example with hexagonal boron nitride particles [61], molybdenum disulfide particles [62], silicate hydroxide-molybdenum disulfide particles [63], silicon dioxide nanoparticles [64] graphene nanosheets [65], and alkyl-functional boric acid nanoparticles [53]. In the present thesis, no nanoparticles were used in the test fluids because they would disturb the AE signals during the tapping

process. In recent applications, nanoparticles are not typically used in water-mixed MWFs that are focused in this work.

Research has recently been carried out in the field of plant-based oils as an alternative for mineral oil. In [66], jojoba oil and soybean oil were chemically transformed to meet the physical requirements of oils for lubricants. Similar investigations were carried out in [67] with rice bran and karanja oils. A comparison with a widely used polyalphaolefin was made in [68] using a trimethylolpropane trioleate as eco-friendly additive. In [69], jathropha oil and palm oil were tested as minimum quantity lubricants in turning of stainless steel. The jatropha oil outperformed the palm oil and the tested synthetic ester in concerns of cutting forces, chip characteristics, and properties of the cutting tool [69]. In milling of stainless steel, different water-mixed MWFs containing more or less vegetable-based additives were tested in [70]. It was found that the developed bio-lubricants achieved lower cutting forces than the tested standard emulsions. Sunflower and rapeseed oil-based fluids showed good results in tool wear behavior. [70] Ionic liquids are also researched as more ecological alternatives to mineral oils. In [30], the absorption strength of the two tested ionic liquids was closely related to the lubricating effect. The complexity of the molecules was found to be significant for tribofilm formation [30]. In [47], physicochemical and frictional properties of two oil soluble ionic liquids have been investigated and the coefficient of friction could be reduced by 50 %. Lubricant based on cotton was developed and tested in [71].

In [72], an oil in water emulsion with lypophilic emulsifiers achieved better lubricity than with hydrophilic emulsifiers. In [40], the chemical structure of the used surfactant had significant impact on the adsorption of a trimethylolpropane oleat in machining of titanium alloy. An increasing number of ethoxylations of an anionic surfactant positively influenced the adhesion of the ester molecule. Furthermore, tapping torque decreased with an increasing carbon chain length of the surfactant [40]. Alkyl glyceryl ethers, belonging to non-ionic surfactants, were tested in combination with xanthan gum as dispersant in a water-mixed MWF by [73]. Longer alkyl chain length of the ethers positively influenced the lubrication performance [73].

In [74], a strong impact on friction behavior was found for additives with long alkyl chains together with the sliding speed of the test specimens. A similar result was achieved in [75]. By studying the effect of polyol ester base oils, the friction was reduced by longer alkyl chains and an increasing number of ester groups [75].

Tribological performance of copolymers in aqueous solutions has been investigated by Lin et al.. The copolymer with a longer polypropylene oxide chain formed thicker tribofilm. The chemical structure of the copolymer significantly influenced the results [76].

In this thesis, a natural ester based on coconut oil (2-ethylhexylcocoate) is used in dataset 2019 in comparison to a synthetic polymeric ester (cf. Table 3.4). Esters

are chemical compounds of acid and alcohol or phenol forming a triglyceride [28]. Vegetable oils contain fatty acids being reactive to oxygen and resulting in faster aging. The long-term and oxidative stability of such oils has to be improved by suitable additives. The viscous behavior of vegetable oils is often more advantageous compared to mineral oils. The tribofilm can even sustain high loads [28].

Results about the performance of coconut oil have been reported by [43, 38, 28, 77, 78]. In [78], coconut oil achieved lower surface roughness and lower tool wear in comparison to a soluble oil with lower viscosity and to a straight cutting oil with higher viscosity. In turning, tool wear was determined using soybean, sunflower, coconut, and groundnut oil as minimum quantity lubricants in [43]. Soyabean oil showed best and coconut oil medium performance [43]. In [77], a water-mixed MWF containing coconut oil was developed and was compared as minimum quantity lubricant with an commercially available MWF and dry machining. With the coconut oil-based emulsion, lower cutting force and lower temperatures than dry machining could be achieved in most experiments. For the lowest tested cutting feed at 0.05 mm/rev, the coconut emulsion even outperformed the commercial MWF [77]. In [28], coconut, sunflower, and mineral oil were used as base oils and were mixed with the same additive. In turning, the performance of the fluids used as minimum quantity lubricants for cryogenic cooling was compared.

Friction properties of coconut and paraffin oil was compared with nanoparticles containing coconut oil and nanoparticles containing paraffin oil in [38]. The coefficient of friction was reduced by molybdenum disulfide in both cases. The coefficient of friction of pure coconut and pure paraffin oil were similar. In [38], a review summarizing the research about the effect of coconut oil in machining applications is included. A review containing findings about coconut oil was provided by Lawal et al. [79].

By Huesmann-Cordes et al., the effect of polysulfides with three and five sulfur atoms and an overbased sodiumsulfonate on the wear behavior was examined for two different steel alloys. With increasing complexity of the molecules, the optimal content of polysulfides decreases for 100Cr6. The larger the molecule, the faster the surface is covered, even at low concentrations. The effect of overbased sodiumsulfonate is stronger for larger polysulfide molecules. Here, an increase in concentration of overbased sodiumsulfonate resulted in a reduction of worn area [52].

Further sulfur compounds have been investigated by other researchers: disulfides in naphtenic oil [45], a biobased fatty acid methyl ester disulfide in two different base oils [80], dialkylpentasulfide in synthetic ester [46], and sulfur and phosphorus compounds of different oxidation states [81]. By Zheng et al., the produced MWF was tested as emulsion and the additive had negative effect on wear scar and friction coefficient in comparison to the same fluid without additive. The built tribofilms mainly contained FeS and FeS_2 that did not have that good AW performance as the $FeSO_4$ tribofilms built during the application of the MWF concentrate [46].

Phosphorus additives are applied for antioxidation properties and for AW tasks. By Phillips et al., the chemical structure of various phosphorus compounds used as lubricants additives are introduced. As friction modifiers mainly act long-chain phosphites and phosphonates. As AW additives, neutral organic phosphates and phospites are used [55].

By Fleming, different additives including phosphate ester are tested in cold forging steel. In comparison to pure mineral oil, phosphate ester reduced the process torque by 13 % and maximum torque by 16 %. The surfaces forged using the phosphate ester showed clear advantages compared to the surfaces using molybdenum disulfide or boron nitride nanoparticles [82].

In [83], phosphorus-based additives showed a positive effect on the adhesion of aluminum on coated tools during tapping of AlSi6.5. The adsorption of phosphorus in dependency with the presence o sulfur was investigated using X-ray Absorption Near Edge Structure Spectroscopy in [84]. Applying diphenyl phosphate and triphenyl phosphate, the tribofilm mainly consisted of iron polyphosphates. Similar results were found by Fu et al. [85]. Najman et al. found out that diphenyl phosphate was able to react at lower temperatures with the substrate than triphenyl phosphate. The authors revealed competitive interactions between phosphorus and sulfur additives [84].

In [85], phosphite esters with longer alkyl chains showed better AW properties than those with shorter alkyl chains. For good EP properties, shorter alkyl chains were better. In [86], the wear behavior of different dithiophosphates and different phosphorothionates was investigated. The phosphorothionates showed poor AW properties. Some dithiophosphate built a functioning tribofilm and some not [86]. Thiophosphates also positively influenced the tribofilm formation in a study of [87].

Chain lengths of glycols effect their lubricating performance. Frictional performance of glycol-based lubricant was investigated in [88]. For glycol-based lubricants, it was observed that increasing glycol chain length decreased friction.

2.1.6 Laboratory tests for fluid qualification

In addition to physical properties such as density, viscosity of the concentrate and pH-value of the emulsion, tribological properties of MWF are determined. The large number of lubricant applications presupposes that a large variability of the contact conditions can be represented. For the variety of contacts and the variety of friction types (Figure 2.5), different test rigs are industrially available. Probably the best known test for characterizing greases and lubricating oils is the 4-ball-apparatus: A single ball rotates on three other identical balls; in between is the lubricant. At the lubricant manufacturer, the lubricants are characterized using various tribological test machines differing in the tested contact condition. Depending on their subsequent application, lubricants are tested in the closest suitable contact condition.

The Reichert test is typical for characterization of water-mixed MWF. The tribological system corresponds to Figure 2.5a 4. A cylinder gets in contact with a rotating ring under a specified pressure. The ring is immersed to a certain depth in a small temperature-controlled basin containing the test fluid. The wear scar area is determined after a defined rotating distance. The smaller the wear scar area, the higher is the lubricity of the test fluid for the tested material pair.

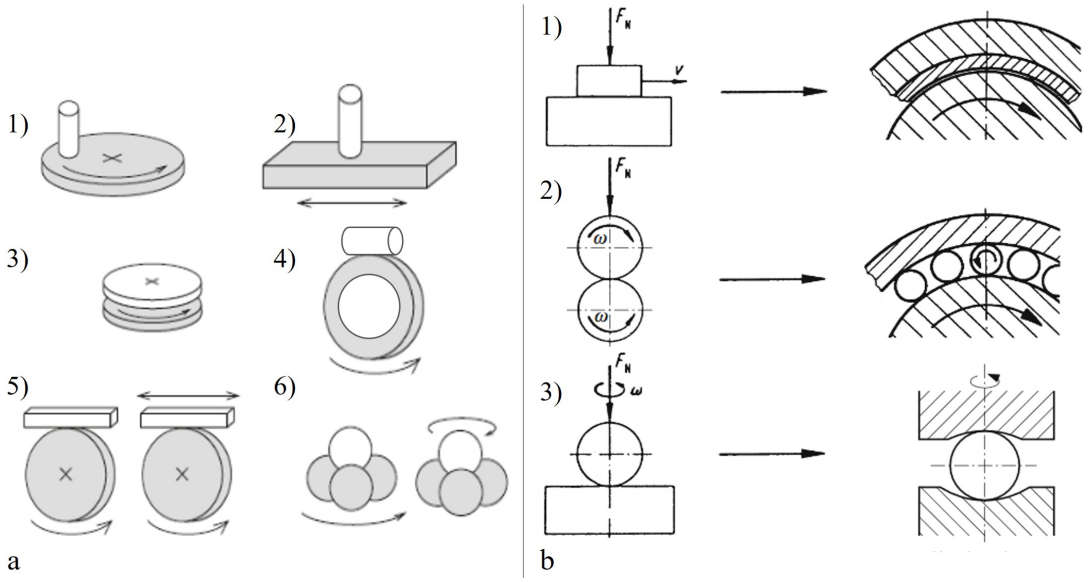

Figure 2.5: a: Principles of tribological testers: 1) Pin-on-disc, 2) Pin-on-plate, 3) Disc-on-disc, 4) Cylinder-on-ring, 5) Roller-on-disc, and 6) 4-ball-test acc. to [89],
b: Friction types: 1) Sliding, 2) Rolling, and 3) Spinning friction [90]

The TTT is a test method to compare lubrication performances of MWFs and to evaluate their suitability for a certain tool-workpiece-combination. This test will be focused in detail in Section 4.1.

2.1.7 Maintenance and monitoring

Ensuring a reliable and not harmful usage of MWFs, the fluid's condition has to be checked regularly. A loss of oil concentration in emulsions or an unintentional introduction of foreign oil into the MWF system can reduce stability and functionality of the MWF. Content of this section and the three subsections is mainly based on the contribution [8].

2.1.7.1 Analyzing methods of MWFs

The condition of a MWF, oil, or lubricant within a tribological system is significant for its functionality. The performance of the used processing fluid is important to provide machine elements of failure and to enhance the reliability of processes. With a processing fluid optimized for the individual application and each metal-to-metal contact a reduction of wear of machine elements or tools is possible. Concerning the machining of metals, a suitable MWF is able to enhance surface qualities and to increase process stability. Regular investigations are necessary to fix the best condition of the MWF. The Technical Rules for Hazardous Substances 611 define the correct use of MWF and prescribe weekly checks of pH value and nitrite content [91]. Other characteristics influencing the MWF's performance can be analyzed by several measurement techniques for example the pH value or the concentration.

For industrial applications, fluid control systems are provided for example by Rhenus Lub, Tiefenbach, and Oemeta [92, 93, 94]. Depending on the system flow, concentration, conductivity, pH value, temperature, germ count, and the filling level of storage tanks – if the system provides automatic refill or dosage – can be monitored. An online measurement of MWF can be realized and a fast intervention in form of an adjustment of concentration or a treatment of microbiological activity is possible.

Here, measurement techniques for analyzing processing fluids are described. Such techniques with applicability for online measurements of water miscible MWF are focused. The aim is to figure out the diversity of techniques and characteristics to be measured and analyzed.

2.1.7.2 Oil concentration in MWF

In practical applications the oil concentration of water mixed MWF is measured with the help of a refractometer. After a short calibration of the refractometer the refraction index of the fluid can be measured. The MWF's concentration can be determined approximately with the known refractive coefficient and the density of the measured fluid. That is a practical and state-of-the-art measuring method in lubricant industry.

An interesting measurement strategy that could be applied in real-time for MWF is the monitoring of oil viscosity by ultrasonic-based testing. A method indicating changes in viscosity was described in [95]. The authors state that the system measures the acoustic absorption by leading an ultrasonic wave through the fluid. The ultrasonic wave sent out is weakened by frictional effects caused by the fluid's viscosity so that a detection of viscosity changes is possible: The higher the viscosity, the longer the relative transit time of the existing emitted ultrasonic waves. The application for concentration measurements in MWF could be considered.

The technique of dynamic light scattering was applied and tested for industrial degreasing baths [96]. To monitor the condition of the degreasing bath the micelles are measured optically. In degreasing baths, the micelles get larger and multiple when the condition of the bath gets worse. The capacity of degreasing declines by rising micelles. With the help of this technique the determination of the micelles' sizes is possible. The contamination rate and the loss of detergent could be concluded from this measurement. Possibly the dynamic light scattering technique could be applied to determine the concentration or the dispersity in emulsified MWF.

2.1.7.3 Fluidic contaminants

A processing fluid can be contaminated with fluidic contaminants such as tramp oils, water, gasoline, or coolant. An optical sensing method was developed in [97]. The object shape-based methodology was able to detect different concentrations of water, gasoline, or coolant by capturing and processing images of the fluid. The online applicability of this system was verified for engine lubricant oil with artificial generated contaminant concentrations. The optical sensing method could be feasible for water miscible MWF concerning the contamination with tramp oil or coolant. Because oil droplets within the fluid could cause incorrect measurements, the method could only be practical for water soluble MWF.

2.1.8 Summary

Lubricants are used to reduce friction. In machining, MWFs have significant impact on tool wear, surface quality, and machining accuracy. Due to their application, MWFs have different constituents. Lubricant additives determine lubricity and performance of a MWF.

Functions and mechanisms of selected lubricant additives are well studied. In general, the mechanisms of tribofilm formation are explained by adsorption, adhesion, and chemical reaction. The latter is only possible through higher temperature and longer contact times. Thus, the mechanisms taking place during machining are mainly adsorption of molecule polar groups and adhesion of atoms with dipoles. From literature review results as well that additives interact. In which way the interaction influences the lubricity of the MWF depends on the molecule structure and the application ratio of the additives. Rather, it has been shown that sulfur can compete with other additives for the surface.

It is not in the focus of the present work, two investigate the composition of tribofilms. No spectroscopy will be performed and no theories of lubricating mechanisms will be developed. But the knowledge about these mechanisms is crucial for the choice of additives and for the development of a base fluid that is then equipped

with these additives. According to the results of the literature research, it is fundamentally important for the experiments in this dissertation that only one active lubricating additive is contained in each lubricant formulation. In this way, such interactions are systematically excluded.

Two polysulfides, different phosphorus additives, two esters and two glycols will be used as additives in the experimental part. They will be used as single additives combined with a constant base fluid and not in combination with other surface-active additives. Sulfur additives are used for EP applications and phosphorus additives are applied as oxidation inhibitors and as AW agents. As esters, the additive 2-ethylhexylcocoate (F07), an ester based on coconut oil, is compared with a synthetic polymeric ester (F08) and a naphtenic mineral oil (Ref). The used glycols differ in their molecular structure. From literature, it is known that molecules with higher polarity adsorb faster on the metal surface than those with lower polarity. The unpolar part builds the tribofilm: The longer it is, the better is the separation of friction partners.

The MWF condition has to be checked regularly. For water-mixed MWF, water evaporates, AW or EP additives are carried out by workpieces, concentration changes, bacteria grow. No real-time capable condition monitoring technique for MWFs is known evaluating the current lubrication performance. The aim of this dissertation is to develop a measuring method which makes for the future of fully-automated machines an in-process qualification of MWF's suitability possible.

2.2 Tapping processes

This section first contains a description of threading processes in general. In the second subsection, the literature review published in [98] concerning conduction and evaluation of TTTs is included.

2.2.1 Basics

In this work, machining of internal threads is focused. Tapping is a manufacturing process that generally appears very late in the process. Errors in this process usually lead to very costly rework or even to complete component rejects. In the present work, torque and AE will be measured during the tapping process. A typical torque curve of cut tapping is mapped in Figure 2.6. Entering the pre-hole, torque increases (1.) until a nearly constant value (2.) is reached. At the end of the thread, tap's rotation is stopped (3.) and the direction of rotation changes.

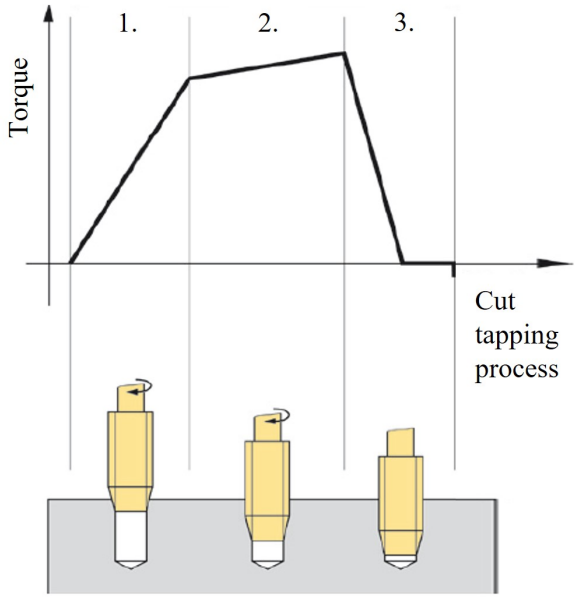

Figure 2.6: General torque curve during the forward process of cut tapping acc. to [99]

Threading is a common application in industry. Internal threads can be realized by cut tapping or form tapping. In cut tapping, material is cut away by the cutting edges of the tap. A new surface is built by forming chips (Figure 2.7a). Threads can also be realized by form tapping where the existing material is elastically and plastically deformed by the tap lobes (Figure 2.7b). Therefore, the diameter of the pre-holes for form tapping is larger than that for cut tapping.

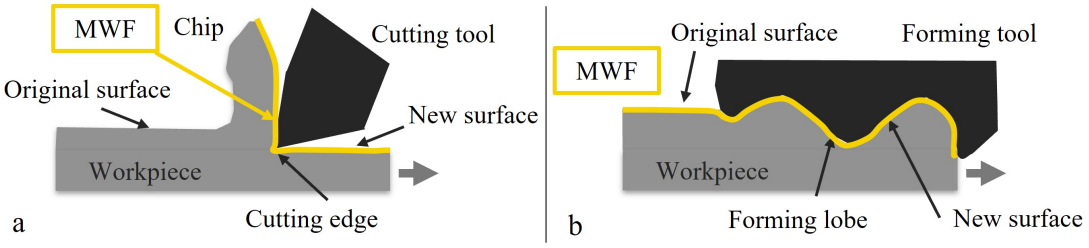

Figure 2.7: a: Thread cutting b: Thread forming

From Figure 2.8, it can be concluded that torque of form tapping (blue line) is generally higher than torque of cut tapping (green line). It is expected that differentiation of MWFs will be easier in form tapping when torque is generally higher. Additionally, tapping torque depends on tap size, material strength, and lubrication. The torque needed for a thread of size M3 is 10 % of that of size M16.

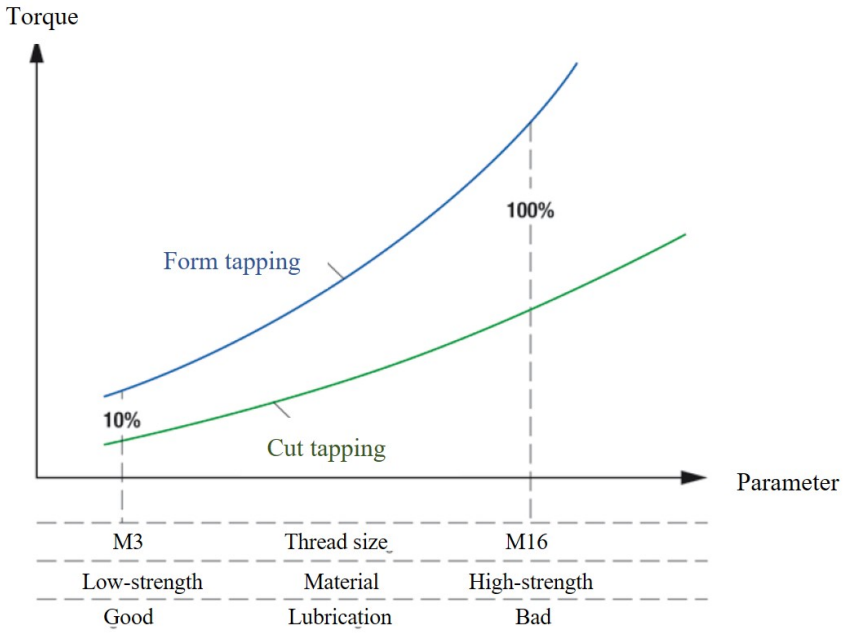

Figure 2.8: Tapping torque depending on various parameters acc. to [99]

Furthermore, chips are built in cut tapping as shown in Figure 2.9. The geometry of the tool ensures that the chips are transported out of the machining zone. For blind holes, the chips are transported out by the twist of the tap but they could get stuck in the thread. In regular distances, chip breaking is necessary for thread cutting. Both processes could interfere with the AE signals.

Form tapping is a non-cutting process; no chips are produced. The diameter of the pre-hole is chosen as big as there is enough remaining material volume to build the

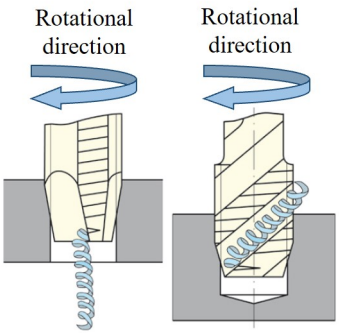

Figure 2.9: Difference between chip curling in through and blind holes due to tap twist [99]

new geometry. The geometry of a formed thread is shown in Figure 2.10. A split crest is built at the top of the thread. The smaller the pre-hole diameter is the smaller the split crest. The lower the provided material volume was, the larger the split crest is. If there is too much material volume or too little lubrication, the tap will get stuck in thread. In this case, the risk of tap breakage is very high. Hardness and stability of formed threads are better than of cut threads [100]. In [100], the microhardness of formed threads was reduced by using lubricating oil instead of emulsion. Obviously, lubrication significantly influences the formation of the metal lattice structures during forming.

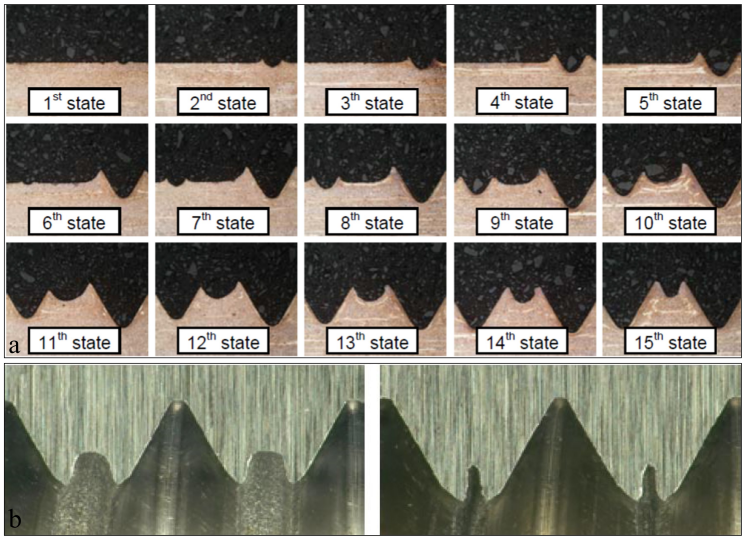

Figure 2.10: a: States of thread formation [101]
b: Geometry of formed threads in dependence on pre-hole diameter [99]

Form tapping is chosen for the experiments by the following reasons:

1. higher torque for possibly better differentiation of lubricants,

2. no chips possibly disturbing the signals, and
3. continuous process over the whole thread depth, no chip breaking necessary.

For performing a correct thread into a pilot hole, a large number of different tools are available: A tap can be chosen from a variety of tapping tools. In Figure 2.11, a small selection is exemplary shown for taps in size of M6. Taps can vary e.g. in coatings, number of flutes, flute's geometry, and number of cutting edges or forming lobes.

Figure 2.11: Various tools for cut or form tapping

The workpiece material also determines i) the type of tap and ii) the type of lubricant. Dependent on workpiece and tool material, tool wear can occur as abrasive (tool material is lost) and/or adhesive wear (extra material is welded on tool). The aim of lubricant application is to prevent tool wear and to elongate tool life. If best lubricating performance is the goal of a machining process, well adjusted MWFs have to be applied. For difficult-to-cut materials such as Nickel based steel alloys (e.g. X5CrNi18-10) a different MWF has to be used than for easier-to-cut materials such as wrought aluminum alloys (e.g. AlMgSi1). The whole process consisting of workpiece material, tool material, and lubricant determines the tribological pair.

2.2.2 Tapping Torque Test

This section is based on publication [98].

A literature review is given on experiences with TTTs with respect to contributions applying the standard of TTTs, ASTM D5619-00, or a modified version. Here, articles are focused using tapping torque as a measure to evaluate the functionality

of tool coatings, effect of different pre-hole diameters, or other test related parameters. At the time of publication, the new standard ASTM D8288-19 has not been published yet.

The use of MWFs in industrial machining processes is widely spread. The fluids cool and lubricate the contact zone between tool and workpiece to prevent tool wear and to ensure manufacturing of required geometries and surface qualities. To recommend the best suitable MWF for each machining process, lubricant manufacturers use empirical data of similar applications as well as results from standard laboratory wear tests e.g. Reichert and Brugger test or cutting force tests e.g. TTT. In comparison to cutting force tests in drilling, turning, or reaming operations, tapping tests show the best relative resolution related to special cutting fluids and work materials [102]. Lubrication reduces friction between tool and workpiece and can increase surface quality and tool life time. A general statement is not possible and the machining result depends on the effects of the fluid's contents. The type of fluid and its contents/additives mainly affect tool wear and surface roughness or make higher machining speeds possible to decrease manufacturing time and increase the output. Apart from good lubricating and cooling properties, other properties such as corrosion inhibition, flushing and defoaming properties, long-term stability, skin and environmental compatibility can also be included in fluid requirements.

Most of these established tests are performed strongly related to conformed standards and rules of relevant institutions. The relevant regulation for TTT is ASTM D5619-00 (2011), *Standard Test Method for Comparing Metal Removal Fluids Using the Tapping Torque Test Machine*. The last active version of ASTM D5619-00 (2011) has been withdrawn in 2016 with no replacement. Due to missing alternative it can be assumed that the last version is still widely used to evaluate the performance of MWFs. The present contribution highlights the problems of the withdrawn standard and proposes changes to improve test conduction, evaluation, and significance of test results for a new version and therefore provides the fundamentals for an alternative.

Threads can be realized in two different ways: cut tapping or form tapping. The diameter of the pre-holes for cut tapping is smaller than that for form tapping because excess material is cut away by the cutting edges of the tap to build the final thread. In form tapping the existing material is elastically and plastically deformed by the lobes of the tap. Tools for cut tapping have flutes for chip transportation. Tools for form tapping can have oil grooves for lubricating aspects. In this case, the forming lobe is located just between the grooves. The fundamental processes of cut and form tapping processes differ strongly [103, 104] and are not focused in this article. Cut tapping is the less reliable process for TTTs because chip curls can drag and jam in the tap's flute and can contribute to the measured tapping torque. Thus, the ASTM D5619 is not only realized and applied for cut tapping but also for form tapping. In the experimental part of this article, tests are conducted in form tapping.

In the present contribution, the fundamental processing of cut and/or form tapping is not focused. Here, the methodology of performing and evaluating tapping tests is discussed in general. The literature review contains contributions dealing with cut or form tapping. The contributions are analyzed regarding test procedure, reference measurements, start parameters/running-in of tools, tool qualification processes, considering of carryover effects, number of replicates and test deviations. The result evaluations of these contributions are investigated due to differences between test fluids and statistical evaluations. These criteria are important for tests using cut taps as well as form taps.

In literature, many contributions have dealt with TTTs or tapping processes. Most of TTTs were performed according to ASTM D5619 [103, 105, 106] or to a modified, similar procedure. Uncoated or coated tools with diameters between M4 and M10 were used in thread cutting and thread forming operations in workpiece materials reaching from carbon steels to highly alloyed steels or various aluminum alloys. The effect of different fluids i.e. base oils, additives on the tapping torque [107, 83, 103, 105, 42, 108] and of different tool geometries [109] was investigated. Exemplary, a less effective oil needs a 53 % higher torque than a highly effective oil in form tapping of hardened steel [42]. Tool coatings have a significant effect on tapping torque and tool wear [83, 110, 104, 111, 112] and on thread surface quality [111]. Lubricants not only influence the tapping torque but can also affect the micro-hardness of the flank of the formed thread [100]. Pre-hole diameters and forming speeds influence the tapping torque [106].

The usability of tapping torque and reaming torque tests for cutting fluid evaluation were investigated. By comparing both tests, reaming torque tests were evaluated to be a viable alternative to TTTs [113]. Different machining methods were tested to evaluate cutting fluid efficiencies [114, 115]. Laboratory lubrication tests were compared with real manufacturing processes: Brugger and TTTs were performed using non-water miscible MWFs with different additive combinations. A transferability of both tests to industrial forming processes was proven using the same workpiece and tool material combination [116]. A good correlation between measurements of TTTs with high resolving power and field performance were obtained using the same fluids [112].

The running-in behavior of tapping tools to be used for TTTs has rarely been investigated. For dry tapping and tapping with minimum quantity lubricant without additives, a running-in behavior of the used cutting taps can be recognized [83]. It can be concluded that the running-in effect is not recognizable for higher lubricating conditions with flooded tap oil or minimum quantity lubricant containing additives. The running-in phase is possibly affected by the lubricating ability of the used fluid.

The necessity to run-in the taps before starting the test sequence is mentioned in several contributions. Details about the number of threads or the tolerated deviation

of the means are often not given. The importance of repeating reference measurements after the running-in is emphasized to verify that tool wear has no effect on the measured tapping torque [112]. The tolerated deviation from the reference value is not mentioned and the repeated reference values are not taken into account in the calculation of tapping torque efficiency.

Before conducting the lubricant's test, the forming taps are firstly used with the reference fluid [103]. It is not mentioned for how many threads the reference fluid is used but the measurement values are used to qualify the taps. Taps with a repeatability of 2 % are qualified [103]. The equation to determine the repeatability is not given.

In a few contributions [116, 117, 118], the test procedure is considered in more detail. Good repeatability and reproducibility of TTTs are obtained applying a suitable order of test sequence for the fluids [117, 118]. Regular reference measurements are performed [116, 117, 118] to monitor the effect of tap wear. In most cases, the changed reference values are not integrated in the calculations of tapping torque efficiencies. Reference values can change up to 12 % when using new forming taps of the same batch [103]. To be able to compare the measurement values of different taps, a coefficient of correction is introduced. Although the calculation of this coefficient is not described, it is used to calculate an average tapping torque corrected [103]. The corrected values are used to directly compare the test results of fluids obtained with different forming taps.

Multiple tapping torque testbeds are proposed to increase the sensitivity of TTTs [112]. The importance of selecting suitable test conditions to be able to distinguish between MWFs is emphasized. Differences between measurement results are analyzed using a statistical significance test (t-test) assuming a normal distribution for the plateau area of the torque curve. As a result, it is stated that tool coatings, tool sizes, and machining speeds significantly affect the resolving power of the tests [112]. Four different tap coatings and four different fluids were evaluated in tapping of carbon steel (SAE 1018) at 500 and 1000 rpm. Coated high performing tools were found to be ineffective for MWF examination because of very small and not statistically significant differences between test fluids [112]. The highest resolving power was gained with an uncoated M6 high speed steel tap at 1000 rpm [112]. A minimum number of replicates of each test condition has been determined to allow statistically distinguishable values for the test fluids [112]. Based on experimental experience, 20 to 30 replicates are proposed depending on the resolving power of the chosen test conditions.

Fluid type, tool coatings, workpiece to workpiece variation, and tool to tool variation have statistical significance on the measurement results [112]. Tool to tool variation is discussed to have less effect on the results than the other three parameters. That means the allowed standard deviation of $\pm$ 2 % between tools defined in ASTM D5619 is surpassed by fluid type, tool coating, and workpiece variation [112]. In

another contribution, the differences between the taps are evaluated as so significant that a correction coefficient is applied to compensate the differences between the taps [103].

To my best knowledge, no contribution is known investigating carryover effects by previously used fluids on TTT results. In some articles [103, 116], the test procedure is described in such a way that the conditions before starting a test run are adapted. A reference fluid is used for one thread to set the same starting conditions before changing the fluid and to monitor a drift of the measurement values [116]. An influence of the previously measured fluid is assumed to be significant but it is not investigated further. A comparison between measurements with and without this initial condition is not made. In another contribution, each tap is only used for the reference fluid and for one lubricant to strictly avoid contamination effects [103].

2.2.3 Summary

Summarizing the literature review, a transferability into field application has been shown for TTTs. The necessity of regular reference measurements or the significance of carryover effects has not been investigated in detail. The strong difference between initial values of taps has been considered only in one case by introducing a correction coefficient. Details about measurement deviations are often missing and measurement results have been statistically analyzed only in few cases. No contribution can be found considering the definition of the initial test condition or dealing with the investigation of the characteristic built-up edge to precisely define the end of running-in phase of a tap. Therefore, suitable measurement methods or useful features have not been discussed.

2.3 Acoustic Emission in machining

This chapter is mainly based on contributions [8, 9].

Acoustic Emission is known as a passive, non-destructive testing technique. In general, AE refers to elastic stress waves that can be detected on structures under load or stress due to damage. These are located in the ultrasound regime and propagate through structures over significant distances. Therefore, the AE signal entails information regarding underlying physical source mechanisms. Due to its origin as a non-destructive testing technique, AE has decisively shaped many structure health monitoring applications such as monitoring of aircraft structures, wind turbines, or bridges. Besides detection and characterization micro-mechanical damages, also monitoring of wear in friction contact is relevant to structure health monitoring. During elastic-plastic interaction of surfaces under sliding motion structural alterations at the surface of the material can be observed, which ultimately cause surface fatigue and loss of material. Here, different principal mechanisms, namely adhesive and abrasive wear, can be distinguished. Since the contact zone is difficult to access, AE has recently been used to study wear in friction contact. It is generally accepted that wear mechanisms can be distinguished based on the frequency content of the related AE. However, relation to corresponding physical mechanisms is not unambiguous.

Asamene et al. studied the effect of different parameters in reciprocating contact of flat steel surfaces on the corresponding AE [119]. In this study, frequencies of 100 kHz and above, up to 700 kHz are considered. Plastic deformation was characterized as weak signal which is close to white noise [120]. Hase et al. studied the AE during pin-on-block experiments to relate properties of the AE signal to distinct wear mechanisms [121]. Here, frequencies between 250 kHz and 1 MHz are attributed to abrasive wear, whereas frequencies of up to 1.1 MHz can be related to adhesive wear. However, mild adhesive wear also excites frequencies in a lower regime between 10 kHz and 100 kHz [122]. Baccar and Söffker proposed novel health-monitoring approach for tribological system using frequency-selective analysis of AE [123]. Three distinct wear phases of metallic plates in sliding contact can be distinguished according to the frequency content of the AE signal.

Acoustic emission technique has already been used as a feature for condition monitoring during machining in [124, 125, 126, 127]. Especially for tool condition monitoring, AE is frequently used as a means for indirect wear estimation in different machining operations. To develop indicators describing tool wear states, correlations between AE signal features and process parameters (i.e. power consumption, torque, or cutting forces) are exploited [128]. Gomez et al. [129] investigated the correlation between AE and torque in drilling operations using mean power and Average Spectral Power in different frequency bands. Burst type-events could be related to chip breakage, whereas continuous AE is attributed to plastic deformation

and friction, respectively. Statistical analysis shows that different types of worn drill bits (i.e. cutting edge and flute edge) can be distinguished. Additionally, increase in tool wear leads to a shift of signal power spectrum to increased frequencies. Using this approach, severely worn tools are identified reliably. Similarly, Ferrari and Gomez [130] addressed relationship between thrust and AE in drilling. Compared to torque, thrust is considered to be particularly well suited to assess time behavior of the drilling process. Sensitivity of AE to tool wear is confirmed. However, correlation between thrust and tool wear was not established.

Similarly, AE has been considered to assess the tool condition in turning. Bhuiyan et al. investigated the effect of tool wear on AE and vibration measurements in turning during dry machining based on root mean square of AE and vibration signals. As a conclusion, AE is sensitive to wear rates of the tool, whereas vibrations are related to surface roughness [125]. Hase et al. [131] identified chip generation (continuous or discontinuous) as major influencing factor on AE. Furthermore, special emphasis is placed on the complex interaction between flank wear, cutting conditions (shear angle), and roughness of the machined surface during generation of chips. Moreover, Maia et al. [122] attempted to distinguish between different source mechanisms (i.e. adhesive and abrasive wear, plastic deformation) using frequency content of AE signal.

From the summary above, it is apparent that most frequently the condition of the tool is subject of investigation. However, machining operations are usually not performed under dry conditions. To achieve improved performance, MWFs suitable for the tribological pair should be used [132]. To date, the underlying mechanisms are partly researched. Formation of tribofilms or lubrication regimes has been researched in connection with AE measurement. It is possible to differentiate between boundary and hydrodynamic lubrication [133].

In [134], AE was measured in lubricated contact conditions in a ring-on-disc and a journal bearing test setup. The root mean square was calculated from the AE signals and a spectral analysis using different ways of Fourier Transformations was performed. The root mean square correlated well with proceeding wear. The power spectrum was analyzed until 425 kHz and the range of 60-225 kHz was found to be related to the tribological contact including oil and material combination [134].

2.3.1 Monitoring techniques during machining

Parts of this and following subsections are based on the contribution [8] published in 2016.

Process control has become more and more important to ensure products with constant quality and to decrease the number of process failures. In engineering there is an increasing demand for higher productivity, reproducible products, and lower

costs. Machining processes like turning, drilling, or milling are monitored in real-time to predict tool breakage and to prevent machine failure. The application of monitoring systems can reduce costs for machining tools and can improve process reliability. Nowadays, tool condition monitoring is implemented into machining centers as standard. The main techniques used are cutting force (thrust, support force, torque), vibration, or AE measurements. Advanced technologies do not only use a measurement system but also contain implemented neural networks for the diversity of tools. The regular process of each tool is trained so that the abnormal process can be detected by changes in measurement results. Additionally, prediction of tool life time is possible as a task of predictive maintenance. The tool change can be predicted by the system after related thresholds had been implemented. Detection rate, amount of false alarms, or the necessity of human intervention are less discussed in literature.

2.3.2 Tool condition monitoring techniques

Reviews with the focus on tool condition monitoring have for example been published by [135, 136, 137, 128, 138].Tool condition plays a significant role in reaching demanded surface qualities or demanded machining accuracy. Tool wear increases with increasing machining time [139]. Tool's lifetime depends on the respective tribo-pair including workpiece material, tool material, the cutting parameters, and the used MWF.

During machining, workpiece material is deformed plastically by tool material. This generates high friction between tool and workpiece. The tool material wears off. Tool wear can appear in several forms: flank wear, crater wear, plastic deformation, chipping, breakage, and built-up edge [140]. A worn tool is not able to fulfill constant qualities of the machined workpieces. A tool breakage can damage the workpiece irreparable. A tool condition monitoring system can warn against highly worn tools so that those can be replaced in time. Process stability can be saved and production failures caused by tool breaks can be reduced. As a result, a tool condition monitoring system can reduce production costs.

2.3.3 Manufacturing solutions

Manufacturers of milling or turning machines recognized the need for tool monitoring and offer several tool condition monitoring systems optionally for their products. In the following, systems of some companies are mentioned focusing on systems with AE technique. Komet Brinkhaus offers monitoring systems for example for tapping processes [141]. The system is able to learn and to differentiate between a normal and an abnormal process. The products of MCU GmbH contain sensors measuring the active power, force, structure-borne noise, vibration/oscillation, and collision.

The limit of tool condition monitoring measurements by power current is given for very small tools. When the current consumed power of the spindle is as low as the no-load current power, a detection of process failures is not possible. Here, AE is used to monitoring the condition of very small tools [142].

Schwer + Kopka developed process monitoring systems for cold and hot forming, stamping, and assembling [143]. Different piezoelectric sensors are used to measure forces, strain, AE signals, electrical power consumption, and tool breakage. Nordmann divide their sensors in seven categories [144]: effective power and torque, force, AE and vibration, distance and gab, tool length and workpiece position control, workpiece dimension control, and tool position control. Acoustic Emission is used to detect tool breakage through the cooling jet or to control the gap for grinding machines. An in-process quality control system from Hufschmied uses artificial intelligence to classify sound images of the machining process [145]. The detection rate was not specified for each of these systems or sensors.

2.3.4 Scientific research

In literature, tool condition monitoring has been investigated on the basis of forces [138, 146, 147, 148, 149, 150, 151, 152, 153], vibrations [139, 154, 155, 156, 157, 158, 159, 160], optical features [161, 162, 163, 164, 165], spindle or feed motor currents [166, 167], wear images [154, 161, 163, 164, 165], sound energy, power consumption, ultrasonic emission, or temperature [128]. In addition, many research has been taken out on the combination of different features for tool condition monitoring for example in [148, 168, 169, 170, 171, 172, 173, 174].

Soft computing techniques with artificial intelligence as neural networks, Support Vector Machine or fuzzy classifier [167, 168, 172, 175, 176] are used to predict process data and to optimize process stability [135]. The main part of the investigated techniques is based on monitoring forces, vibrations, and AE that have been tested for several machining operations like milling, drilling, or turning. Furthermore, AE techniques were used intensively for forming and grinding operations.

This literature research focuses on research concerning AE. There have been several reviews on tool condition monitoring including AE [128, 135, 138, 177]. These reviews give a detailed view over the monitoring techniques in several machining operations. In [128] the application of AE is described for turning, drilling, face milling, and end milling. The authors in [135] focus the monitoring systems using digital images. A review on artificial neural networks during turning is focused in [138]. The paper of [177] was published in 1995 and includes a detailed review on AE techniques.

2.3.5 Different machining processes

For the content of this subsection, publications with monitoring techniques for different machining processes have been investigated. Sensing combination systems based on cutting force, vibration, and/or strain was developed for example in [151, 169]. The fusion of vibration features and digital images was investigated in [178]. This review part focuses on techniques using AE as feature. The machining processes turning, drilling, and milling are included.

2.3.5.1 Turning

Acoustic Emission measurement was combined with other measurement techniques as vibration or cutting forces. The correlation of these methods was investigated for example in [172]. A multiple sensor system based on cutting force, vibration, and AE was tested during turning. The measurement results were evaluated by neural network. Additionally, a tool life time prediction model was implemented. With the help of an online cognitive decision making system it was possible to realize a machine learning algorithm [172].

In turning, the wear of the tool was monitored by AE [122]. A piezoelectric sensor was placed on the tool holder. Acoustic Emission signals were analyzed by power spectral density technique. The value was high for a new tool, decreased at the middle of the tool life, and finally increased until the end of tool life. The average of the power spectral density correlated with the maximum flank wear of the turning tool [122]. By implementing suitable thresholds for each tool, the tool's usability could be limited.

The root mean square value of AE signal in turning was investigated in [126]. Turning tests were performed at different cutting speeds, feed rates, and depths of cut. Flank wear and AE was measured during the tests. It was found out that the important signals mainly occur within a frequency range of 30 to 60 kHz. The root mean square value correlates with the flank wear [126].

The relation of AE and vibration signals during turning was investigated in [125]. With increasing flank wear the surface roughness as well as the signals based on AE first decreased to a minimum value and then increased steadily until the end of tool life. Acoustic Emission and vibration signals were evaluated to be useful to monitor the turning process. The progression of tool wear could be monitored well by AE whereas surface roughness could be indicated better by vibration signals [125].

By Kamarthi et al., flank wear could be estimated using AE signals in wavelet representation. In addition, a recurrent neural network was trained and the results outperformed previous methods using Fourier transformed AE signals [179].

The quality of the machined surfaces was focused in [180]. Acoustic Emission was measured during turning. An indirect correlation between the root mean square value of the AE and the measured surface roughness could be drawn [180].

2.3.5.2 Drilling

By Kimmelmann et al., burr formation mechanisms appearing during drilling of carbon reinforced plastic have been investigated by AE technique. It was shown that burr height could be estimated already during machining by AE signals after Fourier Transformation [181].

By Möhring et al., workpiece quality and tool wear in drilling of stacks have been investigated by AE technique. By two AE sensors and a high speed camera, the drilling of carbon fiber reinforced plastics–aluminum–stacks is monitored. Characteristic features of the AE spectrum can be used to evaluate the bore hole quality. The surface roughness of the aluminum layer could be estimated from the AE signal. The authors did not find a correspondence between tool wear and AE signals [182].

By Ferrari and Gomez, AE in correlation to the thrust force was investigated. Tools with five different wear states were used. Acoustic Emission and thrust force were recorded simultaneously. The AE sensor was placed on the workpiece. The root mean square value, the measured area under the rectified signal envelope energy, the amplitude, and the mean power were selected as AE based features. The author concluded that the mean power could be used for tool wear characterization [130].

By Arul et al., the correlation between AE, flank wear, and drill hole shrinkage was evaluated concerning drilling of glass fiber reinforced epoxy resins. Flank wear, thrust force, and hole shrinkage are influenced by cutting parameters. Acoustic Emission signals were evaluated in frequency domain. The power of the measured signal increases with the number of drilled holes. Furthermore, the root mean square correlates to the thrust force, the flank wear and the hole shrinkage in regard to the number of holes. The values increase with the number of drilled holes. The root mean square of AE correlates best with the flank wear so that a determination of the flank wear via AE was possible in this case [183].

By Quadro and Branco, the effect of tool coatings was investigated using AE based on the quantification of wear and the identification of five different wear states. An increasing tool wear results in an increase of the measured rectified signal envelope of AE. In relation to tool wear, peaks in AE change [184].

2.3.5.3 Milling

By Liu et al., a decision making model was developed based on AE data collected during milling tests. With increasing tool wear amplitude and distribution of the AE signal changed. The signals were analyzed by wavelet packet transform and the wavelet packet energy was calculated. The normalized energy increased with machining time and increasing wear [185].

By Gao et al., Artificial Neural Network based on features of cutting forces, vibrations, and AE was developed and tested during milling tests. The model provided a higher precision than a model based on single features [176].

By Marinescu and Axinte, AE was used to detect tool and workpiece malfunctions during milling. The aims were to identify AE signals independent from the tool path to calibrate AE sensory against proceeding tool wear and to detect surface anomalies resulting from machining failures. Milling tests were conducted at an Inconel 718 workpiece and the AE sensor was placed onto the workpiece. During the tests, AE, forces in three dimensions, and torque were recorded. From the test evaluation resulted that monitoring of the cutting insert's wear was possible by applying Short Time Fourier Transformation (STFT) to the AE signals. With the help of the area underneath the envelope of the resultant cutting force, the measured area of the rectified AE signal envelope, and metallographic investigations a relation between AE, cutting forces, and surface quality could be established [186].

Marinescu and Axinte, investigated further a cutting tool with an intentionally damaged insert. The AE signal was analyzed in time-frequency domain. A differentiation between normal cutting and cutting with resulting surface anomalies could be detected [187].

Jemielniak and Arrazola, explored the application of AE and cutting forces for tool condition monitoring in micro-milling. A strong relation between AE and tool wear was found. Although the cutting force signals were disturbed by vibrations the monitoring of tool wear was possible. The author suggested that the usage of more signals is preferable to minimize the diagnosis uncertainty and to make tool condition monitoring more reliable. Better results are achieved by the measurement of cutting forces and AE than a technique only based on AE measurement [124].

2.3.5.4 Other processes

Dornfeld et al. investigated AE technique for precision machining. It was concluded that AE was very sensitive to control parameters in high frequency range. Normally force or vibration sensors lose accuracy in the high frequency range because of limited band width and due to noise. High frequency signals of AE were measured for a small length scale of material removal whereas the frequency declines for increasing material removal. It was shown that AE is more sensitive for small material removals and high levels of precision whereas the use of forces or vibration signals is better for larger chip thicknesses. Concerning the ultra-precision machining and micro cutting mechanisms, signal measurements based on AE are suitable techniques for monitoring because noise and disturbances caused by machine elements could be minimized [188].

Acoustic Emission was tested to control the wear status of gears [189, 190] or for forming and grinding operations [191, 192, 193]. Friction and wear states of sliding plates were investigated in [123, 194].

By Liu et al., the lubrication effect at a head/disk interface was examined with AE. Three different lubricants were investigated and difference between AE responses has been observed due to higher wear of the disk. Concerning the head/disk interface the lubricant was identified "as one of the most important factors". The occurring debris in the interface could be measured by changes in the AE signal. The levels of AE signal were higher for increasing wear and increasing lubricant degradation [91].

2.3.6 Summary

Using AE, an indirect measurement of tool wear in turning, drilling, and milling is possible. The roughness of turned surfaces is related to AE signals. Special features of AE signal can be used to detect different wear states of a drilling tool. In drilling, the correlation between AE and drill hole shrinkage or between burr formation was found. Changes in cutting speeds, feed rates, and tool coatings could also be detected during drilling. Regarding milling processes, the differentiation between normal and abnormal machining could be made by measuring AE signals. A correlation between AE, tool wear, and surface quality was found. For head/disk interfaces, detection of higher wear caused by lubricant degradation was possible by measuring AE signals.

Tool condition monitoring systems have been using AE for a long time for different tasks including life time prediction tasks. In most of the aforementioned contributions, the use of a lubricant is not mentioned although most of these processes are performed wet. Obviously, the role of lubricant for the tribological contact is often underestimated and not considered. No contribution is known, using AE for real-time monitoring of the lubricant's condition as aging or for predictive maintenance of lubricants during machining.

2.4 Machine Learning in manufacturing processes

Machine Learning is nowadays used in many areas of life as well in the field of tribology [195]. It is more often fundamentally important for process improvements and/or innovative business models [196]. In machining, Machine Learning algorithms are most commonly applied for classification tasks, or prediction of lifetimes of machine parts or machine tools. These self-learning algorithms are first tuned with a training dataset. The quality of the resulting model is then checked with a test dataset. Generally, test data are not included in the training dataset. Reviews about Machine Learning methods applied in tool condition monitoring are given for example in [6, 128, 197, 198]. New research about tool condition monitoring methods without learning processes have become rare. König et al. used a face recognition technique based on an eigenface algorithm for the evaluation of tool wear images. New images are compared with a set of existing reference images. The evaluation is only statistical and learning-free and does not need any training. [162] One advantage of learning-free monitoring systems is that they usually work faster. But main disadvantages are unflexibility and strongly reduced transferability. In this dissertation, learning algorithms are focused.

2.4.1 Machine Learning approaches

Different kinds of machine learning algorithms like Hidden Markov Models, Support Vector Machines, random forest/decision trees, Artificial Neural Networks, Convolutional Neural Networks, etc. have been used in literature to monitor, evaluate, and predict friction contacts. The following part does not represent a complete presentation of the aforementioned algorithms. Rather, the selected references focus on frictional contacts and AE measurements. Parts of this section are related to the publications [10, 11].

2.4.1.1 Hidden Markov Model

A Hidden Markov Model is a stochastic model. States are connected with certain probabilities of occurrence. These states are hidden and have observable outputs occurring with probabilities depending on the respective state. These models have a simple structure allowing fast training, are good in nonlinear and non-stationary signals, and can easily be generalized [136]. Due to these characteristics, Hidden Markov Models are primarily applied for fault recognition for example in rolling bearings [199] and for health state identification of cutting tools [200]. Ertunc et al. used Hidden Markov Models to estimate tool wear status during drilling. A classification into the three conditions sharp, workable, and dull was possible with thrust force and torque signals [149].

2.4.1.2 Support Vector Machine

A Support Vector Machine works as a supervised binary classifier. The classes have to be learned by training data. The algorithm calculates an optimal hyperplane dividing the data in two classes by placing the hyperplane at a position with the maximal possible distance between the nearest data points. In [127], tool condition monitoring during milling was performed using vibration and acoustic data. With both features, AE data after STFT and vibration energy, 98.46 % classification accuracy could be reached using a Support Vector Machine as linear classifier [127]. Brezak et al. used a Support Vector Machine algorithm for tool wear estimation. Feed force, AE, and feed drives nominal current signals were measured and relevant features were selected during an fuzzy logic classification [168].

For fault diagnosis in bearings, Saimurugan et al. used a decision tree algorithm for feature selection and a Support Vector Machine for classification of vibration signals [159]. Saeidi et al. classified AE signals resulting from lubricated sliding contacts using a Support Vector Machine to identify the transition from the steady-state regime to the scuffing regime [194]. In [201], the performance of Support Vector Regressors has been tested for wear identification of taps during thread forming. Bustillo et al. found out that the radial Support Vector Regressor reached better results than the linear Support Vector Regressor. Cho et al. designed a tool condition monitoring system for milling based on multiple sensors by testing two different feature selection methods and three classifiers. The highest accuracy of 97.67 % was reached with fusion of features from force, vibration, and AE signals. The applied support vector machine outperformed the two other machine learning classifiers, Multilayer Perceptron Neural Network and Radial Base Function Neural Network [170]. Comparable results regarding milling were published in [175].

Sun et al. successfully implemented a revised Support Vector Machine and were able to classify tool flank wear based on AE signals [202]. Alves and Poppi identified the contamination of a paraffinic base oil with naphthenic or vegetable oil by processing data of a spectroscopy using a Support Vector Machine [203].

2.4.1.3 Random forest and decision tree

Random forest is a classifier that combines several decision trees. Each tree makes a decision and the majority decides on the final classification [204]. In a decision tree, consecutive decisions are hierarchically arranged. Random forests need training and test data. Bienefeld et al. estimated the remaining useful lifetime of lubricated rolling bearings using structure-borne sound signals. With 500 decision trees in the random forest and different feature combinations, the smallest achievable relative error of prediction was 8.9 % [17]. Bustillo et al. used decision tree based regressors for identification of tap wear. The best performance was achieved by a rotation forest

with reduced-error pruning trees [201]. Prost et al. used a random forest classifier for identification of four states in journal bearings using lateral force signals. The trained algorithm was able to classify the states with an accuracy up to 93.9 % [205]. Krishna Pradeep et al. used decision trees as classifiers of vibration signals and/or digital images for tool condition monitoring. The classification efficiency reached 98 % for the approach with both features fused [173].

2.4.1.4 Mahalanobis-Taguchi system

Mahalanobis-Taguchi systems are used for diagnosis and forecast. The Mahalanobis distance is used as measure for the distance between abnormal and normal observations [206]. Mahalanobis-Taguchi systems were used for prediction of tool breakage during drilling [207] and fastened grip length of bolted joints [208]. Rai et al. measured thrust force and torque during drilling and identified useful features for tool life time prediction. Saygin et al. used torque signals and torque-angle signatures of an optical encoder in a Mahalanobis-Taguchi system for the detection of various grip lengths and achieved an accuracy over 95 % [208]. A review of recent research results obtained with Mahalanobis-Taguchi systems has been made in [206].

2.4.1.5 Artificial Neural Network

Following Rojas, in Artificial Neural Networks, biological neural networks as the human brain are imitated. Principally, artificial neural networks are treated as *black box* which should produce a certain output vector for a certain input vector. Neural networks can have hierarchical structures and transmission of information can take place between layers and between all elements of the network. Data is stored at the contact point between different neurons and partly in the transmission channels. The behavior of the network is only finally determined in a learning process. If there are no feedback loops, the network is feed-forward and the calculation process is unique. If the output of a node is fed back to it as an argument, it is a recursive network and there are countless possible outputs [209].

Neural networks are applied in many fields of industrial applications. A review about the applications of Artificial Neural Networks for tool wear monitoring is given in [210]. Karam et al. developed a prediction model for tool life during turning based on sensor fusion and neural network. Cutting force, vibration, and AE signals were used in differently configured three-layer feed-forward backpropagation neural networks. An online cognitive system continuous learning from new inputs has been developed [172]. A neural network model was developed in [211] to classify force signals to related wear states during turning.

Sadegh et al. used AE for identification of the three lubrication regimes in journal bearings. Features are extracted in time domain and after continuous wavelet

transformation. The extracted features are classified by genetic algorithms in combination with Artificial Neural Network. Lubrication regimes can be identified by using at least four features and a combination of genetic algorithms and Artificial Neural Networks. Root mean square, crest factor, and impulse indicator have been identified as important features [212].

Artificial Neural Network was used for wear distinction by Jafari et al.. Types of valve damages in internal combustion engines were detected by evaluation of AE signals in time domain [213].

2.4.1.6 Convolutional Neural Network

This section deals with the introduction of CNNs and with a review about the use of CNNs in monitoring/classification of frictional contacts. It is mainly based on publication [10].

In the early 1960s, David Hubel and Torsten Wiesel improved the concept of receptive fields. In 1975 and 1980, Kunihiko Fukushima extended the theory basis by implementing the concept of 'cognitron' and 'neocognitron', the biological theory of CNNs. In 1986, Rumelhart et al. raised back propagation. Yann Lecun et al. applied the back propagation algorithm to train neural network and proposed LeNet-5 [214] which is the prototype of recent CNNs. In 2012, Krizhevsky et al. introduced the new deep structure and dropout method in CNNs [215] by raising test accuracy to 84.6 % which aroused people's interest and started a new epoch of CNN. From 2012, many CNN models were developed such as LeNet, AlexNet, VGG, GoogLeNet, ResNet which are widely applied in many fields of living and working.

In this thesis, CNN as a sub-field of Deep Neural Network is applied and this in turn as sub-set of Machine Learning [216]. It can also be called as a type of deep learning model for process data and it usually works supervised. The architectures of CNNs is inspired by the organization of animals' visual cortex. It is designed to automatically and adaptively learn spatial hierarchies of features from low to high level patterns [217]. Nowadays, CNNs are used for pattern recognition, classification, fault diagnosis, and prognosis tasks.

A CNN is typically forward directed (without feedback loops) and designed with three different types of layers: convolutional (conv) layers to extract features, pooling layers to reduce dimensions and calculation time, and the fully connected (fc) layer at the end to classify data into predefined classes [218].

The fundamental block for CNNs is convolution layer which is composed of a stack of mathematical operation called convolution. In convolution operation, the element-wise product between each element of the kernel and the input tensor is calculated and summed to obtain feature map. In convolution layer, the convolution operation

is repeated, applying multiple kernels to form an arbitrary numbers of feature maps which represent different characteristics of the input tensors [219].

Usually, the output of the convolution layer is then passed through a nonlinear activation function which is used to increase the expression ability of neural network model. There are several common nonlinear activation functions like sigmoid, tanh, rectified linear unit (relu) etc.. After multiple stages of conv and nonlinear layers to reduce the computational requirements progressively through the network as well as minimizing the likelihood of overfitting, pooling layers are used. There are four types of pooling: max pooling (mpool), average pooling, global max pooling, and global average pooling.

The output feature maps of the final conv or pooling layer are transformed into a one-dimensional array of numbers or vector and connected to one or more fc layers, in which every input is connected to every output by a learnable weight. The features generated by the final conv and pooling layer correspond to a portion of the input image as its receptive field does not cover the entire spatial dimension of the image, thus, fully connected layer is mandatory in CNN [220].

Besides the classic building blocks in CNN, according to the task, another activation function would be applied to the last fully connected layer. For classification task, softmax would be used to normalize output values to target class probabilities.

In [221], three different wear modes in sliding bearings were detected by AE signals processed in CNN using the method GoogLeNet. The inputs were time-frequency images of AE hits after Continuous Wavelet Transformation (CWT). With particles contaminated oil could be classified with 100 % accuracy whereas the distinction between running-in and inadequate lubrication reduced the overall accuracy to 82.5 % [221]. Prosvirin et al. combined CNN with kurtogram representation of AE signals for bearing fault diagnosis [222]. Wang et al. performed bearing diagnosis by measuring vibrations and acoustic signals. They developed a CNN for classification for the different groups of bearings [223]. Shevchik et al. used spectral CNN for in-situ quality monitoring in additive manufacturing [224].

Möhring et al. developed a CNN to classify the surface roughness from sensory data of a milling process. The trained CNN reached an accuracy of 96 % in determining four predefined classes of surface roughness [225].

For tool condition monitoring, CNN was used to classify vibration signals [226]. Cao et al. combined derived wavelet frames and CNN and successfully identified wear states during milling.

Most commonly used CNNs are feed-forwardly designed. The idea of a full scale training loop was proposed by [227] and successfully used for the prediction of driving behaviors. The loop was used to optimize both model structure and model training [227]. As shown in Figure 2.12, all unknown parameters including prefilter

and hyperparameters are treated as design parameters and are included in the optimization loop. The design of concept used in the present work has a loop between data processing steps and CNN.

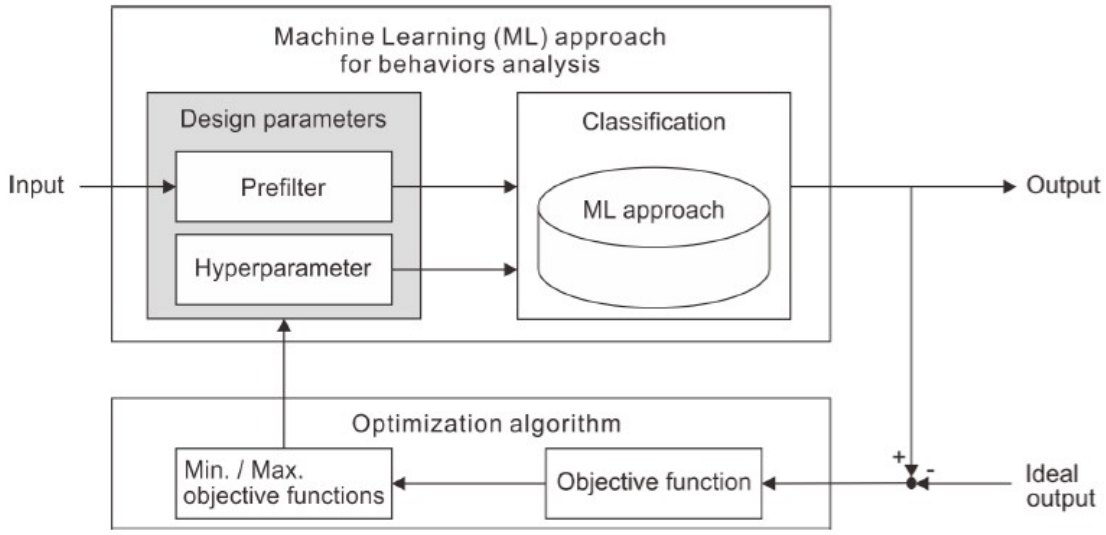

Figure 2.12: Scheme of a full scale training loop [228]

2.4.2 Summary

Machine Learning methods have been applied during machining for various purposes: damage detection in valves, flank wear detection of tools, prediction of tool breakage, and even for identification of lubrication regimes. The mostly used signals were cutting force, vibration and AE. Different features were extracted from these signals and used for classification. As classifiers and/or for feature selection, neural networks, decision trees, or support vector machines were applied. Convolutional Neural Networks have been used for detection of wear in sliding contacts and for quality monitoring during additive manufacturing. A newly developed idea of a full scale training loop for CNN optimization achieved good results in prediction of driving behaviors [228]. No contribution is known investigating the effect of different lubricants during a metal forming or metal removing process using Machine Learning methods.

2.5 Research gaps and scientific goals

In the areas of machining and monitoring of tribological contacts, applications of lubricants in different systems are well researched. Especially in steady frictional contacts as journal bearings, lubrication regimes and reaction of lubricating additives with surfaces are investigated. It is known that special elements adhere or even react – due to contact time and temperature – with metallic surfaces building protective layer(s), the tribofilm. The composition of such tribofilms is only partly researched. Few contributions deal with indirect measurement of tribofilm thickness and lubrication states. For these cases, AE is already used as measure. In this thesis, it is investigated if interactions between tool and workpiece can be measured during thread forming. The contact conditions and process-kinematic effects during thread forming are not analyzed.

For tool condition monitoring, different features of AE are used in several machining operations. It is successfully applied for monitoring of proceeding tool wear, detection of different wear types, and surface qualities. The relation between tool wear and lubrication state remains unnoticed in the examined contributions. Despite of own publications in the last years, during a real machining operation, AE has not yet been used for evaluation of lubrication conditions.

Real-time monitoring of MWFs is still unpopular. Meanwhile, users from industry have realized that a regular control of the MWF in use is necessary in order to maintain its positive properties such as less tool wear or corrosion inhibition for machines and workpieces. Especially for difficult-to-cut materials, acceptance and insight even go so far that special MWFs are required for machining. The composition of MWFs play a significant role for tool wear and qualities of machined surfaces. Real-time condition monitoring systems for MWFs in use are hardly available. In existing systems only the suitability of MWF's characteristics to its target values e.g. concentration is checked but not its suitability to the current machining situation. The development of a technique/system for monitoring of the current tribo-contact would be a novelty. Fundamental research for a suitable and real-time capable technique for the analysis of lubricity does not exist.

The performance of MWFs is determined by mostly standardized tests. Lubricity can be evaluated by TTTs. Results of TTTs are transferable into practice if the same workpiece material is used. Existing researches about TTT often do not discuss standard deviations of means or statistical distinguishability of test results. From own experiences, the sensitivity of TTTs could be improved because small changes in MWFs cannot be detected by torque means. Knowledge and effects occurring in conduction of TTTs are not well researched.

For enhancing the importance of TTTs, AE is implemented as second measure in this thesis. There is no existing research in which different features of AE signals e.g. images of raw data, spectrograms, scalograms, or AE energy have been tested as

classification variable in different algorithms. No contribution is known evaluating AE signals in CNNs or using Transfer Learning (TL) for fluid classification tasks.

The research gaps are arranged by the following points:

- Interaction of tool and workpiece during thread forming has not been analyzed by AE technique in detail.
- The evaluation of lubrication conditions has not been performed during machining using AE.
- Fundamentals of a technique focusing condition monitoring of lubricity in real-time have not been researched well.
- Side effects occurring in TTTs and influencing the differentiability of torque means have not been detailed explored.
- Classification approaches using different features of AE signals to enhance the differentiability of test fluids in TTTs have not been developed.

The scientific goals concerning the qualification of MWFs in TTTs are summarized as

- studying influencing factors on tapping torque means in the current test procedure,
- improving repeatability and comparability of TTT results by proposing new rules and calculation methods,
- investigating the suitability of AE as additional measure to enhance the sensitivity of TTT results,
- developing a series of comparable test fluids to generate suitable experimental datasets,
- searching for limitations of AE signals to evaluate differences in test fluids,
- testing various classification approaches to differentiate MWFs by means of AE, and
- evaluating the developed technique for condition monitoring of MWFs in use in the future.

3 Experimental datasets

The experimental design is described in this chapter. Experiments are carried out with an extended TTT. First, the idea of conducting an extended TTT is introduced. Second, the test rig is described including standard test rig, tool, and workpiece materials. The technique for the additional measurement of AE signals is introduced. Third, datasets of 2016 and 2019 are described and chemical structures of MWF's additives of dataset 2019 are explained.

3.1 Extended Tapping Torque Test

This section was mainly published in [11].

In TTT, test fluids are evaluated by the used tapping torque during threading. Threading is a common operation in industry. By comparing MWFs, a lower tapping torque indicates a higher lubricity. The possibility for testing a greater variety of tribological pairs is given by the TTT. According to ASTM D8288-19, tap and workpiece materials as well as MWF concentration and water hardness has to be chosen by the test operator. In literature, it is reported that results of TTT can be transferred to field applications if the same workpiece material is used [112]. Therefore, TTT are in general very convenient for evaluating MWFs' suitability for a specific material combination.

Because of limited differentiability of test fluids in the TTT by applying ASTM D5619-00, researchers experiment in test procedure and evaluation to increase the importance of TTT. Zimmerman et al. performed multiple testbeds leading to higher sensitivity of TTT and the resolving power of the tests is influenced by tap size, coating, and speed [112]. Demmerling and Söffker recognized carryover effects of the previously measured fluid significantly affecting the differentiability of test fluids. These have to be taken into account by calculating torque mean values. Water-mixed MWFs of 5 and 10 % concentration could be distinguished in C45E with a significance of 99 % by complying with specific test procedures and calculation methods [98].

Wirtz et al. developed an extended TTT by integrating AE technique into the torque measurement. This technique was used to increase the sensitivity of TTT and to find differences in phosphorus contents of test fluids [9]. Acoustic Emission is a passive non-destructive testing technique used e.g. in process monitoring and quality control in manufacturing processes. Acoustic Emission technology is widely applied in metalworking processes but only a few papers refer to the relationship between AE technique and MWFs. Water-mixed MWF with different phosphorus contents can be distinguished by AE energy in a certain frequency range after CWT. A lower sum of AE energy is related to an higher content of phosphorus. [9]

Other contributions deal with AE for identification of contaminants in lubricants, oil viscosity, or lubrication regimes. Hase et al. investigated the relationship of wear and AE signals in time domain. The number of wear elements was directly related to the amplitude of AE [229]. Similar results were found by Strömbergsson et al. by using lubricant during a superfinishing process. The AE signal was stable when the surface roughness was not improved further [230]. By AE and vibration signals, it was possible to monitor the contamination of journal bearings with silica sand in different sizes and concentrations [231]. Root mean square and energy of AE signals increased by increasing particle size and concentration. Here, energy achieved better detectability than root mean square of AE. Miettinen et al. used AE for distinction of contaminated grease in rolling bearings. They found a correlation of grease composition and numbers of signal bursts in time domain of AE signals. It was possible to differentiate between concentration and hardness of the solid contaminants in the grease [232].

The correlation of AE and two types of lubrication oils in an engine test rig was analyzed by Wei et al.: the lower the oil's viscosity, the lower the AE amplitude [233]. Wei et al. obtained similar results for different fuels [234]. In journal bearings, a lower lubricant's viscosity resulted in significant higher AE amplitudes in a frequency range below 100 kHz [235]. Signals of AE in mechanical seals were not only generated by asperity contacts of tribological partners but also by viscous friction in the lubricant. Thus, AE time domain data can be used to identify lubrication regimes [236].

Monitoring of lubrication regimes was studied in pin-on-disc tests for a Nickel-steel and an Argentum-steel tribopair by Moshkovich et al.. The AE waveforms in time domain of elastohydrodynamic lubrication and boundary lubrication differed as well as the waveforms of the two different materials. It has been recognized that AE energy in boundary lubrication was higher than in elastohydrodynamic lubrication. This effect was more significant for the Argentum-steel tribopair [237]. Hamel et al. studied tribofilm thickness by evaluating AE signals in a gearbox. The reduction of oil film thickness correlated with an increase of AE root mean square level [133].

3.2 Test rig

Content of this section is based on publications [9, 98].

The experimental setup is shown in Figure 3.1. The test rig for TTT includes tribometer, test platform, tapping tool for thread forming, different test fluids, and a cleaning station. The nut blanks in the test platform are filled with test fluids. Then, threads are tapped into the nut blanks by measuring tapping torque. By brushes and an air blow system, chips and fluid residues are removed from the tap after every thread.

For the experiments, a tapping tribometer (Tauro®120, Taurox e. K., Germany) with a spindle that is fixed at a weight compensated suspension is used; no rigid tapping is used. The tribometer does not have an automatic feed as it is usual for cutting machines. Before starting the test procedure, the zero point of the z-axis is set at the entry of a nut blank. For the first two revolutions, the tool is pressed into the nut blank with a defined pressure using an air pressure system. This short feed distance is enough that the forming lobes of the tap's entry taper have caught enough material to pull the rest of the tap into the nut blank simply by rotating it. As a result, the axial force only works on the entry taper of the tap.

The used titanium carbon nitride coated tap depicted in Figure 3.1c and d has a five-polygon form, an entry taper with three pitches, and a thread length of about 8 mm.

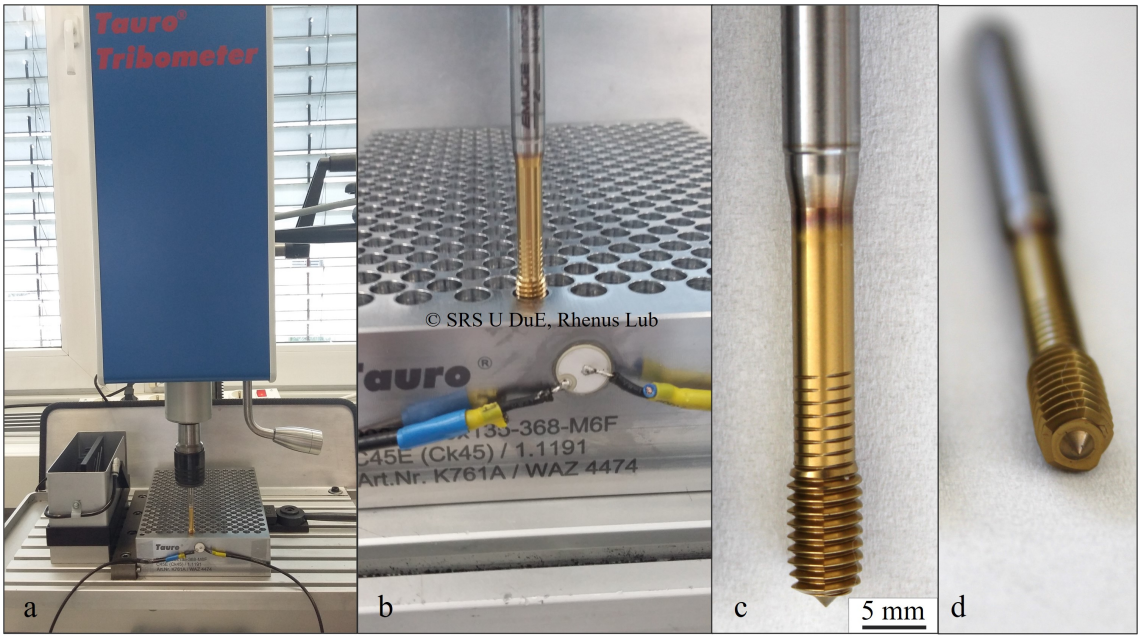

Figure 3.1: Experimental setup [11]
a: Tapping machine, tap, pre-drilled test platform with piezoelectric transducer and cleaning station (Rhenus Lub)
b: Exemplary starting tapping process
c: Titanium carbon nitride coated tap 6 mm diameter
d: Tap: 5-polygon form, without flutes

Torque is directly measured by the tribometer through the power consumption of the spindle. For extended TTTs, a technique based on field programmable gate arrays for measuring AE during threading is added to the setup. To this end, a disc-shaped broadband piezoelectric transducer of dimensions Ø10 mm and 0.55 mm in thickness with corresponding resonant frequency of 3.6 MHz is mounted on

the workpiece using cyanoacrylic glue (Figure 3.1b). The AE waveforms are acquired continuously at a sampling rate of 4 MHz. Test material and parameters are listed in Table 4.1. These parameters are kept during all tests. The AE signal is manually recorded during the forward and the reverse process. The measurement is started before the tap reaches the pilot hole and is stopped after the tap was fully retracted out of the thread. Each measurement lasts about 5 s. During all measurements, torque and AE signals are recorded. Temperatures in the contact zone are not measured.

Table 3.1: Test material and parameters for extended TTT [11]

Workpiece material	C45E
Process	Thread forming
Hole diameter [mm]	5.6 H7
Hole depth [mm]	31.3
Forming speed [m/min]	20
Fluid volume per thread [ml]	≈ 0.8
Tapping depth [mm]	27.3
Torque sample rate [Hz]	500
Diameter of piezoel. transducer [mm]	10
Thickness of piezoel. transducer [mm]	0.55
Resonant frequency of transducer [Hz]	3600
AE sample rate [Hz]	4000

The used workpiece material is made of C45E (1.1191). It is assumed that the micro-structure of this material is homogenous and complies with those of standard applications. The pre-drilled and pre-reamed holes in the test platform are only suitable for M6 forming taps. Diameter, roundness, and cylindricity mainly affect tapping torque. The producer of the test platform guarantees a dimensional accuracy for 99 % of the holes. Additionally, diameters are previously checked using a go/no go-gauge of 5.6H7. The platform has 368 holes in 23 columns of 16 holes. The threads are machined column by column from back to front due to the automatic program of the tribometer. Before tapping the next hole, abrasion particles and other solid residues on the tap are removed by air blow and brushes in the cleaning station.

This experimental setup is used for qualification of MWFs of two different datasets. A dataset consists of numerous measurement series. Measurements within one series are performed applying the same test fluid. Number of series, measurements, and fluids in the two datasets are different. Additionally, types of fluids and components in fluids differ. In the following sections, the datasets, namely dataset 2016 and dataset 2019 due to the year of test conduction, are introduced.

3.3 Dataset 2016

This dataset has been published in [9] for the first time. The aim was to investigate the feasibility to use AE signals for distinction of i) emulsion and oil, ii) phosphorus content in emulsions, and iii) phosphorus content in oils. Besides a reference fluid, two test emulsions and two oils with different phosphorus contents are used in dataset 2016. Compositions of the test fluids are listed in Table 3.2. The composition of MWFs differs in the concentration of phosphorus which is considered as anti-wear additive. For emulsion 1, the phosphorus content is 66 times that of emulsion 2. For oil 2, the phosphorus content is 20 times that of oil 1.

Table 3.2: Fluids applied in dataset 2016 [12]

MWF	**Basis**	**Water**	**Oil**	**Ester**	**Phosphorus**
Reference	Water	95 %	0 %	1.25 %	50 ppm
Emulsion 1	Water	95 %	1.4 %	0 %	3163 ppm
Emulsion 2	Water	95 %	1.4 %	0 %	48 ppm
Oil 1	Oil	0 %	85 %	6.5 %	80 ppm
Oil 2	Oil	0 %	85 %	6.5 %	1600 ppm

The particular sequence of trial series is stated in Table 3.3. First, 32 trials are performed using the reference emulsion to run in the new tap. Then, emulsions are tested before the oils. Each series consists of eight measurements corresponding to half of a column on the test platform. After a repeated reference measurement, oils are tested before the emulsions. The influence of a previously measured fluid on the test result is investigated.

Table 3.3: Sequence of thread forming trials of dataset 2016 [9]

Series	**Synonym**	**MWF**	**Thread no.**
1	ReF	Reference	1-32
2	E1	Emulsion 1	33-40
3	E2	Emulsion 2	41-48
4	O1	Oil 1	49-56
5	O2	Oil 2	57-64
6	ReF	Reference	65-72
7	O2	Oil 2	73-80
8	O1	Oil 1	81-88
9	E1	Emulsion 2	89-96
10	E2	Emulsion 1	97-104
11	ReF	Reference	105-112

The aim of this dataset is to find out whether it is possible to differentiate between oils and emulsions and between different phosphorus contents in both. Three different classification approaches described in Chapter 4 are applied on the recorded tapping torque or AE signals. Related results are presented in Section 5.1.

3.4 Dataset 2019

Dataset 2019 was developed after the evaluation of the results of dataset 2016. First, dataset 2016 was mainly used as a feasibility study. The differences between the fluids were comparatively large. In dataset 2019, the differences between the fluids is much more nuanced. The focus is more on the chemical structure of the additives and on smaller differences between the active substances. The aim of this dataset is to show the usability of the approaches developed for dataset 2016. Additionally, the knowledge obtained during experiments for publication [98] is applied in dataset 2019. The number of measurements per series is increased from 8 to 16 threads considering carryover effects of previously measured fluids. The test sequence is also changed. A complete series with the reference fluid is measured after every test fluid series.

In dataset 2019, a reference fluid and ten test fluids are measured in extended TTTs. The reference fluid used in 2019 is different from that used in 2016. Each series contains 16 threads corresponding to one column on the platform. Reference fluid and test fluids are all emulsions and the compositions are very similar. A water miscible base concentrate is developed to build the core structure of the other MWF concentrates. This base concentrate is not a 100 % receipt. The missing percentages to 100 % are filled up with certain additives. That means test fluids in dataset 2019 have the same basis and only one additive is varied. Before testing, an 8 % emulsion is prepared: 8 g MWF concentrate is added to 92 g demineralized water and the mixture is homogenized using a magnetic stirrer. The additives are described in Table 3.4. The concentration of the active substance is given for the water-mixed emulsion of the specific test fluid. Using a base concentrate for all fluids, comparability is given between all test fluids.

The aim is to distinguish fluids in extended TTTs with chemically similar lubricant additives and only slightly varying contents of active substance. In Group S with sulfur as active lubricating substance are F02 and F03, in Group P with phosphours as active lubricating substance are F04, F05, and F06, in Group E with ester as active lubricating substance are F07 and F08, and in Group G with glycol as varying substance are F09 and F10. The used sodium sulfonate in F01 is applied as emulsifier and could only help indirectly by the adhesion of lubricating additives as stated in [116]. The effect of sodium sulfonate will not be discussed in this work.

The dataset consists of 21 series listed in Table 3.5. The first and the last series are performed with the reference fluid. In between the measurements with the test

fluids, the reference fluid is repeated. With this test sequence, the test differences due to carryover effects of different previously measured fluids are minimized because every test fluid has the same predecessor fluid.

Table 3.4: Water-mixed test fluids and their contents of special additives [11]

Fluid	**Description of additive**	**Active substance [ppm]**	**Group**
Ref	Based on naphthenic mineral oil	-	-
F01	Sodium sulfonate	4800	-
F02	Polysulfide	1600	S
F03	Polysulfide	2400	S
F04	Lauryl ethylene oxide phosphate	160	P
F05	Oleyl ethylene oxide phosphate	160	P
F06	Stearyl ethylene/propylene oxide phosphate	86	P
F07	2-ethylhexylcocoate	8000	E
F08	Synthetic polymeric ester	8000	E
F09	Diethylene glycol	8000	G
F10	Polypropylene glycol	8000	G

Table 3.5: Sequence for thread forming trials of dataset 2019 [11]

Series	m01	m02	m03	m04	m05	m06	m07	m08	m09	m10	
Fluid	Ref	F01	Ref	F02	Ref	F03	Ref	F04	Ref	F05	
Series	m11	m12	m13	m14	m14	m16	m17	m18	m19	m20	m21
Fluid	Ref	F06	Ref	F07	Ref	F08	Ref	F09	Ref	F10	Ref

The aim of this dataset is to find out whether it is possible to differentiate between chemical structures of lubricating additives by evaluating signals during thread forming. Different classification approaches described in Chapter 4 are applied on the recorded tapping torque or AE signals. Results are shown in Section 5.2.

3.5 Lubricant additives of dataset 2019

Additives used in dataset 2019 have similar chemical structures. These are shown and lubricating effects are discussed using knowledge from Section 2.1.5.

Fluids F02 and F03 contain similar sulfur additives with different sulfur concentrations. The chemical structures of the used additives are depicted in Figure 3.2. The polysulfide molecule of F02 contains three sulfur atoms whereas the polysulfide

molecule of F03 has five sulfur atoms. The negative dipole of both molecules is located at the sulfur atoms. The molecule of F03 has a stronger dipole and therefore a higher adhesion effect. A higher lubricating effect is assumed for F03 with an higher sulfur content.

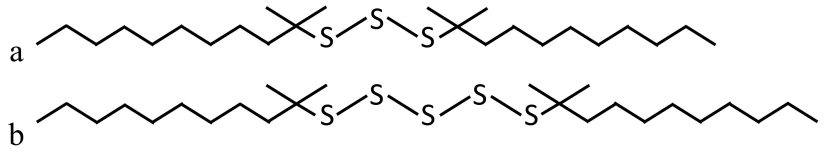

Figure 3.2: a: Polysulfide in F02 with 20 % sulfur
b: Polysulfide in F03 with 32 % sulfur

In fluids F04, F05, and F06, different phosphorus additives are used. The chemical structures of the used additives are depicted in Figure 3.3. The phosphorus content of additives in F04 and F05 is the same but the used phosphate molecules have different side chains. The phosphate in F04 has a lauryl group whereas the phosphate in F05 has oleyl group and the phosphate in F06 a stearyl group. These groups are depicted in Figure 3.3a-c. The negative dipole of all phosphate molecules is located at the oxygen atom with double bond to the phosphorus atom. The strength of dipole of all additives is the same; the difference is only the R-group. The evaluation which additive is expected to have the highest lubrication effect is not trivial. On the one hand the long stearyl chain could build a good tribofilm and separate friction partners. On the other hand the big chain length could be disadvantageous because it prevents further molecules from adhesion. A similar argumentation is possible for the oleyl chain. The chain is not only long but also twisted and could prevent other molecules from adhering.

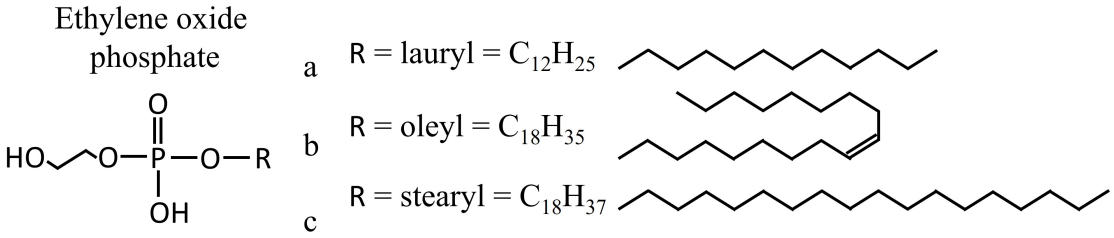

Figure 3.3: a: Lauryl ethylene oxide phosphate in F04
b: Oleyl ethylene oxide phosphate in F05
c: Stearyl ethylene oxide phosphate in F06

Two different ester oils are applied in F07 and F08. The chemical structures of the used additives are shown in Figure 3.4. The ester content in F07 and F08 is the same but molecules' structures differ. Coconut oil is the basis of 2-ethylhexylcocate in F07.

Natural esters are usually less temperature-stable than synthetically produced esters and need additional anti-oxidants. The molecular structure of the synthetic ester is polymeric and therefore more complex. It is expected that the polymeric ester with its numerous polar groups outlined as spheres in Figure 3.4b has a higher lubricating effect than the ester with only one polar group at one end. The adhesion effect of the polymeric ester will most likely be higher.

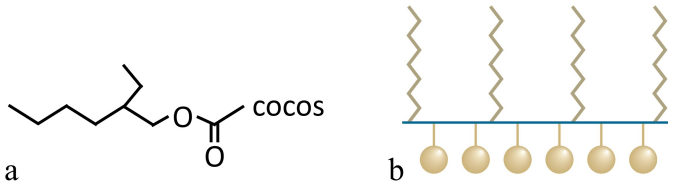

Figure 3.4: a: Naturally based ester in F07
b: Synthetic polymeric ester in F08 [238]

Fluids F09 and F10 differ in the type of glycol additive. In emulsions, glycols are typically used as solubilizer. In fully synthetic and water-soluble MWFs, glycols can act as lubricating additives. This effect is investigated for F09 and F10. Glycols used are diethylene glycol and polypropylene glycol. Diethylene glycol is a linear molecule with hydroxy groups at both ends (Figure 3.5a). Polypropylene glycol has a hydrogen atom on one end and a hydroxyl (OH) group on the other (Figure 3.5b) [239]. A negative dipole is located at each oxygen atom. Due to the poly-chains, polypropylene glycol has a longer chain in comparison to diethylene glycol. It is assumed that polypropylene glycol shows an advantageous lubricating effect in comparison to diethylene glycol.

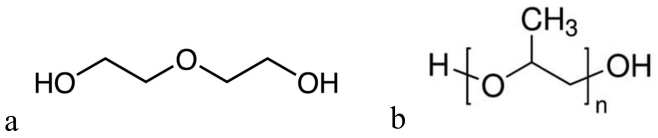

Figure 3.5: a: Diethylene glycol used in F09
b: Polypropylene glycol used in F10

4 Evaluation approaches

Content of this chapter is related to the publications [9, 98, 11, 10, 12].

The following approaches are used to distinguish between test fluids in extended TTTs:

1. Torque means are calculated following [98] and differences are statistically analyzed using two-sided t-tests abbreviated as *norm-TT-means*.
2. AE signals are analyzed in time-frequency domain after CWT and k-means clustering following [9] abbreviated as *clust-CWT-AE-energy*.
3. AE signals are analyzed in time domain. Feature extraction and fluid classification are realized using CNN [10] abbreviated as *raw-AE-CNN*.
4. Transfer Learning is applied from dataset 2019 to dataset 2016 using AE signals in time-frequency domain after STFT [12] abbreviated as *STFT-AE-TL*.

In Figure 4.1, the approaches no. 1 to 3 are applied on relevant data for one exemplary thread. In Figure 4.1a, raw data of tapping torque values are shown. At the beginning of the thread (blue arrow), measurement values nearly start at 0 Nm. Then, torque increases until all forming lobes of the tap are cut in (orange arrow). In the following plateau-region, torque values nearly remain constant until the end of thread (grey arrow). Reaching the demanded end of thread, tap rotation is stopped and turned so that the tap gets out of thread. This so-called reverse process is not recorded by the tribometer. For the first approach due to [98], tapping torque mean values are calculated from the plateau-region.

In Figure 4.1b, raw data of AE signals in time domain are shown. The arrows in this figure point at corresponding events in time as in the previous figure. The measurements are stopped manually and AE recording is started before the tap reaches the test platform. Forward and reverse process are recorded. In the forward process where elastic and plastic deformation takes places, the amplitudes are higher than in the reverse process. In the reverse process, mainly friction between tap and workpiece material generates low amplitudes. These values are used in the third approach developed and tested in [10].

In Figure 4.1c, AE data after CWT are shown. Lower amplitudes are mapped in dark blue and higher amplitudes are mapped in yellow. The positions of the three colored arrows correspond to the arrows in the figures above. The arrival of the tap at the pilot hole surface (blue arrow) is indicated by an higher amplitude in half of the measured frequency range. The same applies to the back turn of the tap at the beginning of the reverse process (after grey arrow). The sum of AE energy in significant frequency ranges is used in the second approach.

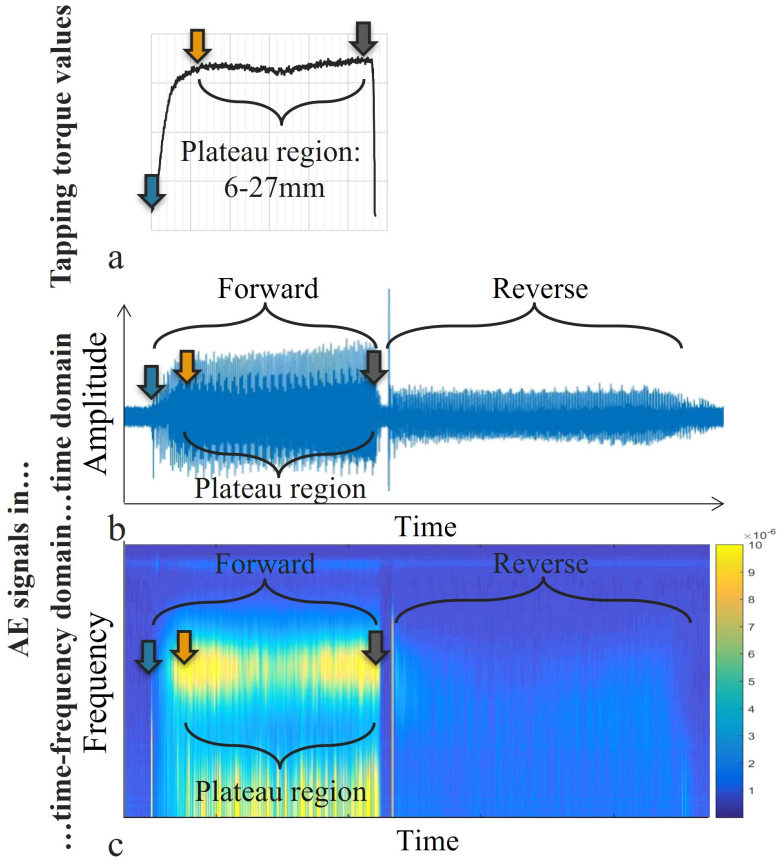

Figure 4.1: Connection between tapping torque and AE [11]
a: Raw data of tapping torque with marked plateau region
b: Raw data of AE measurement in time domain
c: AE signals after CWT in time-frequency domain

4.1 Tapping Torque Test according to ASTM D5619

Content of this section is from contribution [98] published in 2019. At the time of publication, the recent standard for performing TTTs was the withdrawn ASTM D5619-00 of 2000. In the meantime, the standard ASTM D5619-00 for comparison of MWFs has been replaced by ASTM D8288-19 in 2019. The summary at the end of this section briefly describes the changes between the version discussed here and the new version.

Key points of the standard are described in the first subsection so that the reader is able to understand the consequences of existing definitions and the lack of necessary definitions.To highlight the necessity for improvements of the withdrawn standard, the problems are summarized in a critical evaluation in the second subsection. In the

following subsections, experiments' description, results, and conclusions concerning the performed basic research in [98] are given in detail.

4.1.1 Key points of ASTM

The TTT is described as more accurate than previously available laboratory scale tests to predict the performance of MWFs [240]. The aim is to find the best suitable fluid for a specific application i.e. a specific material pair combination. Threads are cut by taps into pre-drilled and pre-reamed holes while lubricating the contact zone between tap and hole wall by a MWF. The required torque to cut a thread is recorded and serves as the main feature to evaluate the test fluid in comparison to a reference fluid. As defined in ASTM D5619, only measurement values from the plateau region (Figure 4.2) of each thread have to be taken into account for mean calculation. The lower the tapping torque mean, the higher the test fluid's lubricity for the tested material pair combination.

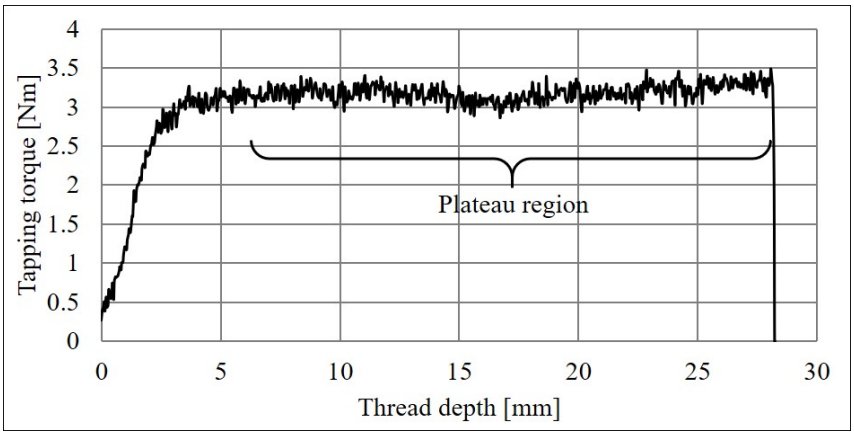

Figure 4.2: Plateau region from 6 to 27 mm of an exemplary torque measurement in AlMgSi1 [98]

The final resulting characteristic value of a test fluid is the tapping torque efficiency TT_{eff} describing the quotient of reference fluid and test fluid as [240]

$$TT_{eff}[\%] = 100 \times M_{ref}/M_{test} \tag{4.1}$$

with M_{ref} denoting the mean of the reference condition and M_{test} the mean of the test condition.

Different taps and different workpiece materials can be used for TTTs. Each material pair combination can result in another best suitable MWF. Test results strongly depend on the chosen experimental design. To achieve results with best significance and best transferability into practice, it is recommended to use the same material

pair combination in the TTT as it is used in the real application [116]. To exploit this main advantage of high flexibility of TTTs, workpiece and cutting materials are not bindingly defined in ASTM D5619 as well as machining speeds and fluid types.

The ASTM D5619 prescribes a running-in and a qualification process for the taps to be used for TTTs. New taps have to finish their running-in phase first, then to be checked as qualified before using them for TTTs [240]. The necessity to run-in new taps is established to achieve characteristic built-up edges on the tap. The term *built-up edge* is given by ASTM to describe a characteristic wear state of the used tap. These specific built-up edges are built on the cutting edges of the tap and belong to the chosen test condition of tap and workpiece material, fluid, and machining speed. How these built-up edges should be examined (microscopic wear images, torque, or...) to obtain equal initial conditions is not described in ASTM D5619.

The test conditions of running-in are not defined. It has to be assumed that they match with those of the tap qualification process directly following the running-in. Thus, the running-in of the tap would simultaneous be the qualification process. The tap qualification is recommended to be performed in a 1215 steel alloy - regardless in which material the test run later will be performed. The built-up edge on the tap will be characteristic for cutting 1215 steel alloy using the reference fluid. The fluid to be chosen as reference fluid should not contain surface activating additives and should produce minimal built-up edges [240].

In the tap qualification process, five threads are performed. The standard deviation is calculated according to the usual formula as

$$stdd_{\overline{x}} = \sqrt{\frac{\sum (x - \overline{x})^2}{n - 1}} \tag{4.2}$$

with x denoting a single measurement value, $\overline{x}$ the sample mean, and n the sample size.

The allowed standard deviation of the mean of each tap is ± 2 %. The allowed difference between the mean of the reference tap and the mean of another tap is ± 2 %. Concluding, the mean of the other tap has to lie in between the lower and upper 2 % bounds of the reference tap. Taps not fitting into this requirement have to be discarded leading to high test effort and high tool costs.

After running-in and tap qualification, the test sequence can begin. At this point, it is unclear if the reference fluid should be used in the same workpiece material before using the test fluid or if the reference fluid is only tested in 1215 steel. Additionally, it is not defined if regular reference measurements shall be performed between test runs to monitor proceeding tool wear.

The test fluid is measured for five threads. To calculate the test fluid's mean, only values of the last three threads are taken into account [240]. Possible carryover effects of the previously used fluid are so taken into account by two threads. Reducing the amount of values contributing to the mean implies a higher standard deviation and worse statistical differentiability between test fluids.

4.1.2 Critical evaluation

This contribution focuses on a critical evaluation of the conduction and evaluation of TTTs exclusively according to [240]. The ASTM D5619 provides many opportunities to choose different workpiece materials, reference fluids, or manufacturers for tapping tools. Recommendations for suitable reference fluids and the number of replicates are given. A tap qualification process (2 % deviation) and an initial criterion (built-up edge) are defined. Evaluation criteria for the built-up edge are not detailed. Based on experimental experience, questions concerning the test conduction and some problems with definitions of ASTM D5619 appear. These are not clearly defined and should be more detailed to obtain unambiguous and repeatable test results. The following points need to be improved:

1. The completion of a running-in phase is required before starting tests with new taps. The running-in phase is finished when a characteristic built-up edge has been built belonging to the specific type of tool and the specific fluid used for running-in. Technical utilities to be used to evaluate built-up edges (optical microscope for wear inspection, TTT rig for torque monitoring) are not described. A systematic procedure to clearly identify the end of running-in of a new tap is not explained.
2. For tap qualification, the use of a SAE 1215 carbon steel alloy is recommended. Although the test method allows tests on other workpiece materials, the taps should all be qualified on the same workpiece material. It should be noted that not every tool has been developed for machining of SAE 1215 steel and is possibly not suitable for this material. The workpiece material could cause premature tool damage or the tool would even get stuck in the thread. As consequence, misleading conclusions may occur when using workpiece materials not recommended by tool manufacturers.
3. For qualified taps, a 2 % deviation of the means is allowed. This feature has to be checked only during the tap qualification procedure by using the reference fluid. Over the whole life of the tap, wear proceeds and the tap possibly does not fulfill the qualification definition further. Regular reference measurements to monitor the tool's condition are not recommended. A criteria for the end of tool life is not defined.

4. Taps not fulfilling the recommended 2 % deviation are not qualified for TTTs and have to be sorted out into appropriate qualified groups. Taps within one group are comparable with each other. Taps between groups are not comparable with each other. This recommendation increases experimental costs because many taps are needed.
5. A strong effect of the workpiece material's quality on the measurement results is described. A procedure to qualify test platforms is not proposed. The material composition of test platforms may significantly affect repeatability and comparability of measurement results. This makes the development of a data base containing directly comparable TTT results impossible. A reference value valid for a specific material pair combination is missing that could be used to normalize mean torques and to ensure comparability of test data.
6. Neither a special tool type or tool coating nor a geometry of flutes/grooves and edges are recommended. Uncoated tools have higher resolving power than coated tools so fluids can more often be distinguished using uncoated tools than using coated tools [112]. High performance coatings can mask the fluid's performance so that uncoated tools seems more suitable than coated tools. The aim of TTTs is to replicate field conditions as good as possible. Coated tools are used in field applications. Using only uncoated tools reduces the transferability into practice.
7. The number of threads per fluid is set to five. For the test run, the mean torques of the first two threads are not included in the calculation of the overall fluid's mean. The fluid's mean and its standard deviation are based on three measurements. This small number of measurements leads to high standard deviations, wide confidence intervals, and finally to non-suitable differentiability of test fluids.
8. Carryover effects of previously measured fluids can affect the following test run. By taking these effects into account, the first two of five single measurements are discarded and the mean torque is calculated for the last three measurements. Depending on reactions of the previously measured fluid with the tool's surface, two threads could be insufficient to eliminate carryover effects, especially when thread depth is not defined.

As illustrated, several problems with the current test procedure occur based on reasonable considerations as well as on practical experiences. The existing regulations lead to high tooling costs, not clearly defined initial test conditions, bad comparability between test fluids over the whole tap life, possible not significant differentiability between test fluids, and less transferability into practice. These points could be avoided or significantly improved.

In this paper, first experimental results of TTTs are presented and statistically validated. The aim is not to find a best suitable fluid for a specific application but to improve the standard's test procedure and the evaluation of test results. Second,

suggestions are developed to overcome problems due to quality differences of taps, proceeding wear, fluid carryover effects, and statistical significance of test results. Third, comparisons based on statistical tests are made between the recent regulation and two new approaches to show the effectiveness of the suggested changes.

4.1.3 Experiments for research on test procedure

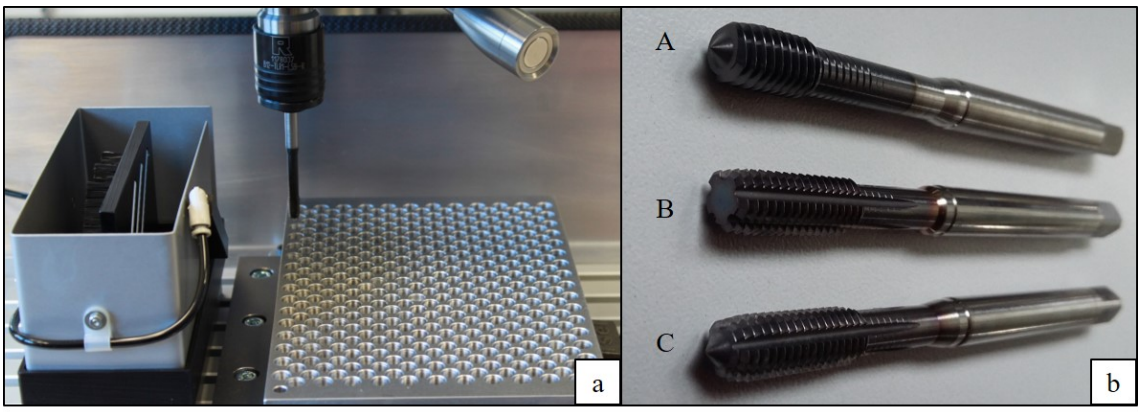

Figure 4.3: Test rig and tools [98]
a: Tapping machine, tapping tool, pre-drilled test platform and cleaning station used for TTTs (Rhenus Lub)
b: Different tapping tools for thread forming used in the tests

Table 4.1: Used test materials and parameters for TTT conduction and evaluation acc. to [98]

Parameter	**AlMgSi1**	**C45E**	**AlSi7Mg**
Hole diameter [mm]	5.6 H7	5.6 H7	5.6 H7
Hole depth [mm]	31.3	31.3	26.5
Forming speed [m/min]	25	20	20
Water hardness [°dH]	0	0	0
Fluid volume per thread [ml]	≈ 0.8	≈ 0.8	≈ 0.6
Tapping depth [mm]	27.3	27.3	24.3
Evaluated thread length [mm]	6-27	6-27	4-24
Sample rate [Hz]	500	500	500

The experimental test rig partly shown in Figure 4.3a consists of a tribometer (Tauro®120, Taurox e. K., Germany), test platform, tapping tool for thread forming, different test fluids, and a cleaning station with brushes and air blow system to remove chips and fluid residues. In the present tests, no rigid tapping is used. The spindle is fixed at a weight compensated suspension. During threading, the spindle

Table 4.2: Characteristics of used forming taps [98]

Tap	**Specification acc. to DIN 371, form C and DIN 2174**
A	Without grooves, entry taper 3 pitches, 10 mm thread length, 4-polygon form, HSS-E, multi layer coated, M6
B	Five grooves, entry taper 3 pitches, 17 mm thread length, 5-polygon form, HSS-E-PM, TiCN coated, M6
C	Five grooves, entry taper 3 pitches, 17 mm thread length, 5-polygon form, HSS-E, TiCN coated, M6

is turned into the nut blank through the thread flanks of the tap. The axial force only works at the entry taper until the first thread flanks have caught material.

In Table 4.1, materials and test parameters are listed. The displayed forming speeds are recommended by the tool manufacturer for his tap and the concerned workpiece material.

Although fluids could be easier distinguished using uncoated tools in TTTs [112], coated tools are chosen for the experiments (Table 4.2, Figure 4.3b). In practice, coated tools are often preferred because higher speeds and longer tool life can be achieved. Uncoated tools lead to early tool failure in comparison to coated tools [111]. Another disadvantage of uncoated tools is that they may entail higher material adhesion and wear. The use of uncoated tools can lead to a shortened steady-state wear phase in comparison to coated tools. Less test measurements could be performed with one tool leading to a higher number of tools to be acquired and qualified. In this contribution, tapping of AlMgSi1, C45E, and AlSi7Mg is investigated. It is assumed that the micro-structure of these materials complies with those of standard applications and is homogenous. Similar alloys have been tapped in other researches [83, 111, 241, 5, 242].

The contents of the used workpiece materials are listed in Table 4.3. Each test platform has pre-drilled and pre-reamed holes with 5.6 H7 mm diameter suitable for M6 forming taps. Platforms made of AlMgSi1 and C45E have 368 holes in 23 columns of 16 holes (Figure 4.4) and platforms made of AlSi7Mg have 112 holes in 8 columns of 14 holes. The machining table of the tribometer is programmed in such a way that the threads are machined column by column from back to front.

The pre-hole diameter has a significant impact on tapping torque and thread geometry [111, 243]. It is assumed that the given H7 tolerance ensures a comparability between the holes and hence between the test results. Before testing, the holes are proven by a GO/NO GO pin gauge. The maximum thread depth of the forming process is limited either by the depth of the pre-hole (AlSi7Mg) or by the length of the tapping tool up to its wider shaft (AlMgSi1, C45E). Before testing, platforms

Table 4.3: Alloying elements of the used workpiece materials in % [98]

Alloy/Element	**C**	**Si**	**Mn**	**P**	**S**	**Cr**	**Ni**	**Cu**
C45E	0.444	0.232	0.683	0.014	0.005	0.016	0.005	0.008
	Al	**Nb**	**Mo**	**V**	**Ti**			
C45E	0.03	0.002	0.001	0.001	0.001			
	Si	**Fe**	**Cu**	**Mn**	**Mg**	**Cr**	**Zn**	**Ti**
AlMgSi1	1.2	0.16	0.07	0.63	0.7	0.01	0.01	0.01
AlSi7Mg	7.0	0.45	0.15	0.35	0.5	-	0.15	0.2
	Sn	**Ni**	**Pb**					
AlSi7Mg	0.05	0.15	0.15					

are cleaned in an ultrasonic bath for 15 min. using a cleaning solvent (1:1 mixture of naphta and isopropyl alcohol) and dried in a drying oven at 50 °C for 15 min.. New taps are cleaned by repeated washing and wiping steps using the same solvent mixture before using them for the first thread.

Due to the automatic program of the tribometer, the tap is automatically cleaned in the cleaning station after every thread before the tapping process proceeds with the next hole. To determine the mean of a single thread, the plateau region (Figure 4.2) of the torque curve is chosen [240, 112, 42]. The values of the single measurement curves are not filtered or smoothed as can be seen in Figure 4.2. Mean and standard deviation of a single thread (Equation 4.2) are calculated by the software of the tribometer according to the chosen definition range. Details about the used materials and fluids used are given in the diagrams and figure captions.

4.1.4 Results about running-in

According to ASTM D5619, a cutting tap is finally broken-in when a characteristic built-up edge has been formed by cutting threads using a reference fluid. The appropriate term to *built-up edge* is *adhered layer* on the forming lobes. This term does not specify if hard material or a chemical layer has occurred.The term *a broken-in tap* means that the tap has finished its running-in phase. After the tap is broken-in, a nearly stationary phase follows in which wear and resulting mean torque are quasi constant.

The evaluation of built-up edges requires special equipment such as magnifiers or microscopes and high expertise by the operator. To continuously control the edges consumes time and increases measurement costs. To facilitate the determination

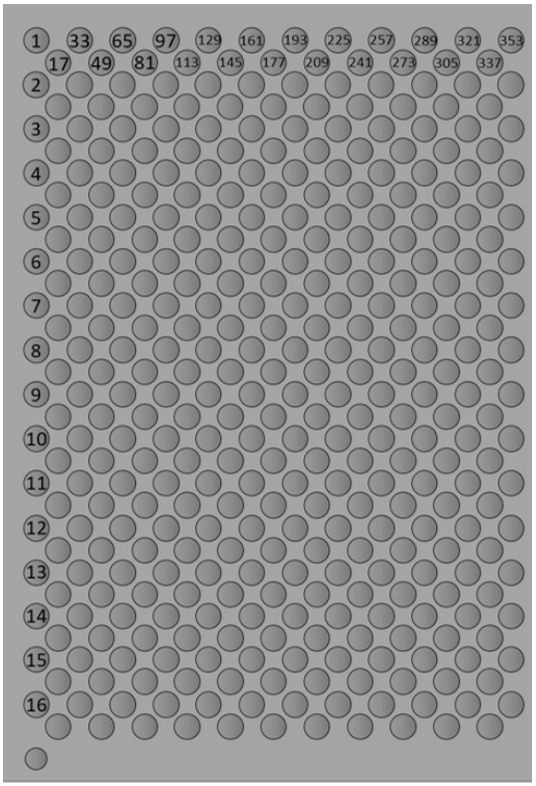

Figure 4.4: Order of pilot holes and tapping scheme of a typical Tauro®test platform

of a broken-in tap, it is proposed to use the same features as are already used for the final test procedure i.e. mean torques. Derived from the specific order of pre-holes on the test platform (Figure 4.4, k number of holes per column), the following criterion for a broken-in tap at thread number i is proposed

$$|M_{i+k\text{-}1} - M_i| < stdd_{M_i} \tag{4.3}$$

with M_i denoting the torque for thread number i, k the number of threads per series (k=16 for AlMgSi1 and C45E), and $stdd_{M_i}$ the standard deviation of the mean torque of thread number i. In the stationary phase, single outliers are tolerated.

The criterion is used to characterize the end of running-in phases of taps. The fulfillment of this criterion is exemplary shown for taps A-9 and B-4 in Figure 4.5a. For tap A-9, the criterion is fulfilled beginning from thread number 15. For tap B-4, Equation 4.3 is always fulfilled. The assumption arises that tap type B shows a shorter running-in phase because of higher production accuracy or additional downstream production steps.

In Figure 4.5b, Equation 4.3 is applied to the measurement values of every tap to find the end of their running-in phases. Thread numbers fulfilling Equation 4.3 for

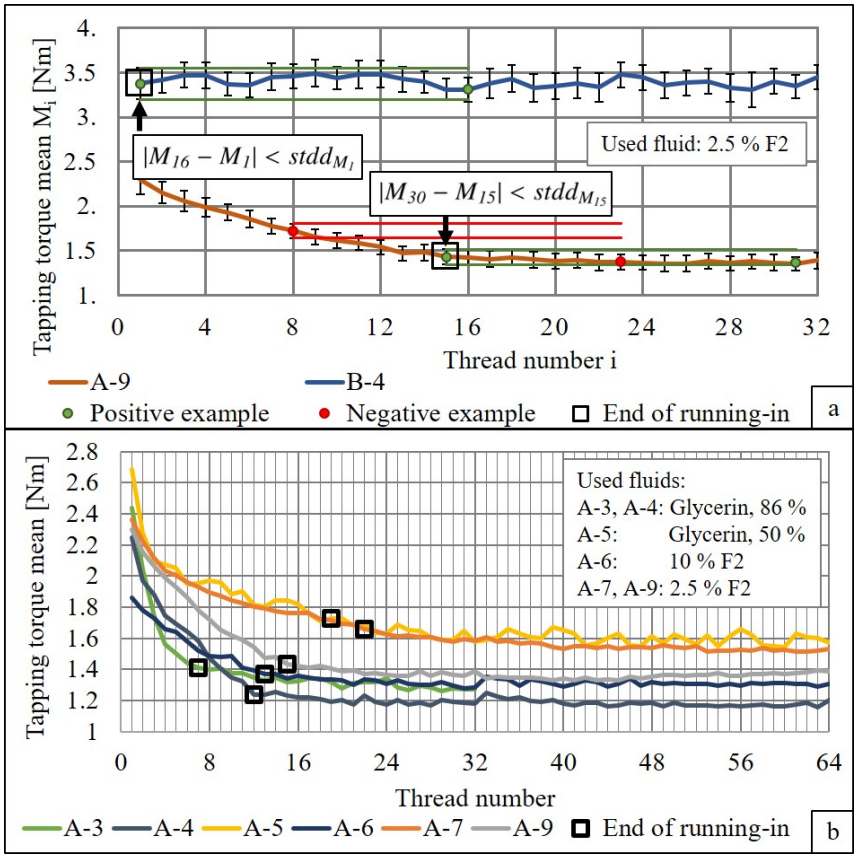

Figure 4.5: Running-in behavior of different taps [98]
a: Running-in behavior of two different tap types in AlMgSi1
b: Determination of broken-in taps by mean torques.

the first time are marked by black boxes. Different lengths of running-in phases are observed for taps of type A: The running-in ends between thread no. 7 and 22. A correlation between k-value and the length of running-in phase can not be recognized. A conclusion if the fluid affects the running-in behavior can not be drawn from Figure 4.5b. As a consequence, the need for a running-in and the length of the running-in depends on the tap and has to be investigated in each specific case before performing TTTs.

4.1.5 Results about tap type

Subsequently, the running-in behavior of two different tapping tools is exemplary investigated. In Figure 4.6a, the mean torques of the first 32 threads of tap types A and B in AlMgSi1 are shown. Taps A-1, A-2, and A-3 as well as taps A-7 and A-9 as well as taps B-2, B-3, and B-4 are used on the same test platforms and with the same fluids so a comparison between tools of the same group is possible.

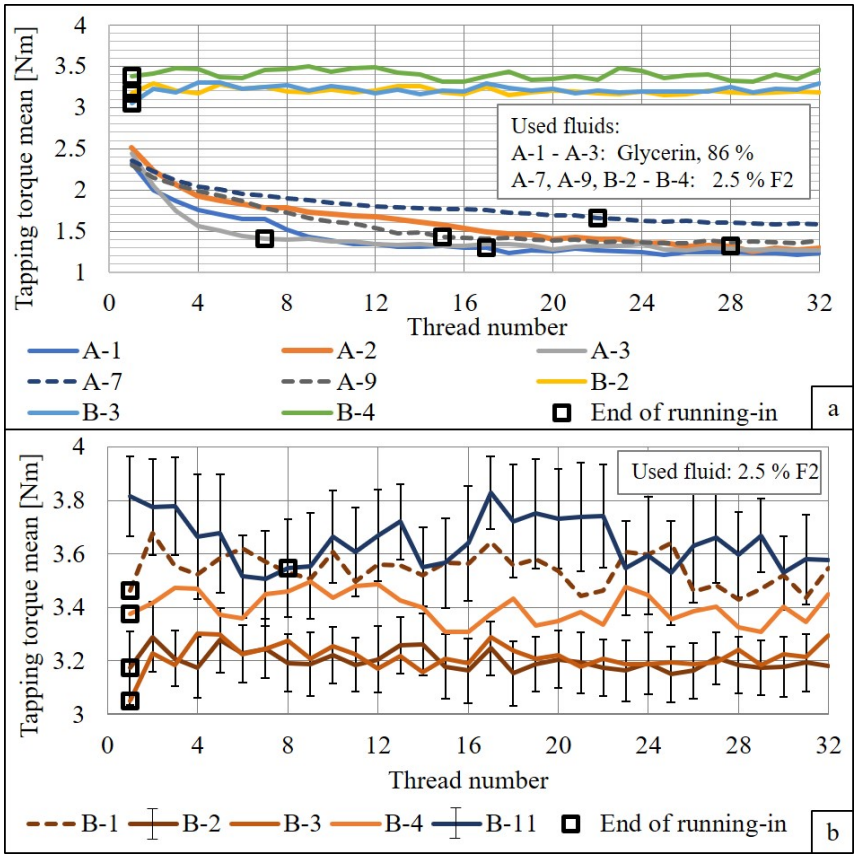

Figure 4.6: Comparison of running-in phases of different tap types [98]
a: Tap type A and B in AlMgSi1
b: Various taps of type B in AlMgSi1 (B-1 to B-4) and C45E (B-11)

The mean torques of tap type A start at around 2.4 Nm. Increasing the thread number leads to a decreasing tapping torque until a steady-state is reached. A running-in process can be detected. Taps of type B generally need a higher torque for the threading process than taps of type A. For tap type B, a running-in phase cannot be detected.

The strong impact of the tap type on the torque level can also be recognized by comparing measurements of A-7 with A-9 (dotted lines) and taps of type B with each other (Figure 4.6a). The slope of the mean torque can vary although the same tap type and the same fluid are used. The example depicted in Figure 4.6a can be used to explain tap qualification. The tap qualification process prescribes a maximum allowed deviation of 2 % between taps. The allowed 2 % tolerance range is applied to taps of type A and B and are listed in Table 4.4.

Taps A-1, A-2 and A-3 are in one group, A-7 and A-9, and B-2, B-3, and B-4. For each reference tap, lower and upper bound are noted. By comparing the means with the lower and upper bound of the reference tap, it is checked if the means are within

the range. Tap A-1 is within the range of A-2 and a qualified tap. Tap A-3 is out of the range of A-2 and is evaluated as disqualified. The mean of A-9 is out of the range of A-7. Taps B-3 and B-4 are out of range of B-2. Following the criterion for tap qualification defined by ASTM D5619, only one tap would be qualified and four of eight taps of three different groups have to be discarded. Therefore, the defined 2 % range has a strong impact on experimental costs. Quantifying torque tolerances for each tap type and conducting significance tests to statistically evaluate the differences between taps could be more economic than testing a very high number of taps. Changing the equation of tapping torque efficiency (Equation 4.5) would be efficient by implementing a normalization factor that is calculated from means obtained during tap qualification. An equation for this purpose is introduced in Section 4.1.7.

Table 4.4: Applying the 2 % tolerance range for tap qualification [98]

Tap	**Mean [Nm]**	**Lower 2 % bound [Nm]**	**Upper 2 % bound [Nm]**
A-1	1.296	qualified	
A-2	1.317	1.291	1.343
A-3	1.408	disqualified	
A-7	1.658	1.628	1.691
A-9	1.433	disqualified	
B-2	3.173	3.110	3.236
B-3	3.049	disqualified	
B-4	3.376	disqualified	

4.1.6 Results about workpiece materials

From Figure 4.6b, conclusions can be drawn regarding the effect of two different workpiece materials on the tapping torque level. The effect of workpiece material on the running-in behavior has been investigated for tap type B. Taps B-1 to B-4 are used in AlMgSi1 and tap B-11 in C45E. Taps B-1 to B-4 are broken-in from the first thread on whereas B-11 is broken-in after eight threads. The workpiece material may significantly affect the running-in phase of a tap.

Tap B-1 (dotted line) was used in another platform than taps B-2, B-3, and B-4. The torque level of B-1 is higher than those of B-2 to B-4 so an effect of platforms of the same workpiece material can be assumed. Summarizing, different platforms of the same material can influence the level of mean torque and the workpiece material can affect the running-in phase of the taps.

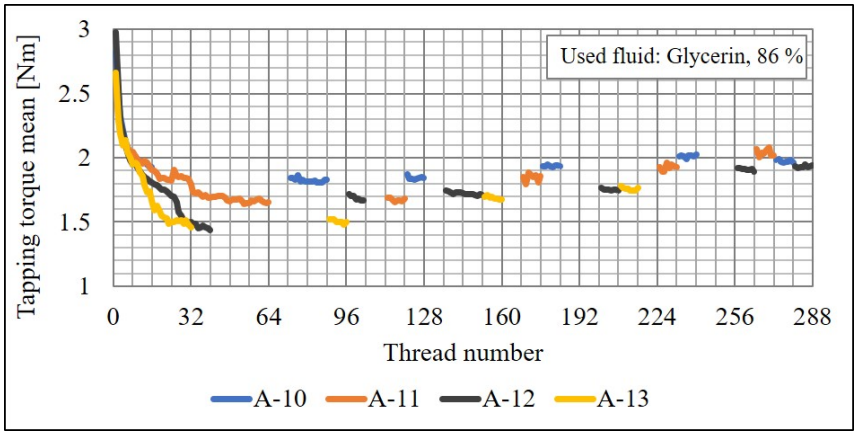

Figure 4.7: Regular reference measurements in AlMgSi1 for checking and monitoring the reference value [98]

4.1.7 Reference measurements

The test procedure of ASTM D5619 does neither consider nor recommend regular reference measurements. Regular reference measurements will be important if one tap is used for many test series with different MWFs and/or on different test platforms. The introduction of a theoretical reference value at test series no. i will be the basic of comparable measurement values when performing many test series with the same tap. To show the importance and necessity of regular reference measurements, experimental tests are performed (Figure 4.7). Taps A-10 to A-13 are used in AlMgSi1 platforms to investigate the development of reference measurements up to 288 threads. After tap's running-in, the reference values slightly increase. Exemplary, for tap A-11 the reference value starts at about 1.7 Nm (thread no. 64), increases steadily and exceeds 2.0 Nm at thread no. 264. Applying Equation 4.1 to a fictitious test mean of 1.9 Nm, the tapping torque efficiency could vary between 89 % (1.7 Nm as reference value) and 105 % (2.0 Nm as reference value). For correct efficiency calculations, the operator has to know the recent reference value corresponding to the recent test measurement. As a consequence, not checking the reference value in regular measurements could result in wrong test results and misinterpretations.

A verification of the reference value before and after each test measurement, would lead to immense experimental effort and costs. To get a sufficient approximation to a real reference value, the following procedure is proposed: performing reference measurements before and latest after every sixth test run. This means after the first/beginning reference series, up to six test series are performed. The seventh series is again a reference series. From each series, a mean is calculated representing the measurement value of each series. Between the beginning and end reference value, a linear slope is assumed so that a linear interpolation between these values

is used to established a corresponding theoretical reference value of each test measurement. This theoretical reference value is introduced to deal with tap wear over the whole life of the tap.

The theoretical mean reference is calculated as

$$M_{ref,i} = M_{ref,\alpha} + (M_{ref,\omega} - M_{ref,\alpha}) \times (z_i - z_\alpha)/(z_\omega - z_\alpha), \tag{4.4}$$

with $M_{ref,i}$ denoting the theoretical mean reference at test series no. i, $M_{ref,\alpha}$ the measured mean reference before the test series, $M_{ref,\omega}$ the measured mean reference after the test series, z_i the test series no. i to be compared with the reference, z_α the number of reference measurement before the test series, and z_ω the number of reference measurement after the test series.

As a result, the tapping torque efficiency is calculated as

$$TTT_{eff,i}[\%] = 100 \times M_{ref,i}/M_i. \tag{4.5}$$

Considering the equations for the theoretical reference value and the normalized tapping torque efficiency, it is possible to compare the measurement obtained at thread no. 40 with the measurement obtained at thread no. 200. For illustration, measurement values of A-11 are given in Table 4.5. Tapping torque efficiencies calculated according to Equation 4.1 (ASTM D5619) significantly vary in comparison to the results obtained by the new Equations 4.4 and 4.5. For Lub 3 in Table 4.5, tapping torque efficiencies range from 110 % to 118 %. These experimental results show that monitoring of the reference value and normalization of the measurements values are required.

In some cases, the comparison of mean torques is expedient, especially when comparing test results of different fluids statistically. For this issue, the introduction of an overall reference value valid for all tools and platforms of the same material combination becomes necessary. To use only normalized and thus comparable data, the equation

$$M_{i,norm} = M_{ref,fix} \times M_i/M_{ref,i} \tag{4.6}$$

for calculation of normalized mean torques $M_{i,norm}$ is proposed, with $M_{ref,fix}$ denoting a fixed and overall reference value valid for the combination of the same tool type, same platform alloy, and same reference fluid. The normalized mean torque $M_{i,norm}$ is similar to the value of average tapping torque corrected introduced in [103] because of differences between taps of the same type. Adjustment and normalization according to Equations 4.4, 4.5, and 4.6 makes comparisons between test results obtained with different tools and platforms of the same material combination possible. Discarding of taps or platforms becomes redundant.

Summarizing the conclusions from Figure 4.7 and from the derived equations, regular reference measurements are indispensable for comparable tapping torque results and can be used to eliminate the effect of changed tools and platforms by applying the developed equations.

Table 4.5: Measured data of A-11 normalized acc. to ASTM and Equation 4.5 [98]

Series i	**Fluid**	M_i	$M_{ref,i}$	$TTT_{eff,i}$	TTT_{eff} **acc. to ASTM**
5	Reference	1.673	1.673	100	100
6	Lub 1	1.825	1.825	94	92
7	Lub 2	1.722	1.722	102	97
8	Lub 3	1.523	1.802	118	110
9	Reference	1.845	1.845	100	-

4.1.8 Results about carryover effects

Carryover effects due to an impact of the previously used fluid on the tap's surface can cause variability in the first test results with the following fluid. This effect is considered in ASTM D5619 and leads to an elimination of the first two measurement values of the following fluid. Other researchers met the risk of carryover effects by using the reference fluid for one thread before each test run [116].

To investigate carryover effects, tap B-4 was used with three different test fluids in AlMgSi1 (Figure 4.8a). The abscissa is divided in steps of 16 threads equivalent to the number of holes per series on the test platform. Linear trend lines numerically determined show the slope of tapping torque per series. From thread 1 to 96, a slow falling tendency can be detected for B-4 and reference fluid F2.

Using F12 in the same concentration leads to an increase in tapping torque. The series of F12 itself has a slightly decreasing tendency as well as the following measurement with F11. The measurement with F11 starts at a slightly lower value in comparison to F12. The end reference measurement with F2 starts at a significant higher value than the last measurement of the first reference series. Torque decreases to a similar value as of the first reference measurement. A carryover effect resulting from the fluid change can be detected. The test results are interpreted as follows: Fluid F11 shows a better lubricity than F12. The reference fluid lubricates better than F12.

The carryover effect can be recognized for tap type C in AlSi7Mg (Figure 4.8b). In this figure, the gradients of the trend lines are added to examine the carryover effect. From Lub K to Lub P, a decreasing tendency per series of seven threads can be detected (14 holes per column on AlSi7Mg-platform). An increasing tendency is detectable for Lub U. Carryover effects differently influence the following measurement series. Taking the gradient of the trend lines as a feature to evaluate the effect of the previously used fluid, Lub M (lower gradient) is not affected to the same extent by Lub L as Lub L (higher gradient) is affected by Lub K.

Most of the measurement values level off only for the last three or four values (Lub M, O, P, and U). For Lub K and L the values do not level off for the number of

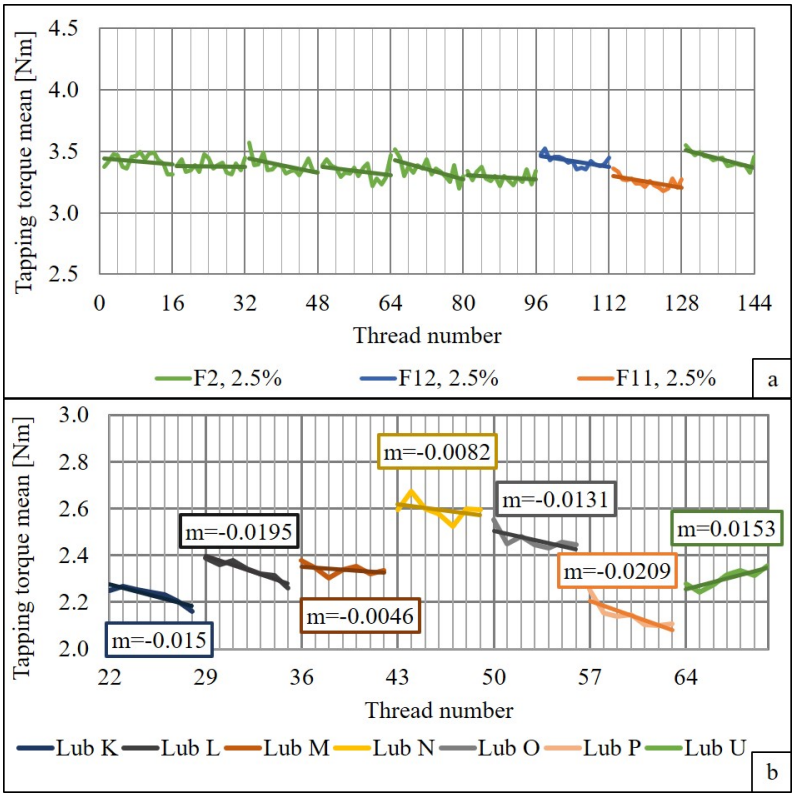

Figure 4.8: Torque slopes of different fluids [98]
a: Measurements of B-4 in AlMgSi1 to investigate carryover effects from fluid to fluid
b: Test series and gradients of numerical trend lines for tap C-2 in AlSi7Mg

measured values. Concluding the experimental results, the carryover effect exceeds the two threads defined in ASTM D5619. Possible reasons for the observed behavior may be the existence of the tribological film built by the previously used fluid or the formation of a characteristic adhered layer belonging to a specific test parameter combination. Ignoring carryover effects leads to less statistical relevant effects and misinterpretations.

4.1.9 Effect of the new methodology on the significance of test results

In the following, results of TTTs (Figure 4.9a) are statistically analyzed to show the improvement of the new developed methodology by means of an improved statistical significance. The tests were conceived in such a way to be able to compare the results of the standard methodology with the new developed methodology. A reference fluid and the fluids Lub R, S, and T are tested at 10 % concentration in

C45E. The fluid Lub T is also tested at 5 % concentration. The fluids significantly vary in lubricating ingredients. Tapping Torque Tests are performed to show the differences in lubricity for all fluids and for the higher concentration. The reference measurements have similar torque levels and slopes (Ref 1 and Ref 2 in Figure 4.9a). Significant differences between Ref 1 and Ref 2 are not expected.

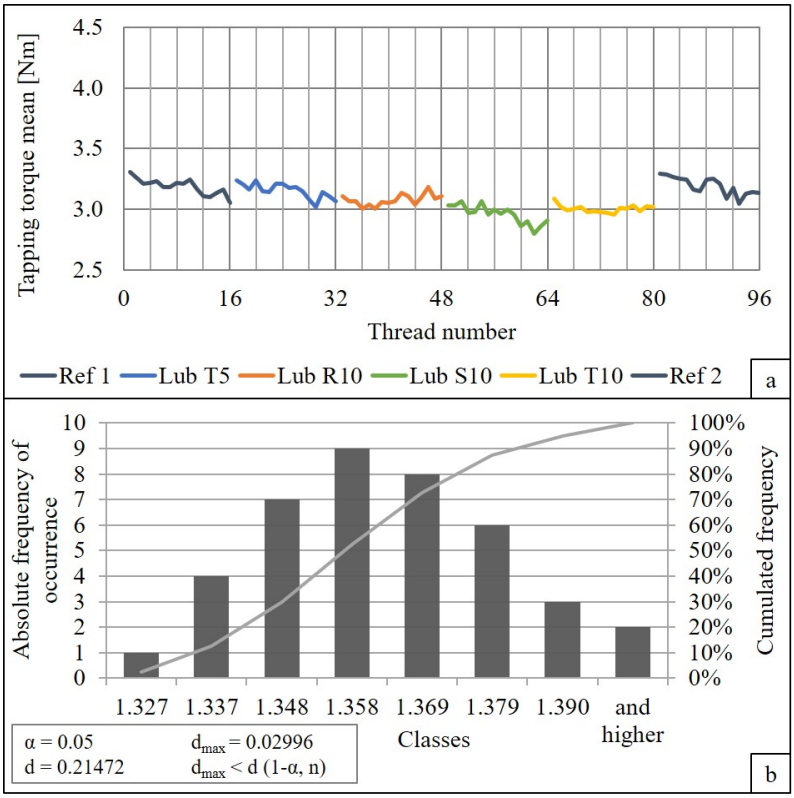

Figure 4.9: Means and distribution of single measurements [98]
a: Raw data of exemplary measurement series in C45E and subsequent significance tests
b: Distribution of a single tapping torque measurement for Kolmogoroff-Smirnov test

Mean torques obtained by ASTM D5619 (approach named *ASTM*) and by two improved approaches are compared to show the necessity of considering a stronger carryover effect and to increase the thread numbers per test run. In the first improved approach *ASTM-16*, 16 threads are performed and the mean is calculated from the last three threads. In the second improved approach *RL-8-8*, 16 threads are performed and the mean is calculated from the last eight threads.

All means are statistically analyzed similar to the analysis in [112]. The torques from the plateau area of the measurement are exemplary checked for normal distribution applying the Kolmogoroff-Smirnov test (Figure 4.9b). For the significance test, the

variances of the means are tested to be equal (F-test). Then, the means are analyzed using a two-sided t-test [244] applying a confidence level of 95 % ($\alpha = 5$ %) and 99 % ($\alpha = 1$ %) to compare these with the resulting p-values.

Results obtained by ASTM D5619 and by the improved approach are given in Table 4.6. In both approaches, the number of contributing values is held constant to investigate only carryover effects. Applying *ASTM*, a significant difference between Ref 1 and Ref 2 and between Lub T5 and Lub T10 can be detected. Differences between Lub S10 and T10 or Lub S10 and R10 are not obtained. In one of four cases, approach *ASTM* provides sufficient test results. In comparison, approach *ASTM-16* gives sufficient results in all cases. Assuming a carryover effect for 15 threads instead of two threads leads to a better differentiability of test fluids in the shown example.

Table 4.6: Results of significance test with $\alpha = 0.05$.
Approach *ASTM-16* achieves better results than *ASTM*. [98]

Compared fluids	**Difference expected?**	**Result acc. to *ASTM***	**Result acc. to *ASTM-16***
Ref 1 vs. Ref 2	no	yes p=0.0012	no p=0.3064
Lub T5 vs. T10	yes	yes p=0.0036	yes p=0.0172
Lub S10 vs. T10	yes	no p=1.0000	yes p=0.0119
Lub S10 vs. R10	yes	no p=0.4535	yes p=0.0034

Table 4.7: Results of significance test with $\alpha = 0.01$.
Approach *RL-8-8* achieves better results than *ASTM-16*. [98]

Compared fluids	**Difference expected?**	**Result acc. to *ASTM-16***	**Result acc. to *RL-8-8***
Ref 1 vs. Ref 2	no	no p=0.4070	no p=0.9664
Lub T5 vs. T10	yes	no p=0.0172	yes p=9.7E-5
Lub S10 vs. T10	yes	no p=0.0118	yes p=0.0047
Lub S10 vs. R10	yes	yes p=5.1E-6	yes p=0.0034

Results from Table 4.6 are based on a 95 % confidence level. To increase the reliability of TTT results, the confidence level can be increased. A confidence level of 99 % makes a differentiability more difficult so that approach *RL-8-8* is applied to obtain distinguishable test results further. New results obtained by approach *ASTM-16* and by approach *RL-8-8* at a 99 % confidence level are given in Table 4.7.

As a result of higher confidence level, the effectivity of approach *ASTM-16* decreases from four to two cases: A difference between Lub S10 and R10 can not be obtained

anymore but a difference between the reference measurements Ref 1 and 2. The improved approach *RL-8-8* is successful in all four cases: Significant differences can be detected between the two different concentrations of Lub T and between the fluids Lub S10 and T10 or R10. The reference measurements are evaluated to be statistically equal. Concluding, increasing the number of torque values contributing to the mean leads to a better differentiability of test fluids especially for higher confidence levels.

4.1.10 Summary and conclusions

Tapping Torque Tests are used to evaluate the performance of MWFs. The standard ASTM D5619-00 has been withdrawn in 2016 and replaced by ASTM D8288-19 in 2019. In comparison, the test procedure of ASTM D8288-19 includes improvements concerning regular reference measurements and tap qualification process. In [98], carryover effects of the previously measured fluid have been recognized significantly affecting the differentiability of test fluids. These have to be taken into account by calculating torque mean values [98]. In ASTM D8288-19, carryover effects of previously measured fluids or slowly but steadily proceeding tool wear are still not considered. Better comparability or distinguishability between test fluids in comparison to ASTM D5619 is not provided by ASTM D8288.

Metalworking fluids have to be evaluated with a laboratory test transferable into practice and flexible enough to reflect the numerous possibilities of tool material and workpiece material combinations. In this section, problems with the last version ASTM D5619 are discussed and improvements are proposed to increase comparability and significance of test results for a new version. Content of this section does not deal with the finding of the best suitable fluid for a specific application. Here, test procedures and evaluation methods are focused. It is found out that the previously fixed definitions lead to high experimental cost, no comparability between taps or workpieces, and less significance of test results. In Section 2.2, tapping processes used to evaluate the performance of MWFs and especially the used test procedures and evaluation methods are reviewed.

The aim of the present investigations is to overcome the disadvantages discussed and therefore to increase significance and comparability of TTT results obtained with coated forming taps. To illustrate the real problems, as example three different workpiece materials (AlMgSi1, C45E, and AlSi7Mg) are used to evaluate the effect of tool, platform, or fluid changes on the test results. The running-in behavior of two different forming taps is investigated. Strongly varying results are obtained for the same tool-fluid-workpiece combination. A criterion to determine the end of a tap's running-in phase is proposed and exemplary applied for the tap qualification defined in ASTM D5619. From the experimental results, it can be clearly concluded

that the qualification criterion defined in ASTM D5619 is too strict and leads to an high amount of disqualified taps.

The need for regular reference measurements is shown by appropriate tests over a higher amount of threads. New definitions (equations) are introduced to normalize the measurement values by the changed reference value. Concurrently, these new equations meet the requirements to integrate disqualified taps into the test evaluation. Applying the suggested definitions, the comparability of test results between taps and platforms of the same material pair combination can be clearly enhanced.

The phenomenon of carryover effects when changing test fluids during a TTT is investigated by applying statistical significance tests. For the chosen fluid sequence, the carryover effect exceeds the two threads defined in ASTM D5619. The analysis of different examination approaches shows that considering a stronger carryover effect and increasing the number of threads per test series enhances the differentiability between test fluids even by applying a higher confidence level. The results can be summarized as follows:

1. The running-in phase has to be checked for each tap: Even taps of the same material and type can have different running-in phases. The workpiece material can also affect the running-in behavior. A criterion based on the measure torque mean is introduced to identify the end of running-in. The optical examination of built-up edges or adhered layers becomes redundant and saves time for test conduction. The starting condition for TTTs is clearly defined.
2. Regular reference measurements are indispensable for comparable TTTs: The tap continuously wears off and the reference value changes over the increasing number of TTTs. Test results are significantly affected and may lead to misinterpretations. Regular reference measurements lead to more reliable data and comparable test results over the whole life time of the tool. The results show that repetitive reference series after every sixth test series are necessary.
3. New calculation methods normalizing the measurement values by the theoretical recent reference value are introduced. These equations make comparisons between disqualified taps and workpieces of the same material possible although such comparisons were not intended in ASTM D5619. Then, taps being disqualified according to the allowed 2 % range can be used for TTTs. Comparability is improved and costs for experiments are saved.
4. More threads have to be discarded because of carryover effects. The effect of the previously used fluid on the following measurement result is stronger than the two threads defined in ASTM D5619. Eight threads are evaluated to be sufficient and reliable. Test fluids are easier to distinguish because of smaller deviations of the contributing values. The usefulness of TTTs is significantly improved.

5. The thread number per test fluid has to be increased. The test procedure according to ASTM D5619 leads to worse distinguishability between test fluids because the mean calculation is only based on three single values. Increasing the number of contributing values to eight leads to differentiability even at higher confidence levels. Reliability and significance of TTT results are increased.
6. Using the proposed test procedure and evaluation approach, coated tools can be used for TTTs. Coated tools are used in field applications because of better performance and longer tool life. The proposed changes lead to results with smaller deviations and clearer differentiation options. As a result of the improvements, it is possible to reflect field conditions more accurately.

For the core experiments in this dissertation, the knowledge of proceeding tool wear is essential. Experiments in both datasets are performed with only one tap because differences between taps even of the same type are significant (cf. Figure 4.6 in Section 4.1.5). As will be described in Chapter 3, in dataset 2016 112 threads and in dataset 2019 336 threads are performed. The aim of this work is to find differences between MWF additives in an extended TTT. For this purpose, a variety of MWFs is measured. Carryover effects can play a significant role in experiments of both datasets (cf. Figure 4.8 in Section 4.1.8). For calculating torque means, effects of tap wear and previously measured fluids have to be considered and their significance has to be evaluated in each case.

4.1.11 Torque mean value calculation for datasets 2016 and 2019

In the first approach, normalized torque means for a statistical analysis are calculated as follows:

1. Means are calculated in the plateau region, i.e. between 6 and 27 mm as shown in Figure 4.1a with orange and grey arrow.
2. With respect to carry over effects by the previously measured fluids, the slope of the single means are depicted for one fluid. According to the recommendation in [98], first measurement values are excluded from the subsequent mean calculation. Later, the remaining single means have to be normalized depending on the reference value.
3. Reference fluids are firstly treated like test fluids as described before. An overall mean is calculated from the remained single means as described in Section 4.1.7 by Equation 4.4.
4. The means of the reference fluid are used to normalize the means of the test fluid. The equation for normalization has been described in Section 4.1.7 by Equation 4.6.

5. The normalized means of two test fluids are used for a statistical two-sided t-test. P-values are calculated and compared with the error probability. If the p-value is higher than the error probability, the examined means are statistically equal.

Normalized tapping torque means and their standard deviations are graphically shown in bar charts.

4.2 K-means clustering of Acoustic Emission energy

In parallel to each torque measurement, AE measurement is conducted. The measurement is manually started and stopped and lasts about 5 s for each thread. At a sampling rate of 4 MHz, this results in about 20 million data points for each measurement. These data points in time-domain can be further processed to get a time-frequency representation. Typical methods are here for example STFT and CWT. By applying such transformation methods, raw data are divided into wavelets so that a time-frequency representation is possible. An exemplary result of both transformation methods is depicted in Figure 4.10. Raw signals containing two higher magnitudes in quick succession and the related transformed signals using STFT or CWT are shown.

The result of STFT (Figure 4.10b) is a so called spectrogram. Here, events in time are not clearly detectable but frequency resolution is better. For Fourier Transformation, different parameters and window functions can be chosen. The result of CWT (Figure 4.10c) is a so called scalogram: Events in time in higher frequency bands are easier to detect. For wavelet transformation, different parameters and wavelet functions can be chosen. The choice of parameters and functions depends on the data and on the analytical goal. If data is recorded during an experiment for the first time, the analytical goal is not clear. If frequencies or events in time are more important, this will be found out during the investigation.

For the second approach, AE raw data are processed using CWT. The hypothesis that tearing or thinning of lubricating film is characteristic for a certain lubricant and results in AE events in time lead to this decision. After CWT, AE energies in previously chosen frequency ranges are calculated. These energies are graphically depicted as one data point for one thread in a dot chart. K-means clustering with a 95 % confidence bound is applied on the data according to [9].

K-means clustering is a partitioning clustering method. Data is not viewed point by point. Clusters are assigned at once for the whole dataset. Using k-means, the number of clusters k is predefined. The goal is to divide data into clusters so that the relative distance between all data points and their corresponding centroid is minimized. Although k-means algorithms can work differently due to implementation ways, the general process is structured as follows [246]:

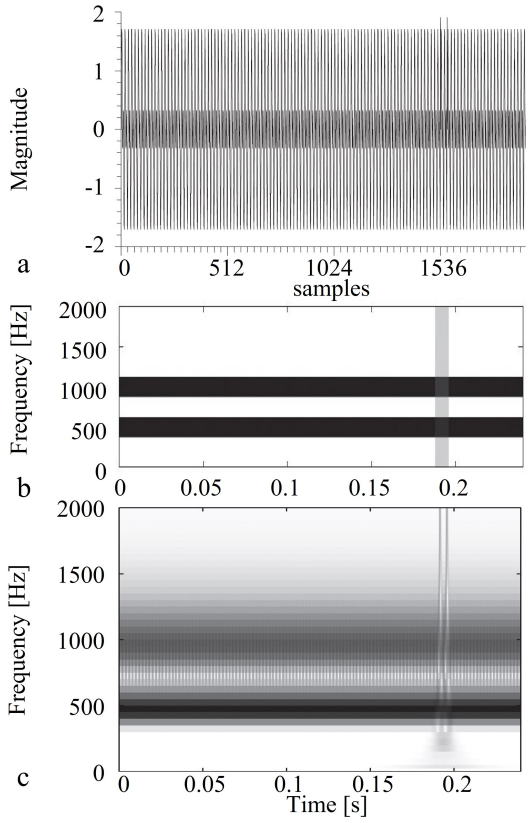

Figure 4.10: Exemplary comparison of STFT and CWT result acc. to [245]
a: Raw signals
b: Time-frequency representation after STFT: Spectrogram
c: Time-frequency representation after CWT: Scalogram

1. Each data point is assigned to a random cluster.
2. Centers of clusters are determined.
3. Each data point is assigned to that cluster whose center it is closest to.
4. Steps 2 and 3 are repeated until the solution no longer changes.

How fast a stable solution is reached is significantly influenced by the start solution. With usual cluster procedures, there is no evaluation of true or false. By clustering, classes are discovered/found. In this thesis, clustering is used as a classification method: The class of each data point is known from the experiment and can be evaluated as true or false clustered point.

In literature, k-means algorithms are used for clustering of AE data for damage type identification in composite material [247, 248, 249]. A health monitoring framework for wind turbines using k-means clustering has been introduced in [250]. Wear states in journal bearings were classified using an unsupervised k-means clustering

algorithm in [205]. The AE burst signals of proceeding tool wear has been analyzed by k-means clustering in [251].

The data points within the clusters are checked whether the true value really belongs to this cluster or not. True clustered (TC) and false clustered (FC) data points are counted for the accuracy calculation. The results can be presented in a confusion matrix shown in Figure 4.11.

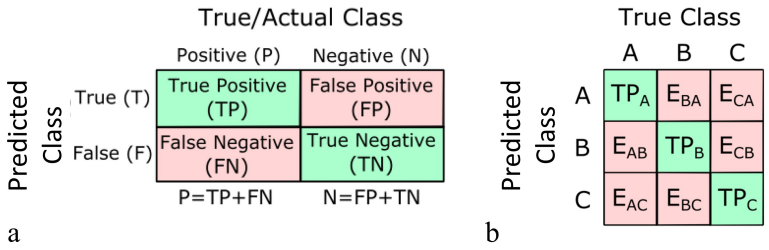

Figure 4.11: Principle of confusion matrices [252]
a: Confusion matrix of binary classification task
b: Confusion matrix of multi classification task

The choice of the relevant frequency bands acts as a prefilter. It could be necessary to exclude certain frequency bands from the calculation of the AE energies. Some frequencies could be influenced by dynamical effects. One example is the distance between piezoelectric transducer and pilot hole. Initially, the distance is wider because the measurement series starts at the rear end of the workpiece. With proceeding measurement series, the distance becomes smaller. As shown in Figure 4.12, this effect is visible in AE energy of the higher frequency range 232 - 464 kHz. For the last measurements of each series – when the process comes nearer to the sensor (red) – the AE energy increases. This effect seems to be independent from the used fluid. Compared to the AE energies in the other two frequency ranges, the energy in this range is very small. Applying a k-means clustering approach on AE energies from certain frequency ranges, this effect has to be considered.

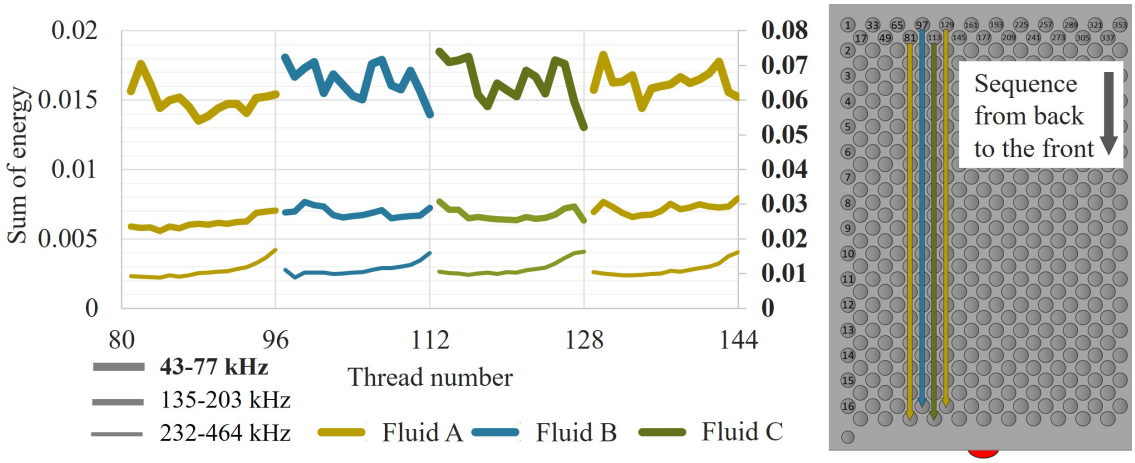

Figure 4.12: Influence of distance between sensor and thread in the range of 232 - 464 kHz and related series on platform

4.3 Application of Convolutional Neural Network

This section and related subsections are published in [10, 12].

As a class of artificial neural networks, CNN is prevalent in various tasks as a type of deep learning for processing data with grid patterns, such as images. The CNN architectures are inspired and designed to automatically and adaptively learn spatial hierarchies of features from low- to high-level pattern [217].

For deep neural network, so-called hyperparameters determine the neural network structure and have to be defined by training. The choice of hyperparameters influences the results. For this reason, hyperparameter optimization, called tuning, is of importance. Hyperparameters can be divided into those related to CNN architecture and those related to training algorithm.

For CNN architecture, basic layers such as conv layers, pooling layers, and fc layers are applied in the proposed models. Besides that, batch normalization (bnorm) layers are added to speed up training and reduce network initialization sensitivity. In addition, relu layers are used to increase the expression ability of neural network model. Applying the relu function, inputs are converted to positive numbers, all negative numbers are converted to zero and all positive numbers remain their value. Furthermore, according to [253], dropout (drop) layers are employed in the proposed models to reduce overfitting. This layer can improve generalization errors in CNN.

4.3.1 Structure of optimization process

In Figure 4.13, the principle flow of the proposed CNN approaches is depicted. Thread forming experiments are carried out using different MWFs. During these experiments, AE signals are acquired for a subsequent use in CNNs. In datasets 2016 and 2019, a single measurement contains about 20 million data points. Due to calculation time, the amount of data has to be reduced. Therefore, AE signals are divided into samples and signals are selected.

According to the flowchart in Figure 4.13, hyperparameters have to be tuned next. If hyperparameters are well tuned, the model could minimize a predefined loss function and give better results. As a large number of hyperparameters is needed to be optimized, cross validation is applied for hyperparameter tuning. For one hyperparameter, different values are tried and the related performance is compared. For the proposed CNN models, a systematic approach for hyperparameter tuning is used. Several CNNs are trained differing only in the value of one hyperparameter. After comparing the performance of these CNNs, the best setting is chosen. This optimized setting is used for the future CNN. As a next step, another hyperparameter is tuned and so on. In this way, the set of hyperparameters are optimized step by step.

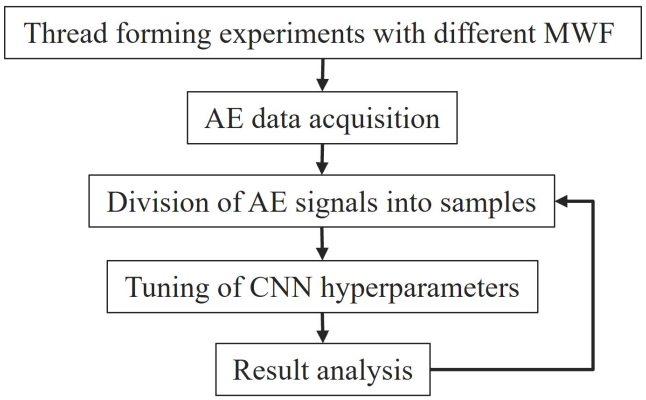

Figure 4.13: Flowchart of proposed CNN optimization loop acc. to [10]

4.3.2 Data segmentation

Data used for training and test of the CNNs in this work are i) AE raw data in time domain ii) AE data after CWT and iii) AE data after STFT in time-frequency domain. As already mentioned, one measurement contains about 20 million data points which have to be reduced due to calculation time. To reduce the amount of data for the CNN, signal selection and segmentation are necessary. In Figure 4.14, different segments of one AE measurement are displayed. From the raw signal

in Figure 4.14a, three process phases can be recognized: air part, forward forming process, and reverse process. From the technical point of view, more AE events occur in the forward forming parts where elastic and plastic deformation take place. Therefore, the forward part of each measurement is chosen for the calculations in the CNN. In the measured raw signal, noise from the environment is included as has been shown in Figure 4.1b.

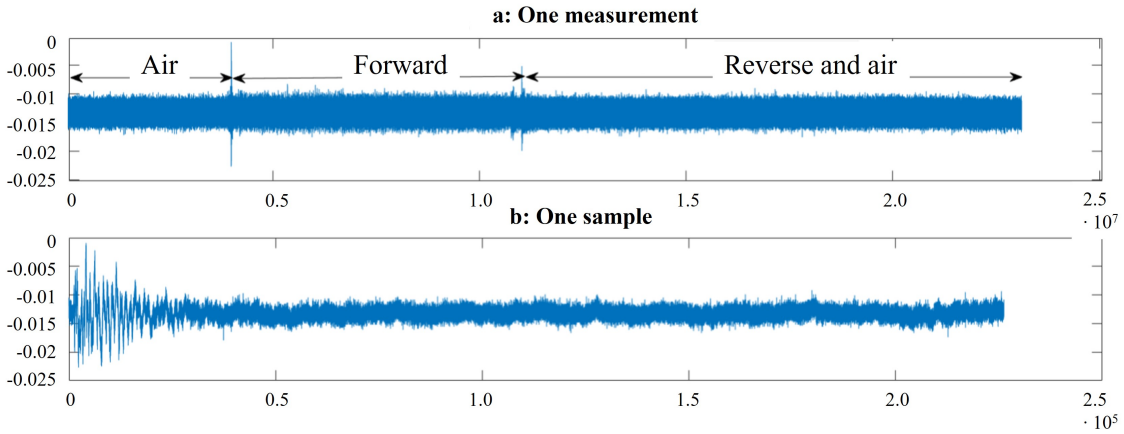

Figure 4.14: Segmentation of raw data [11] a: One measurement b: One sample

Signal segments have not only be selected from one measurement. In dataset 2019, certain measurements are selected from one measurement series. This will be detailed in Section 4.3.4.

4.3.3 Dataset 2016

The AE signals acquired during threading are classified by CNN to check if the fluids can be distinguished. The fluids have been introduced in Table 3.2 and the measurement order has been listed in Table 3.3. The flowchart of this CNN approach is shown in Figure 4.13. Trial series 2 to 11 each contain eight threads. To reduce the impact of carryover effects and the pre-hole location on the platform, four measurements are chosen in the middle of each trial series. For example in series 2, the measurement of threads no. 35 to 38 are chosen from the possible threads no. 33 to 40. Series 1 contains 32 measurements. For balancing the sample numbers in every class, four threads are chosen from the middle of series no. 1.

A single measurement contains about 20 million data. For reduction of CNN calculation time, the amount of data is reduced by segmentation. To maintain the key points of each sample, data overlaps with adjacent samples. In this experiment, different data (3400, 6800, 13600, and 27200 data for each sample) are used as CNN input. After comparing the results, 13600 as best data/sample combination is chosen as the CNN input. In order to maintain the key points of each sample, data

overlap with adjacent samples by factor 0.5. The comparison of one measurement and one sample has already been given in Figure 4.14.

For the proposed CNN model, a systematic approach for hyperparameter tuning is cross-validation between different sets of hyperparameters [254]. Hyperparameters are tuned and optimized step by step. Since there are many tunable hyperparameters, only those are examined that yield the best performance improvement. Values of important hyperparameters are shown in Table 4.8.

Table 4.8: Hyperparameters of CNN for dataset 2016 [10]

Hyperparameter	**Value**
Initial learning rate	0.01
Batch size	1380
Maximum number of epochs	40
Normalization factor	0.001
Drop probability	0.5
Receptive input size conv1	1 x 109 x 1
Receptive input size conv2	1 x 67 x 1
Receptive input size conv3	1 x 29 x 1
Receptive input size conv4	1 x 15 x 1

In Figure 4.15, the architecture of the proposed approach is shown. The layers of this deep neural network are concatenating into a 'layer'-object which describes the network's architecture. It can be described as a 4-layer CNN because it consists of four conv layers. Following [254], bnorm layers and one drop layer are integrated into the model. As nonlinear activation function, relu function is chosen. For the pooling layer, mpool function is elected. For classification, one fc layer and one softmax layer are used. Softmax layers are involved in CNN to reduce calculation time and avoid overfitting.

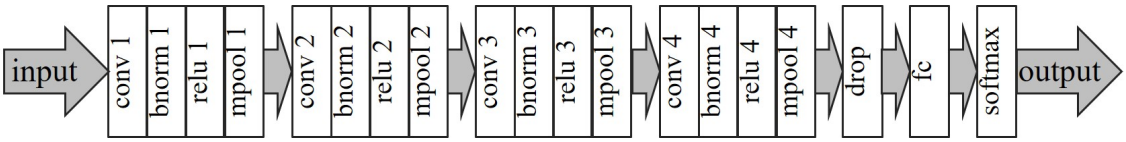

Figure 4.15: Architecture of CNN model applied on dataset 2016 acc. to [10]

4.3.4 Dataset 2019

A CNN model is used to distinguish between test fluids within one group listed in Table 3.4. Signals of AE are analyzed in time domain.

Each series consists of 16 measurements. With about 20 million data points for each measurement, this means about 320 million data points for one series. Due to this large amount of data, data has to be segmented and selected. In this case, each series is divided into four parts

- Part 1: from the first to the fourth measurement (m01 - m04),
- Part 2: from the fifth to the eighth measurement (m05 - m08),
- Part 3: from the ninth to the twelfth measurement (m09 - m12), and
- Part 4: from the thirteenth to the sixteenth measurement (m13 - m16).

The first threads of each series could be effected by previously measured fluids [98]. Therefore, part 1 and part 2 are not chosen. Measurements in part 4 are very near to the piezoelectric transducer. As it has been shown in Figure 4.12, these measurements could contain additional features in specific frequency ranges that could disturb the classification task. Thus, data of part 3 is selected.

Besides measurement selection for each series, specific data segments are additionally selected in dataset 2019. From the technical point of view, more AE events occur in the forward process than in the reverse process. In the forward process, elastic and plastic deformation take place. The forward process is further segmented into segments representing one round of the tap. The amount of data in this segment can be calculated from the test parameters. The spindle speed is 1061 rpm, the tool diameter is 6 mm and the tool pitch is 1 mm. For a sampling rate of 4 MHz, this means that one tap round contains 226200 data points.

After the two prefiltering steps selection and segmentation, the remaining data represents the input into the CNN model. In the proposed CNN model, eight conv, bnorm, relu, and pool layers are used. Aside from that, one drop, fc, and softmax layer are implemented. To maintain the characteristic value of each sample, 0.5 overlap of adjacent samples is applied. Detailed architecture of the CNN used for dataset 2019 is shown in Figure 4.16.

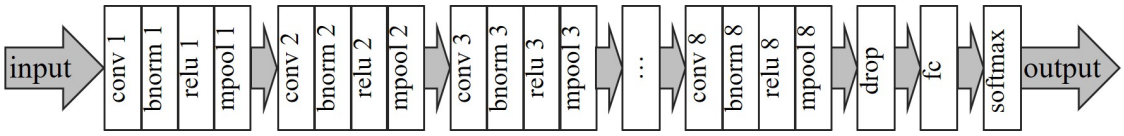

Figure 4.16: Architecture of CNN model applied on dataset 2019 acc. to [11]

For training of algorithm hyperparameters, optimizer selection is critical in CNN as it is used to solve optimization problems by minimizing the function. Stochastic gradient descent with momentum optimizer is employed. It combines advantages of stochastic gradient descent and momentum and provide a boost to learning speed [255]. Other hyperparameters related to model training are also tuned in the proposed approach. These are for example initial learning rate, batch size, maximal number of epochs, L2-regulation factor, drop probability, and kernel size. The result of the optimized hyperparameters is shown in Table 4.9.

Table 4.9: Hyperparameters of CNN for dataset 2019 [11]

Hyperparameter	**Value**
Optimizer	SGDM
Initial learning rate	0.001
Batch size	1380
Maximum number of epochs	40
L2-regularization factor	0.0001
Drop probability	0.5
Kernel size_conv1	1 x 109 x 1
Kernel size_conv2	1 x 67 x 1
Kernel size_conv3	1 x 57 x 1
Kernel size_conv4	1 x 29 x 1
Kernel size_conv5	1 x 15 x 1
Kernel size_conv6	1 x 9 x 1
Kernel size_conv7	1 x 5 x 1
Kernel size_conv8	1 x 3 x 1

4.3.5 Transfer Learning between dataset 2016 and 2019

Content of this section is from [12, 256].

Transfer Learning is a machine learning method to adapt models developed for a task for reusage as the starting point for a model on a second task [257]. In addition that TL can train deep neural networks with comparatively little data, it is also an optimization allowing rapid progress and improved performance to model the second task. Models which are transferred to the second task could be pre-trained outstanding models or models developed by users themselves. Many research institutions release models developed on large and challenging datasets like VGG-16, ResNet50, Inceptionv3, and EfficientNet etc.. It is an effective way by selecting proper pre-trained models or parts of models and adapt or refine them to the target task. Source data should be selected being related to the target dataset. Then, a suitable model for the source dataset should be developed. Afterward, the new model could be tuned and reused for the target dataset.

Transfer Learning is applied from dataset 2019 on dataset 2016. In both datasets, the same workpiece material and the same tap type are used. Unlike previous work [10, 11], where five or eleven MWFs are distinguished, for the developed TL approach 16 different types of MWFs are classified. Most of these MWFs belong to emulsions. Two non-water miscible oil-based MWFs are also included.

In the procedure of classifying fluids of dataset 2019, a CNN-based model is designed. For this classification approach, AE signals are previously transformed by STFT. Images of spectrograms are the inputs to the CNN. The use of CWT and

related scalograms revealed worse classification results. Hyperparameters are optimized on dataset 2019. The model is trained and tested on dataset 2019. The best configuration is chosen and the same model is applied on dataset 2016 to distinguish fluids of this dataset.

Dataset 2019 contains more measurement series than dataset 2016. Besides, all AE data in dataset 2019 are from water-based MWFs. In dataset 2016, water-based and oil-based MWF are used. Furthermore, the series of measurements for each MWF in dataset 2016 is more complicated than in dataset 2019. Data processing in dataset 2016 is more complex than in dataset 2019. With respect to the above considerations, dataset 2019 is chosen as source domain while dataset 2016 is the target domain. Except for the reference fluid, 16 measurements are realized for other MWFs in both experiments i.e. 16 samples can be used for training in each class.

Due to the fact that the temporal start and end of tapping are performed manually, the tapping process can be divided into an air, a forward, and a reverse part as shown in Figure 4.14a. In the air part, there are no usable AE data because the tap is not in contact with the platform. For this reason, the data in this part are removed as a pre-processing step. From a physical point of view, threads are mainly formed in the forward part of the motion. Therefore, the relevant AE events occur in this part.

The data processing procedure can be divided into data selection, segmentation, transformation, and normalization. Due to the fact that the reference fluid is tested more frequently than other fluids, only the data from the first series of the reference fluid are selected in both experiments. Only the data from the front part of each measurement are used. By selecting the data, the number of measurements in each class is the same. The data used are divided into appropriate segments according to the travel speed. To obtain the main characteristics of each sample, the data of adjacent segments overlap. Therefore, after data segmentation, there are enough samples in each class for the deep learning approach, even if fewer measurements are used for each class in total.

By adjusting parameters in STFT, segments are transformed from time domain to time-frequency domain. Spectrograms are generated. In Figure 4.17, one segment spectrogram is shown. Finally, to get rid of a number of anomalies which make analysis of the data more complicated and to reduce database space, spectrograms are normalized by Z-Score and Min-Max techniques. To get better results, parameters in each step are optimized by exhaustive sweep algorithm.

For spectrogram-based distinction, a deep learning approach based on CNN is used. Hyperparameters determining the network structure and variables determining how the network is trained have significant impact on classification.

The structure of the proposed model considered for training is a basic CNN with six conv layers denoted as Basic6. The first layer of the Basic6 model is the image

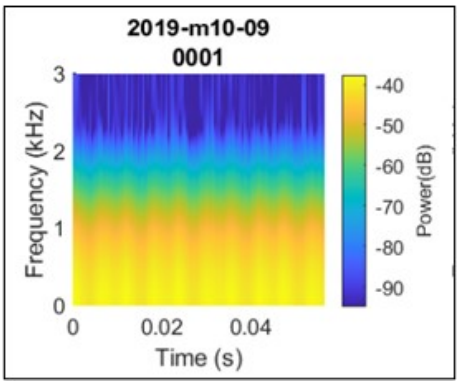

Figure 4.17: Spectrogram of one segment [256]

input normalized by Min-Max. Every input is normalized in the range from 0 to 1. Feature extraction is done by six convolutional blocks containing conv layers, bnorm layers, relu activation function layer. Pool layers are applied to extract the biggest value of each feature map in between conv blocks. To prevent the model from overfitting, three drop layers are used between conv layer 2 to 5. The classification is realized by a fc layer which has as many neurons as class numbers and softmax layer. Final classification results are presented in the output layer. All layers of the Basic6 network are shown in Figure 4.18.

Hyperparameters tuning on training algorithm is time-consuming. Many hyperparameters have to be tuned like optimizer, minimum batch size, initial learn rate, maximum epochs etc.. To define proper hyperparameters, exhaustive sweep and Bayesian optimization techniques are applied for the proposed CNN model. First, an exhaustive sweep algorithm is used to sweep all possible combinations of hyperparameters values. In this step, a rough overview about good parameter ranges is obtained. Second, Bayesian optimization is applied to minimize the distance of the evaluation feature from its optimal value by changing the initial hyperparameter values in a given ranked sequence. After hyperparameter optimization, the best value of every hyperparameter and the best combination have been determined.

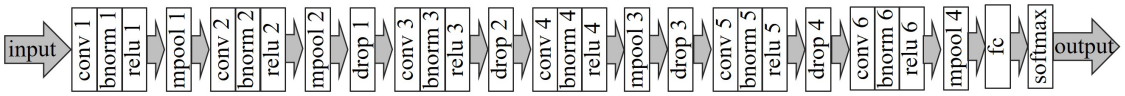

Figure 4.18: Architecture of CNN model used for TL task acc. to [256]

Like data processing in dataset 2019, AE data in dataset 2016 are selected, segmented, transformed, and normalized. The threading process of one thread consists of 27 tap spins that can be divided into segments due to one tap round. Tap speed in the first experiment is 1061 rpm while tap speed in the second experiment is 1000 rpm. Considering sampling rate for both experiments is 4 MHz, each round

contains 226200 data in the first experiment while each round contains 240000 data in the second experiment. When selected part (forward) of each measurement are partitioned into segments, segment's length is designed based on data number of one tap round. As result, segment length in the second experiment is larger than in the first experiment. To keep the main properties of each segment, overlap among adjacent segments is needed. In dataset 2019 and 2016, the overlap among adjacent segments is similar but not identical. Other parameters related to the processes of data segmentation, STFT, and normalization are equal. In the data processing step, parameters in each step are transferred from dataset 2019 to dataset 2016.

Besides different data in dataset 2019 and 2016, the task for both datasets is MWF classification. A model of CNN is trained using dataset 2019. This model is then transferred to dataset 2016. Hyperparameters related to network structure are equal in both datasets. The classification task of dataset 2019 is the distinction of eleven different MWFs. Consecutively, the class number in the last layer is eleven. In dataset 2016, five different MWFs have to be classified so that the class number is set to five. Briefly, the class number needs to be changed by transferring the model from dataset 2019 to 2016. According to the subsettings of these two datasets, transductive TL is applied. Although the last classes numbers are different, other hyperparameters in the CNN model are the same. Transfer of hyperparameters is realized in this approach.

5 Test results

In this chapter, results of the different approaches applied on datasets 2016 and 2019 are presented. These results have in main parts been published in [9, 10, 11, 12].The approaches have been described and explained in Chapter 4. Where necessary, some additional information is given for understanding or scientific completeness issues.

5.1 Dataset 2016

During an extended TTT, tapping torque and AE signals are acquired. Threads are formed in alloyed steel C45E using different MWFs. For dataset 2016, a reference fluid (ReF), two emulsions (E1 and E2), and two oils (O1 and O2) are used for in total 112 threads of 28 mm depth. Test order has already been introduced in Table 3.3. After completing the running-in of the tap, eight threads are tapped with each test fluid. The aim is to differentiate between the test fluids of the same type but with different phosphorus contents. As described in Section 2.1, phosphorus acts as an AW additive during metalworking processes.

5.1.1 Tapping torque means for dataset 2016

As presented in Table 3.3, each test fluid has been measured in eight threading operations. As there are only eight measurements per series, the carryover effects which were found and published later in [98] are not considered for dataset 2016. Single means are calculated from the plateau region of the thread from 7.5 to 28 mm thread depth. All single means are taken into account for the tapping torque mean of one test fluid. After normalization according to [98] considering proceeding tap wear, the normalized means are depicted with means of raw data in Figure 5.1. Normalized means are depicted in yellow and raw means in blue. Additionally, test fluids E1 and E2 and test fluids O1 and O2 are compared using a statistical two-sided t-test. The results of the statistical test are shown in tabular form in the same figure.

From Figure 5.1, the slope of the three ReF means is analyzed first. Fluid ReF has been used in series 1, 6, and 11. Raw means show that ReF mean of series 6 is the highest one. The three means fluctuate by up to 0.024 Nm around a mean of 3.101 Nm. In respect to the standard deviation of about 0.025 Nm for ReF, this means that tool wear was rather low over the experiment. Tool wear remained within a limited range during the entire test procedure. Based on this comparison of ReF means, only a small change is expected for the means of test fluids after normalization according to [98].

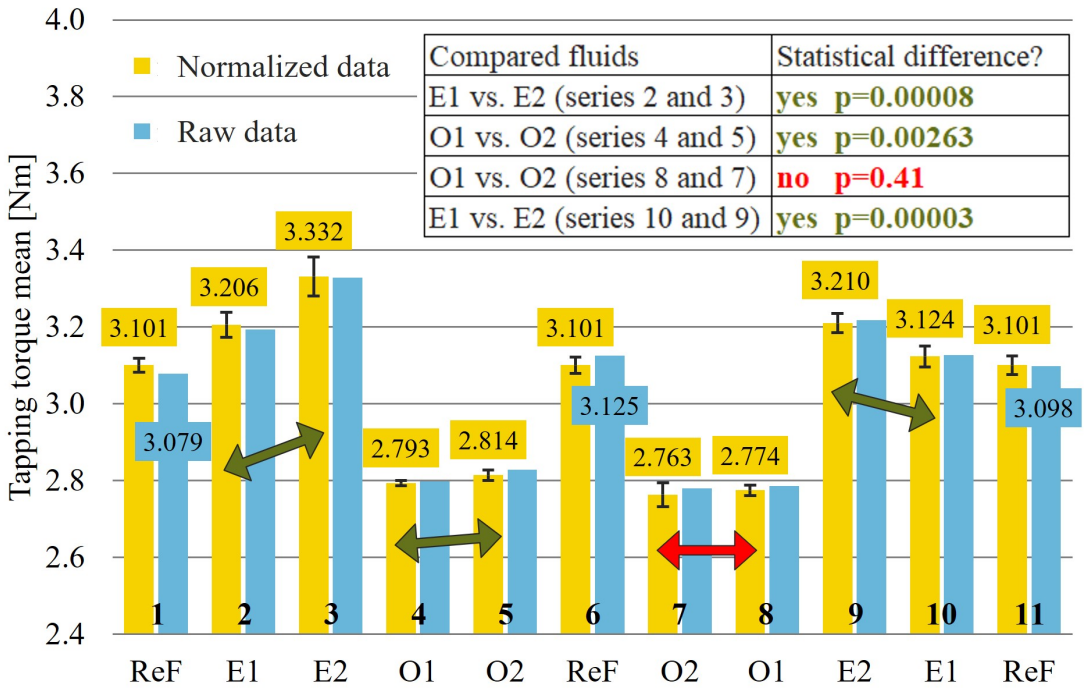

Figure 5.1: Tapping torque means of dataset 2016 and results of significance test with $\alpha = 0.05$

Obviously, differences between means of oils (O1 and O2) and means of emulsions (ReF, E1, and E2) are large. Oil means are about 2.8 Nm and emulsion means greater than 3.1 Nm. Here, a statistical analysis is not necessary to recognize that oils and emulsions can be detected by tapping torque. As next step, the normalized means of E1 and E2 and of O1 and O2 are compared. E1 and E2 as well as O1 and O2 differ in their phosphorus contents. The statistical comparison is performed using a two-sided t-test with a confidence level of 95 %. If p-values are obtained that are smaller than the error probability, then the compared means are significantly different [244]. The obtained p-values are listed in the table in Figure 5.1. The probability of error is $\alpha = 0.05$ for all cases.

For E1 and E2, series 2 with 3 and series 9 with 10 have to be compared. In both cases, means are significantly different . For O1 and O2, series 4 with 5 and series 7 with 8 have to be compared. Here, two different results are obtained. In the comparison of means of series 4 and 5, the p-value is 0.00263 and therefore just smaller than the assumed error probability of 0.05. For series 7 and 8, p-value is 0.41 and therefore greater than 0.05. The test result is not reproducible for O1 and O2 and is apparently influenced by variables that have not yet been taken into account.

A similar effect can be recognized for the means of E2 in series 3 and 9. The mean of

series 9 is significantly lower than of series 3, presumably influenced by the previous measurements with the oils. The measurements in series 6 with ReF have obviously not been influenced by the measurements of the oils in series 4 and 5.

In conclusion, a carryover effect by previously measured fluids, is recognizable for E1 and E2. Why torque means of emulsion ReF are less affected, could be related to additional lubricating ingredients of ReF. As listed in Table 3.2, ReF contains ester in addition to phosphorus. Only phosphorus containing emulsions could be significantly influenced by previously measured oils. For better lubricating emulsions, this effect is no more noticeable. Those results could be good indicators for the lubricating effect of esters in material C45E. At this point, the question could be asked whether this reference fluid is suitable for monitoring tool wear in this experimental design. This point will be taken up again in Section 5.1.4.

In summary, different phosphorus contents in emulsions can be distinguished by tapping torque means. For lubricating oils, this is not reliably possible.

5.1.2 K-means clustering of Acoustic Emission energy for dataset 2016

In this section, k-means clustering is used as a statistical analyzing method for distinction of different MWFs based on AE signals. For the test sequence introduced in Table 3.3, it is checked if changes in the interaction of surfaces during frictional contacts can be detected by means of AE. As has been shown in previous sections, torque and AE have frequently used as features for tool condition monitoring.

Before clustering, raw signals of AE have been previously transformed by CWT. In Figure 5.2, raw signals in time domain and AE energies in time–frequency domain are depicted. From Figure 5.2a and b, it can be concluded that amplitudes are not very significant and that measurements include much noise. In Figure 5.2c and d, two central frequency ranges f2 = 115 kHz and f1 = 57 kHz can be recognized with high energies (in yellow).

In Figure 5.3, torque means and sums of AE energies in the complete analyzable frequency range are depicted for each thread. A high AE energy tends to go hand in hand with a high torque. By AE energy, additional features can be obtained that are not observed by torque. In particular, in trial series 1 AE energy decreases which can be related to the running-in of the tap. In contrast, torque means remain nearly constant. Additionally, several peaks in AE energy e.g. in trial series 6, 10, and 11 are not recognizable in torque.

Torque and AE energy are clearly affected by the used MWF. Using lubricating oils (O1 and O2), lower values are achieved for torque and AE energy. Using E1 and E2, increased torque and increased AE energy can be detected. Moreover, lubricating oils show more similar results for their two trial series than the emulsions. In comparison to E1, E2 can be related to increased values of torque and of AE

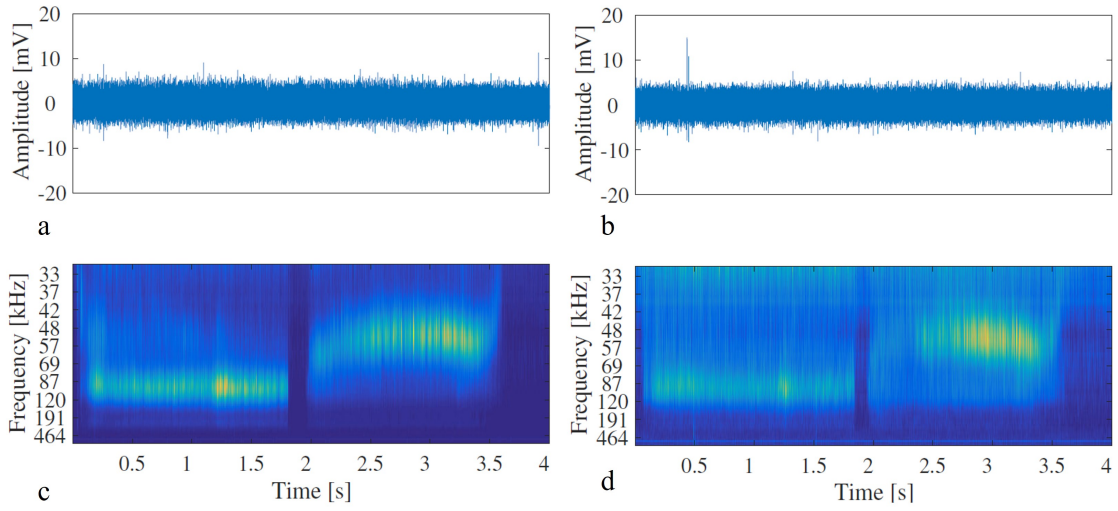

Figure 5.2: Exemplary measurements [9]
a: Raw AE data of Emulsion 2
b: Raw AE data of Oil 1
c: Data of Emulsion 2 after CWT
d: Data of Oil 1 after CWT

energy. For emulsions, it is additionally recognizable that the reduction in torque and AE energy after the use of lubricating oils is permanent. In trial series 9 and 10, lower torque means and lower AE energies are detected compared to trial series 2 and 3. Fluid ReF shows similar torque means over all trial series and torque seems to be less affected by previously measured fluids. This fluid has significantly higher AE energy in trial series 1 than in series 6 or 11. Probably, the running-in effect of the tap is much more than the assumed 32 threads that have been recognized in torque values. Acoustic Emission seems to be a more sensitive measurement feature than torque.

To conclude, AE energy and torque seem to be both related to the tribological interaction between tool and workpiece. Trends that are not apparent in torque are possible to detect in AE energy. Differences between individual trials are reflected to an greater extend by AE energy.

In this section, statistical analysis using k-means clustering is conducted to investigate the distinction of different MWFs using AE energies in dominant frequency bands. Energies in two central frequencies f2 = 115 kHz and f1 = 57 kHz are used as features. The single peaks in AE energy in series 6 and 10 are excluded from the evaluation. In Figure 5.4, clustering results of different MWF trial series are shown. The confidence bound is set to 95 %.

Results for E1 and E2 that are presented in Figure 5.4a and b are in good agreement with known ground truth. The clusters are well separated in f2 (forward process)

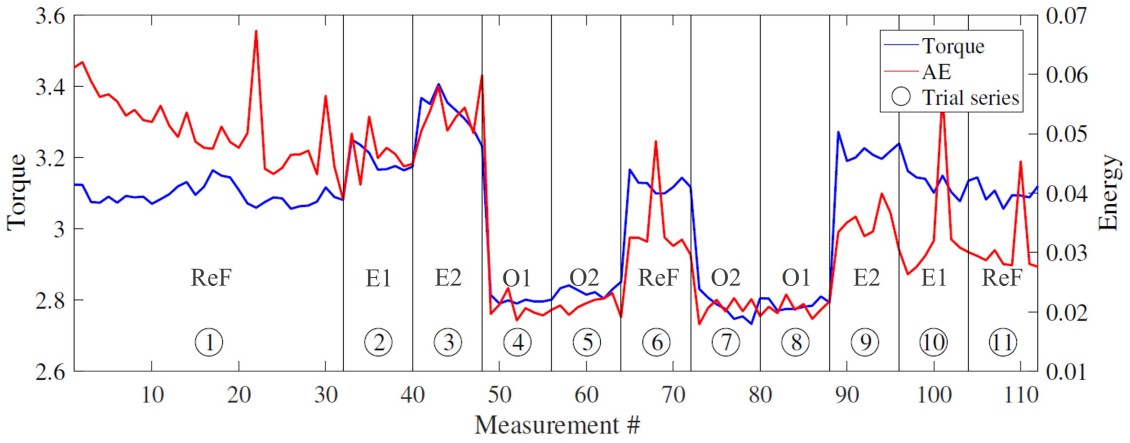

Figure 5.3: Torque means and sums of AE energy [9]

but are overlapping with respect to f1 (reverse process). Apparently, each process phase is affected to a different degree. Using E1, a lower AE energy is observed in the forward forming process than using E2. Emulsion E1 contains a higher concentration of phosphorus leading to improved lubrication. As a result, higher lubricity leads to lower AE signals. In contrast to the possible distinction of the emulsions, a distinction of lubricating oils is not possible (cf. Figure 5.4c). The clusters can not clearly be separated and are overlapping.

The results for different MWF types (E2, O1, and ReF) are provided in Figure 5.4d. The clusters are well separated and the data points are in good agreement with known ground truth. This indicates a strong dependence of AE energy on the MWF's composition. Lower energy is detected using well lubricating oils, whereas higher AE energy is related to oil-in-water emulsions. The reference fluid is located in between because of its higher lubrication activity resulting from a small amount of ester. That higher lubricity leads to lower AE signals, this is confirmed by the results in Figure 5.4d. Lower AE energy is observed using O1 than using the oil-in-water emulsions ReF or E2.

From the data points in Figure 5.4, the accuracy is calculated and listed in Table 5.1. Very high accuracies of 100 % and 93 % are achieved for E1 and E2. The different phosphorus contents are detected as two different clusters using k-means clustering at a 95 % confidence level. The different phosphorus contents in the two lubricating oils cannot be distinguished. The accuracy is only about 50 %. The AE energies of the three different MWFs ReF, E2, and O2 can be accurately clustered with 96 %.

In cases of the three tested emulsions, the used clustering algorithm delivers a satisfactory result. The emulsions with different compositions are clustered with 100 % accuracy for series 2 and 3 and with 93 % accuracy for series 9 and 10. For the tested lubricating oils, the clustering approach is not successful.

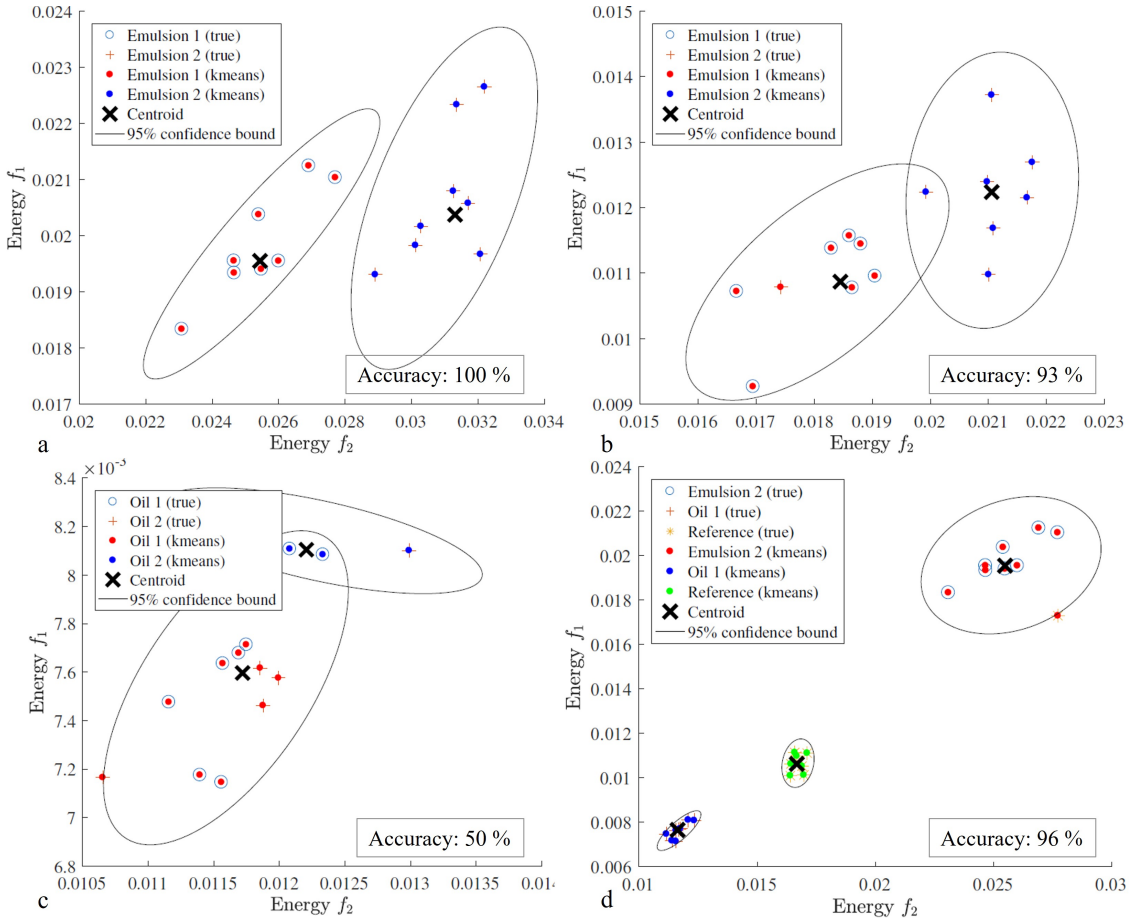

Figure 5.4: Clustering results for dataset 2016 [9]
a: Emulsion series 2 and 3
b: Emulsion series 9 and 10
c: Oil series 4 and 5
d: Different MWF types

Table 5.1: Accuracy of k-means clustering results for dataset 2016

Series	**TC**	**FC**	**Accuracy=TC/(TC+FC)**
E1 and E2, series 2 and 3	16	0	100 %
E1 and E2, series 10 and 9	14	1	93 %
O1 and O2, series 4 and 5	8	8	50 %
ReF, E2, and O1	22	1	96 %

5.1.3 Acoustic Emission signal classification in time-domain by CNN for dataset 2016

Results in this subsection have been published in [10].

The third approach, application of CNN on AE raw data, is applied on dataset 2016. Using data from eleven measurement series, it is the aim to classify five different fluids: ReF, E1, E2, O1, and O2. The fluids have been described in Table 3.2. For ReF, AE data is taken from series: 1, 6, and 11. For the other MWFs, AE data comes from two different series listed in Table 3.3. The process of signal selection and segmentation has been described in Section 4.3.3. By describing the results, the following classification goals are aimed at:

1. rough sample division into three classes: ReF, water-based (E1, E2), and oil-based (O1, O2). For ReF, data from series 1 is employed. For water-based MWFs, AE data in series 2, 3, 9, and 10 are categorized into one class. For oil-based MWFs, AE data in series 4, 5, 7, and 8 are categorized in one class.
2. sub-division of water-based MWF into two classes: E1 and E2. To distinguish between E1 and E2, data acquired in series 2 and 10 are put in one class and data gotten from series 3 and 9 are categorized in a second class.
3. sub-division of oil-based fluids into two classes: O1 and O2. To distinguish between O1 and O2, data acquired in series 4 and 8 are put in one class and data gotten from series 5 and 7 are categorized in a second class.

Table 5.2: Classification results for dataset 2016 and CNN approach acc. to [10]

Step	**MWF type**	**Test accuracy [%]**					
		1	2	3	4	5	Mean
1	ReF/Oil/ Emulsion	70.17	71.20	71.84	70.18	72.95	71.27
2	E1/ E2	80.71	78.47	79.09	81.00	79.87	79.83
3	O1/ O2	70.21	73.87	61.71	70.48	67.54	68.76

The results for the proposed CNN approach are given in Table 5.2. The following conclusions can be drawn:

1. Test accuracies in all steps range from 61.71 to 81.00 %.
2. The lowest deviation between the five calculated test accuracies is in step 2, the widest in step 3.
3. The highest mean test accuracy is reached in step 2 with 79.83 %.
4. Test accuracy in step 3 is the lowest with 68.76 % in average.
5. From the results of step 2 and step 3, the following assumption can be drawn: E1 and E2 can be easier distinguished than O1 and O2. Concluding, water-based MWF are easier to distinguish by the proposed CNN model than oil-based MWF. This result is similar to the k-means clustering result.

5.1.4 Summary and conclusions for dataset 2016

This section includes comparison and discussion of the results of all approaches for dataset 2016. Furthermore, open or unresolved points will be taken up again.

Table 5.3: Ability of approaches to classify fluids in dataset 2016

Classification goal	***Norm-TT-means***	***Clust-CWT-AE-energy***	***Raw-AE-CNN***
ReF/Oil/Emulsion	Yes (95 %)	Yes (96 %)	No (71.27 %)
E1/E2	Yes (95 %)	Yes (100 %)/ No (93 %)	No (79.83 %)
O1/O2	Yes (95 %)/No	No (50 %)	No (68.76 %)

There were three classification goals: at a confidence level of 95 %, distinction i) between ReF, lubricating oils, and emulsions, ii) between E1 and E2, and iii) between O1 and O2. By the approach *norm-TT-means*, all three classification goals could be reached but for oils, the distinction was only possible for one of two comparisons. By approach *clust-CWT-AE-energy*, it was possible to distinguish between ReF, E2, and O1 wit an accuracy of 96 %. The classification accuracy of emulsions was only for one of two comparisons higher than 95 %. The distinction of oils was not possible. By approach *raw-AE-CNN*, the classification goal of 95 % confidence level could not be reached in any case. The highest accuracy was 79.83 % for the emulsions.

As a result for dataset 2016, the approaches *norm-TT-means* and *clust-CWT-AE-energy* performed satisfactory. The results of *raw-AE-CNN* were not good. Possibly, AE raw signals are not suitable for classification tasks or the proposed CNN architecture including signal selection and segmentation would have to be improved for dataset 2016.

As has been shown in Section 5.1.1, means of ReF are less affected by the lubricating oils than E1 and E2. From these results could be concluded that ester containing reference fluid could lubricate too well and thus could mask progressing tool wear. For detection of tap wear during TTT, an ester-free emulsion could be more suitable. This fluid would probably be subject to larger fluctuations around the mean value because the measurements are more strongly influenced by the previously measured fluids. This disadvantage must be weighed against the eventual masking of wear. Further experiments must be performed for identification of the best suitable reference fluid for monitoring tap wear in this experimental design.

5.2 Dataset 2019

The result part for datset 2019 is subdivided into four parts. Firstly, results of tapping torque mean values according to approach *norm-TT-means* are explained. Secondly, clustering results of AE energies according to approach *clust-CWT-AE-energy* are shown. Thirdly, CNN results of approach *raw-AE-CNN* are presented. In the fourth part, these three approaches are compared in respect to their classification ability.

5.2.1 Tapping torque means for dataset 2019

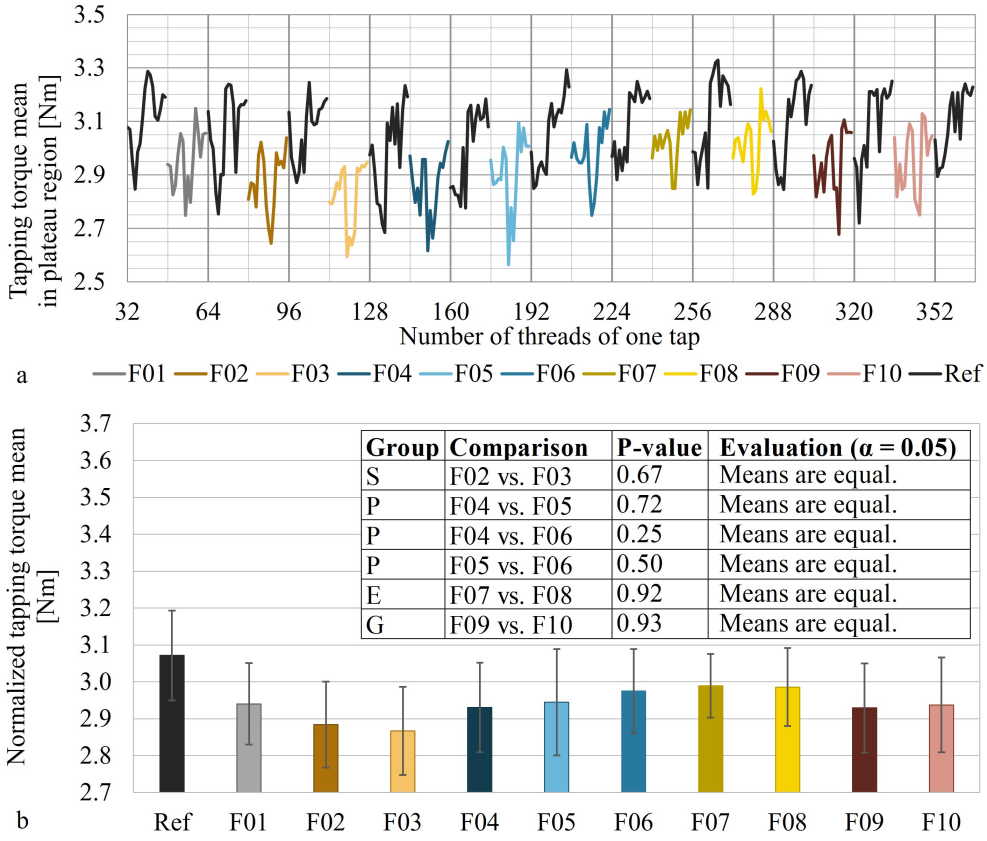

Group	Comparison	P-value	Evaluation (α = 0.05)
S	F02 vs. F03	0.67	Means are equal.
P	F04 vs. F05	0.72	Means are equal.
P	F04 vs. F06	0.25	Means are equal.
P	F05 vs. F06	0.50	Means are equal.
E	F07 vs. F08	0.92	Means are equal.
G	F09 vs. F10	0.93	Means are equal.

Figure 5.5: Results of *norm-TT-means* [11]
a: Mean of tapping torque per thread
b: Results of two-sided t-test with $\alpha = 0.05$ and normalized means including standard deviation

The results of TTT are depicted in Figure 5.5. In Figure 5.5a, raw data of tapping torque in the plateau region of each thread is shown. Raw data is highly fluctuating.

Even carryover effects of previously measured fluids are not recognizable. Wide standard deviations are expected for the means.

The normalized means and their standard deviations are depicted in Figure 5.5b. These means are analyzed using a two-sided t-test applying a confidence level of 95% (error probability $\alpha = 5$ %). For evaluation of statistical differences, the error probability α is compared with the resulting p-values. The p-values are listed in the integrated table in Figure 5.5b. If the p-value is smaller than the corresponding error probability α of 0.05, the compared values are significantly different. In the present cases, the statistical tests reveal that all compared means are not distinguishable. Conclusively, it is not possible to differentiate between the fluids within one group by tapping torque mean evaluation.

5.2.2 K-means clustering of Acoustic Emission energy for dataset 2019

For the current measurements, the main frequency bands are chosen manually. From Figure 4.1, it can be concluded that the main frequency bands of the present experiments are from 50 to 108 kHz and from 217 to 464 kHz. Within these bands the sum of AE energy is calculated. Energies are mapped as data points in diagrams according to [9] and depicted in Figure 5.6a-d. Then, k-means clustering with a confidence bound of 95 % is applied for each comparison. Clustering is evaluated as being true clustered if a blue point is surrounded by a blue circle and a red point is covered by a red cross. The compared fluids are more distinguishable if more (true) data points are within their corresponding cluster (kmeans).

Table 5.4: Accuracy of results of approach *clust-CWT-AE-energy* [11]

Comparison	**TC**	**FC**	**Accuracy=TC/(TC+FC)**
Group S	22	8	73 %
Group P	16	23	41 %
Group E	12	18	40 %
Group G	28	4	88 %

In Table 5.4, the numbers of true and false clustered data points resulting from the pictures in Figure 5.6 are noted. Accuracies listed in the last column are calculated from true and false clustered data points.

The comparison in group G reaches the highest accuracy of all groups: Fluids F09 and F10 are truly clustered with 88 % accuracy. The two different glycol types used as additives in these fluids can be distinguished. Fluid F02 and F03 can be clustered correctly with 73 % accuracy. The other comparisons only reach accuracies even lower than 50 %. Conclusively, the approach does not reach accuracies

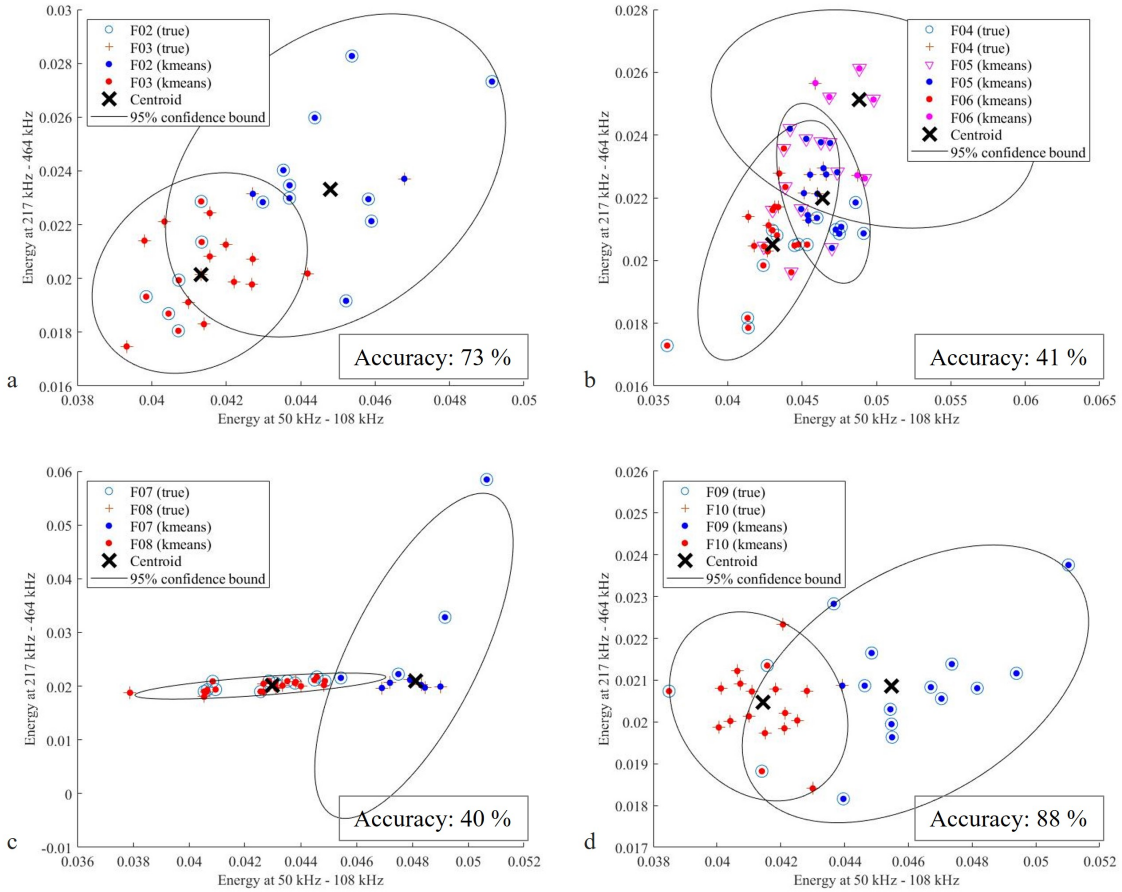

Figure 5.6: K-means clustering results of *clust-CWT-AE-energy* [11] for
a: F02 and F03
b: F04, F05, and F06
c: F07 and F08
d: F09 and F10

higher than 95 %. The approach *clust-CWT-AE-energy* is not suitable for the differentiation of fluids that contain chemically very similar additives. Using k-means clustering, it is not possible to differentiate the investigated polysulfides. Phosphates and ester additives are clustered with no satisfying accuracy. It remains unsolved to differentiate all fluids within one additive group using *clust-CWT-AE-energy*.

5.2.3 Acoustic Emission signal classification in time-domain by CNN for dataset 2019

Results of CNNs are mainly affected by division of the used samples. In the used approach, samples are divided into training, validation, and test data. The ration

among them is: 0.7 : 0.15 : 0.15 according to [258].

To verify the robustness of the model, each step is calculated five times by shuffling the samples each time. Resulting test and average accuracies are shown in Table 5.5.

Table 5.5: Test accuracy [%] for approach *raw-AE-CNN* acc. to [11]

Method no.	**Output classes**	**1st**	**2nd**	**3rd**	**4th**	**5th**	**Mean**
1	11 categories	95.8	93.7	97.9	97.9	97.9	96.6
2	6 categories	96.4	97.3	96.4	97.8	96.0	96.8
2	Fluids 02/03	98.5	98.5	95.6	95.6	100.0	97.7
2	Fluids 04/05/06	96.2	94.2	98.1	94.2	93.3	95.2
2	Fluids 07/08	100.0	100.0	100.0	100.0	100.0	100.0
2	Fluids 09/10	98.6	98.6	100.0	100.0	100.0	99.4

Metalworking fluids are divided differently to compare the accuracies of the different methods. For method no. 1, eleven MWFs are categorized into eleven classes. For method no. 2, eleven MWFs are divided firstly into six classes and then secondly each class is sub-categorized in detail. The average test accuracy for method no. 1 and for eleven MWFs is 96.6 %. For method no. 2, the test accuracy is 96.8 % for six classes. Sub-categorization into additive groups achieves test accuracies between 95.2 and 100 %. These results are very satisfactory for MWF distinction.

5.2.4 Summary and conclusions for dataset 2019

The objectives of this work are to investigate advantages and limits of the three known evaluation approaches by means of a very challenging dataset. The performance of each approach is examined to evaluate if it is usable or not. The best performing approach is chosen by its ability to differentiate fluids within one additive group.

To evaluate usability and performance of the three applied approaches, the ability of each approach to differentiate fluids of one group are summarized in Table 5.6. If a differentiation is possible with a confidence level of minimum 95 %, the corresponding accuracy is inserted. The statistical two-sided t-test of normalized torque means (*norm-TT-means*) showed that tapping torque means cannot be statistically distinguished. Although the approach of k-means clustering of AE energies (*clust-CWT-AE-energy*) reached partly better results than *norm-TT-means*, there was no result higher than 95 %. Only the approach applying a CNN on the raw data of AE

Table 5.6: Ability of approaches to classify fluids within one additive group [11]

Group	***Norm-TT-means***	***Clust-CWT-AE-energy***	***Raw-AE-CNN***
S	No	No	Yes (97.7 %)
P	No	No	Yes (95.2 %)
E	No	No	Yes (100.0 %)
G	No	No	Yes (99.4 %)

signals (*raw-AE-CNN*) achieved successful classification results for all fluid groups with averaged test accuracies even up to 100 %.

Tapping Torque Tests are used in industry to evaluate the lubricity of MWF. Test methods relying only on torque measurement provide a limited differentiability between test fluids of the same type. Especially for very small differences regarding the chemical structure of the used fluid components, so called additives, tapping torque alone is not sensitive enough to show these differences between the fluids. To enhance sensitivity and interpretability of TTT, AE measurement is added to the torque measurement. This new test setup can be denoted as extended TTT.

In this contribution, eleven different water-mixed MWFs are investigated during an extended TTT. These test fluids differ only in one additive and are structured into known additive groups related to the used chemical additives. The specialty of this dataset is the high similarity between the fluids. The main objective is to clarify whether it is possible to detect these very specific chemical differences in MWF using an extended TTT. The fluids are investigated during thread forming in unalloyed steel using a coated tap. Acoustic Emission signals are recorded in parallel to the torque measurement.

The differentiability of the fluids is evaluated by three different approaches. The first approach evaluates the normalized tapping torque means by a statistical two-sided t-test. At a confidence level of 95 %, no differentiation of fluids within one additive group is possible. The second approach uses data of the AE measurement. After CWT, energies of AE signals from two main frequency ranges are summarized. Sums of AE energy of fluids in one group are plotted in one diagram. By applying a k-means clustering algorithm, it is checked if the fluids are true or false clustered. The highest accuracy of 88 % is obtained for the fluids in the glycol group. The required accuracy is 95 %. Thus, the proposed approach is evaluated as not suitable.

The best classification results are obtained by the third approach using AE raw data. Applying a suitably designed CNN with tuned hyperparameters and several different layers, test accuracies between 95 and 100 % can be achieved. Diethylene glycol and polypropylene glycol can be distinguished. In the phosphorus group, an averaged accuracy of 95 % can be achieved so it is possible to distinguish between

a lauryl ethylene oxide phosphate and an oleyl ethylene oxide phosphate. The best classification result is obtained for the fluids in the ester group. Here, an accuracy of 100 % can be achieved so it is possible to distinguish between a 2-ethylhexylcocoate and a synthetic polymeric ester. Applying the third approach using CNN, a distinction of chemically very similar additives in water-mixed MWFs is possible.

The AE-based classification of MWFs in TTTs is possible even for a small MWF change. The additives can be differentiated directly but the lubricity can not be determined by the proposed approach.

Therefore, it is not possible to decide which additives result in higher or lower lubrication. Analyzing tapping torque means the conclusion – the lower the resulting values the better the lubricating effect – can be drawn. A similar connection for AE-related features could be possible: The lower the AE energy the higher is the lubricity of the test fluid which had to verified by practical wear tests. By the CNN approaches presented in this work, this statement is not possible yet. The ultimate goal to differentiate MWFs for evaluation of lubricity is actually not reached.

5.3 Transfer Learning

This section is mainly taken from publication [12].

Different metrics can be used to evaluate training and test. In many recent contributions [10, 217, 252], accuracy as the metric denoting the ration between the total number of correct predictions and the total number of predictions for a dataset is applied. However, as performance measure, accuracy is inappropriate for imbalanced classification problems. Precision and recall are alternatives. Precision quantifies the number of positive class predictions that actually belong to the positive class while recall quantifies the number of positive class predictions made out of all positive examples in the dataset. F-score provides a suitable step that balance both the concerns of precision and recall in one number [252].

In most classification problems, imbalanced class distribution exists, so F-score is a suitable alternative metric. For the proposed approach *STFT-AE-TL*, F-score is applied as main metric. To compare with results in other contribution, accuracy is applied as metrics in both datasets. Cross validation is a re-sampling procedure used to evaluate machine learning models. Generally, results from cross validation have a lower bias than other methods [259]. To eliminate bias and check robustness of proposed approach, 4-fold cross validation is applied to evaluate trained models.

Knowledge and parameters in data processing as well as hyperparameter in convolutional neural networks are transferred from dataset 2019 to dataset 2016. Detailed results of both datasets are shown in Table 5.7. For dataset 2019, F-score for each

Table 5.7: Test results [%] of 4-fold cross validation of approach *STFT-AE-TL* [12]

Dataset	**Result [%]**					
	F-score of each fold					**Accuracy**
	1st	**2nd**	**3rd**	**4th**	**Mean**	
2019	98.58	98.80	98.15	98.92	98.61	98.58
2016	70.30	91.30	94.51	91.30	86.85	86.20

fold ranges from 98.15 % to 98.92 % and the mean F-score is 98.61 %. The accuracy for dataset 2019 is 98.58 %. When the CNN model is transferred to dataset 2016, the F-score ranges from 70.30 % to 94.51 % and mean F-score is 86.85 %. Accuracy for dataset 2016 is 86.20 %. It can be concluded that approach *STFT-AE-TL* trained from water-based MWF distinction could be successfully transferred to other kinds of MWF classification tasks.

As conclusion, classification results for dataset 2016 are better than in Section 5.1.3. AE signals of same kinds of MWFs are classified by CNN which trained by dataset 2016 itself. AE signal features are extracted in time domain. Five kinds of MWF are firstly divided into three categories and then water-based and oil-based MWF are subdivided. The best classification accuracy is 79.87 % and the worse result is 67.54 %. Approach *STFT-AE-TL* using TL from dataset 2019 to dataset 2016 outperforms approach *raw-AE-CNN*.

Comparing with approach *raw-AE-CNN*, the following conclusions can be drawn from the results of TL:

- Two datasets are calculated and 16 MWFs are classified in total.
- Segments are transformed into time-frequency domain and the resulting spectrograms are used as CNN input. In approach *raw-AE-CNN*, images of AE raw data have been used.
- Spectrograms are normalized before their features are extracted in CNN.
- Structure of CNN is more detailed and hyperparameters are optimized automatically. In approach *raw-AE-CNN*, hyperparameters are tuned manually.
- Although results in dataset 2016 are not as good as in dataset 2019, they have been significantly improved in comparison to the obtained classification accuracy of approach *raw-AE-CNN*.

6 Summary, conclusion, and outlook

Measurement and evaluation of lubricity are necessary to qualify lubrication performance of MWFs. Tapping Torque Tests conducted in laboratory scale are near-to-practice tests transferable into real industrial applications. Current challenges are related to the sensitivity of this test. Test fluids often cannot be distinguished. The goal is the detection of even very small differences in MWFs in order to i) save resources in the development of new MWFs – following the principle "only as much as necessary", ii) monitor the condition of MWFs in use – always keeping the best lubrication condition, iii) predict maintenance tasks – when change of aged MWF is necessary. Related contributions presented in this thesis contribute to the fundamentals of these goals. The first part deals with a critical discussion of the current TTT method and includes proposals for better distinguishability based on the existing measurement system. The second part is about a feasibility study of implementing AE measurement into the TTT system, namely extended TTT. In the third part, benefits and limitations of AE signals are shown by testing different classification approaches for a dataset of challenging MWF compositions. In this chapter, the whole thesis work is summarized, the important conclusions are repeated, and suggestions for future work are given.

6.1 Summary and conclusion

Regarding the use of AE for qualification of MWFs and real-time techniques for monitoring of tribological conditions, the following main research questions are established in this thesis:

- Do changes in test procedure and tapping torque mean calculation lead to improved distinguishability of test fluids in TTTs?
- Can changes in the interaction between tool and workpiece surfaces and in MWF compositions be detected by AE signals?
- Is AE more suitable than torque as measure in TTTs?
- Can clustering or CNN classification approaches enhance the accuracy of MWF distinction?
- Is AE technique suitable for online process monitoring especially for MWF's condition and/or tribological state evaluation?
- Could predictive maintenance tasks for MWFs be realizable through AE signals and neural networks?
- Could AE technique significantly contribute to resource saving in development of new MWFs?

These questions are mostly addressed in this thesis by presenting research results contributed to journals or conferences.

In Chapter 2, literature research of MWFs in machining is presented focusing recent monitoring techniques and lubricating mechanisms of additives. No online measurement technique is available monitoring the performance of MWFs during the process.

Additionally, Chapter 2 contains a review about AE techniques used in process monitoring. Contents of this part are related to publication [8]. Tool condition monitoring techniques are widely spread and AE technique has already been used in turning, drilling, and milling processes. There are only few contributions about AE technique used to examine lubrication states or different lubricants in tribological contacts. No contribution is known examining single components of MWF by AE during a real machining operation.

Basics of Machine Learning approaches are also introduced in Chapter 2. Different approaches have been successfully used in tribological processes to detect tool wear and to identify lubrication regimes. The functionality of CNNs is described. No contribution is known applying Machine Learning for condition monitoring of MWFs or for identification of different MWF additives.

In Chapter 3, two experimental datasets are introduced: datasets 2016 and 2019. Dataset 2016 consists of five different fluids. Fluids to be distinguished vary in phosphorus contents. Dataset 2019 consists of eleven different fluids. One novelty of this work are the specifically designed water-mixed test fluids of dataset 2019. A special MWF base concentrate has been developed allowing a direct comparison of the changed additives. These additives can be sorted into four groups: sulfur, phosphorus, ester, glycol. The goal is to distinguish fluids that are in the same group and vary only in concentration of one element or in the molecule structure of the used additive.

The evaluation approaches to classify fluids of datasets 2016 and 2019 are introduced in Chapter 4. Research on TTT is presented in this chapter including findings published in [98]. The current test method ASTM D8288-19 does not always allow a distinction of MWFs. The following suggestions for enhancement of distinguishability and repeatability are made:

- The running-in phase of new taps have to be completed before starting the test procedure with test fluids. End of this phase can be determined by a stationary criterion based on previously determined means. Misinterpretations could be avoided.
- Carryover effects of previously measured fluids have to be considered in the calculation of torque means. The extent of their influence depends on the composition of the fluids. Each measurement series has to be evaluated individually. Repeatability and distinguishability of TTT results could be improved.

- Regular reference measurements are necessary to observe proceeding tool wear over all measurement series with one tap. The reference means have to be used to normalize the torque means of test fluids. Comparability between measurements with new taps and workpieces is established.

By implementing regular reference measurements in the test order and considering running-in and carryover effects in mean calculations, repeatability, comparability, and distinguishability of TTTs can already be improved. In this chapter, the method of k-means clustering is introduced. Sum of AE energy is calculated in two main frequency bands as first has been used in [9]. Concerning CNNs, the architectures are described. Optimization loop and pre-filtering of data are explained. The principle of TL and the architecture of the used CNN model are presented. The CNN is trained and optimized with dataset 2019. Afterwards, knowledge and parameters in data processing as well as hyperparameters of CNN are transferred to dataset 2016.

In Chapter 5, results for both datasets are presented. These can be summarized by the following points:

- Tapping torque means allow distinction of MWFs if their differences are larger as they are in dataset 2016. Different chain lengths of molecules or element concentrations differing only around factor 2 as they are in dataset 2019 cannot be reliably differentiated.
- Using k-means clustering technique, dependence between AE and lubrication conditions can be used to distinguish MWF types. Emulsions can be reliably separated from oils.
- Approaches evaluating tapping torque means and methods using k-means clustering of AE energies have similar classification abilities. Their sensitivity is not good enough to differentiate very small changes in MWFs.
- Applying CNN as classification method, MWFs even with very small differences can be distinguished. Images of AE signals transformed by STFT are more suitable than images of raw AE signals.
- Transfer Learning from dataset 2019 to dataset 2016 using AE data in time-frequency domain reaches better classification results than a CNN specifically designed for dataset 2016 but using AE data in time-domain.

To address the research gaps and scientific goals from Section 2.5, new findings and claims of this thesis can be summarized as follows:

- In performing TTTs, running-in phase of taps, carryover effects of fluids, and regular reference measurements can increase repeatability, comparability, and distinguishability of test results. Large differences in concentrations of same lubricating additives are detectable by considering these principles.

- Interactions between tool and workpiece can be detected by AE measurements. Acoustic Emission energy and torque are closely related to changes in lubrication conditions. However, AE provides a more accurate representation of the thread forming process.
- Only certain and specifically designed pre-filters allow a detailed look into the temporal behavior of the machining operation by AE signals. Wear and/or lubrication monitoring are possible by applying specific methods of data processing.
- Tapping torque measurement is not as sensitive as AE measurement for very small MWF changes. But for good classification accuracies, Machine Learning algorithms such as neural networks have to be applied on AE signals. Signal processing, selection, and segmentation have significant impact on the classification results.
- Signal transformation, selection of measurements, and segmentation of signals improve the extracting process of signals features. The optimization process of these pre-filters in a CNN can be designed time-saving by including them into the optimization loop of the complete training procedure including filters and hyperparameters. The best result is the parameter set achieving the highest classification accuracy.
- Applying an optimized CNN using spectrograms of AE signals as input, MWFs that differ only slightly chemically can be distinguished with an accuracy higher than 95 %. This approach is very sensitive for very small MWF changes and opens new possibilities for fluid condition monitoring systems.
- Structure and other hyperparameters of trained models from water-based MWF classification can be transferred to similar classification tasks to successfully distinguish other water-based and oil-based MWFs.
- The MWF additives are successfully distinguished in the classification using CNN. However, no statement can be made about the lubricating effect of the individual additives. The neural network only detects differences in images of AE signals. A conclusion which test fluid performs better is recently not possible from this point.

The recent work shows relevant potential of neural networks and AE technique for process monitoring during machining. The results reveal that tribological interaction – friction, wear, and lubrication – can be measured by AE. Monitoring of the tribological contact including tool and MWF could be realized using AE technique and artificial intelligence.

6.2 Outlook

The shown results open completely new possibilities for fluid development, analysis, and monitoring in use. Further developments of neural networks for AE signals

could focus the lubricity of MWFs so that the statement which additive is better for the tribological process would be possible. For this, real machining trials would be necessary to evaluate the MWF's effects on tool wear and surface qualities. Chemical analysis of surfaces would be important to support results and to increase the knowledge about reactions of additives.

If classification of such small changes in MWFs is possible by AE signals, it will probably be possible to monitor the aging of MWFs. This could be addressed in future work. Additionally, the shown results could be interpreted with focus on the evaluation of fluids' lubricity. To the best of my knowledge, no explanation is known so far why MWF additives generate different AE signals. Deeper investigations about the lubrication mechanism for each additive may contribute to a better understanding of lubricants' functionality in tribological contacts.

AE is considered as a valuable tool for in-situ monitoring of wear to be used in future investigations to develop an in depth understanding of the fundamental mechanisms in surface interactions governing wear phenomena.

In the future, an in-situ condition monitoring and fluid management could be used during a fully automated machining process without human interruption. Changes in fluid characteristics would be detected by the automation system and relevant additives automatically dosed. Additionally, the MWF could be adapted to another workpiece material. Using artificial intelligence algorithms in such monitoring systems could make processes more reliable. Predictive maintenance could be an interesting application field for saving resources in manufacturing.

Bibliography

[1] V. N. Kostyukov, A. V. Kostyukov, Real-time condition monitoring of machinery malfunctions, Procedia Eng 113 (2015) 316–323.

[2] J. Tlusty, G. C. Andrews, A Critical Review of Sensors for Unmanned Machining, Annals of the CIRP 32 (2) (1983) 563–572.

[3] R. S. Pawade, S. S. Joshi, P. K. Brahmankar, M. Rahman, An investigation of cutting forces and surface damage in high-speed turning of Inconel 718, J Mater Process Technol 193 (2007) 139–146.

[4] B. J. Roylance, Machine failure and its avoidance - what is tribology ' s contribution to effective maintenance of critical machinery ?, in: Donald Julius Groen Prize Lecture 2002, 2002, pp. 349–364.

[5] A. Steininger, A. Siller, F. Bleicher, Investigations regarding process stability aspects in thread tapping Al-Si alloys, Procedia Eng 100 (January) (2015) 1124–1132.

[6] R. Teti, K. Jemielniak, G. O. Donnell, D. Dornfeld, Advanced monitoring of machining operations, CIRP Ann Manuf Technol 59 (2010) 717–739.

[7] A. Verl, U. Heisel, M. Walther, D. Maier, Sensorless automated condition monitoring for the control of the predictive maintenance of machine tools, CIRP Ann Manuf Technol 58 (2009) 375–378.

[8] A. L. Demmerling, D. Söffker, Condition monitoring: A review on real-time measurement techniques for tool condition monitoring and analysis of metalworking fluids, in: K. Nienhaus (Ed.), AKIDA - The Maintenance, Monitoring and Control Conference, Aachen, 2016, pp. 191–208.

[9] S. F. Wirtz, A. L. Demmerling, D. Söffker, In-situ wear monitoring: An experimental investigation of Acoustic Emission during thread forming, in: Proceedings of Structural Health Monitoring, USA, Stanford, 2017, pp. 1198–1205.

[10] X. Wei, A. L. Demmerling, D. Söffker, Metalworking Fluid Classification Based on Acoustic Emission Signals and Convolutional Neural Network, in: Proceedings of the 6th European Conference Prognostics and Health Management Society, 2021, pp. 471–476.

[11] A. L. Demmerling, X. Wei, D. Söffker, Extended tapping torque test to differentiate metalworking fluids, Tribol Int 175 (107819) (2022) 1–9.

[12] X. Wei, F. Jochmann, A. L. Demmerling, D. Söffker, Application of Transfer Learning in metalworking fluid distinction, in: Proc ASME 2022, IDETC-CIE, St. Louis, Missouri, 2022.

[13] L. Shuyi, G. Feng, W. Pat, L. Xinming, Numerical analysis of lubrication of conformal contact with discontinuous oil droplets, Tribol Int 173 (107632) (2022) 1–11.

[14] V. G. Shram, A. V. Lysyannikov, M. A. Kovaleva, The Mechanism of Lubricants Protective Layers Formation in Friction Sliding, Procedia Eng 150 (2016) 458–463.

[15] M. Moghadam, M. Villa, P. Moreau, A. Dubois, L. Dubar, C. V. Nielsen, N. Bay, Analysis of lubricant performance in punching and blanking, Tribol Int 141 (105949) (2020) 1–8.

[16] J. L. Teh, R. Walvekar, T. Nagarajan, Z. Said, M. Khalid, N. M. Mubarak, A review on the properties and tribological performance of recent non-aqueous miscible lubricants, J Mol Liq 366 (120274).

[17] C. Bienefeld, E. Kirchner, A. Vogt, M. Kacmar, On the Importance of Temporal Information for Remaining Useful Life Prediction of Rolling Bearings Using a Random Forest Regressor, Lubricants 10 (67) (2022) 1–12.

[18] D. E. Sander, H. Allmaier, H. H. Priebsch, M. Witt, A. Skiadas, Simulation of journal bearing friction in severe mixed lubrication – Validation and effect of surface smoothing due to running-in, Tribol Int 96 (2016) 173–183.

[19] S. Jiang, S. Li, L. Liu, L. Wang, N. Mominou, The tribological properties and tribochemical analysis of blends of poly alpha-olefins with neopentyl polyol esters, Tribol Int 86 (2015) 42–51.

[20] X. Jin, T. W. S. Chow, Anomaly detection of cooling fan and fault classification of induction motor using Mahalanobis – Taguchi system, Expert Syst Appl 40 (15) (2013) 5787–5795.

[21] J. Hu, L. Zhang, W. Liang, Dynamic degradation observer for bearing fault by MTS – SOM system, Mech Syst Signal Process 36 (2) (2013) 385–400.

[22] X. Yan, Z. Li, C. Yuan, Z. Guo, Z. Tian, C. Sheng, On-line Condition Monitoring and Remote Fault Diagnosis for Marine Diesel Engines Using Tribological Information, Chemical Engineering Transactions 33 (2013) 805–810.

[23] A. Soylemezoglu, S. Jagannathan, C. Saygin, Mahalanobis-Taguchi System as a Multi-Sensor Based Decision Making Prognostics Tool for Centrifugal Pump Failures 60 (4) (2011) 864–878.

[24] B. Denkena, B. Bergmann, L. Ellersiek, Kühlschmierstoff-Einsatz unter der Lupe, Diamond Business 4 (2022) 62–63.

[25] D. Biermann, M. Kirschner, Wahl des Kühlschmierstoffkonzeptes als Schlüssel zum Erfolg, Werkstoffe in der Fertigung 5 (2015) 26–29.

[26] Q.-P. Tran, V.-N. Nguyen, S. Huang, Drilling Process on CFRP : Multi-Criteria Decision-Making with Entropy Weight Using Grey-TOPSIS method, Appl Sci 10 (20) (2020) 7207.

[27] Deutsche Gesetzliche Unfallversicherung, Minimum quantity lubrication for machining operations, DGUV Information 209-025 November (2010) 1–84.

[28] T. Meier, M. Seydaack, D. Gross, N. Hanenkamp, Investigation of the influence of the additivation of a biological metalworking oil in cryogenic machining, Procedia CIRP 105 (2022) 694–699.

[29] M. Q. Saleem, A. Mehmood, Eco-friendly precision turning of superalloy Inconel 718 using MQL based vegetable oils : Tool wear and surface integrity evaluation, J Manuf Process 73 (July 2021) (2022) 112–127.

[30] G. Wu, G. Li, W. Pan, I. Raja, X. Wang, S. Ding, Experimental investigation of eco-friendly cryogenic minimum quantity lubrication (CMQL) strategy in machining of Ti–6Al–4V thin-wall part, J Clean Prod 357 (131993).

[31] W. Yu, J. Chen, W. Ming, Q. An, M. Chen, Feasibility of supercritical CO2-based minimum quantity lubrication to improve the surface integrity of 50% Sip/Al composites, J Manuf Process 73 (2022) 364–374.

[32] C. P. Khunt, M. A. Makhesana, K. M. Patel, B. K. Mawandiya, Performance assessment of vegetable oil-based minimum quantity lubrication (MQL) in drilling, Mater Today Proc 44 (2021) 341–345.

[33] I. C. Pereira, M. B. Da Silva, D. F. Da Cunha, W. F. Sales, Analysis of tapping process in three types of cast iron, Int J Adv Manuf Technol 82 (5-8) (2016) 1041–1048.

[34] M. Liu, C. Li, Y. Zhang, Q. An, M. Yang, T. Gao, C. Mao, B. Liu, H. Cao, X. Xu, Z. Said, S. Debnath, M. Jamil, H. M. Ali, S. Sharma, Cryogenic minimum quantity lubrication machining : from mechanism to application, Front Mech Eng 16 (4) (2021) 649–697.

[35] J. Lopes, F. Ribeiro, S. Linkevicius, M. De Souza Rodrigues, R. R. De Souza, B. K. Sato, D. L. De Moraes, M. V. Garcia, L. E. De Angelo Sanchez, E. C. Bianchi, Manufacturing process linked to the MQL compared to flood lubrication applied to the grinding of VP50IM steel using black silicon carbide wheel, Int J Adv Manuf Technol 120 (2022) 4179–4190.

[36] Deutsche Gesetzliche Unfallversicherung, Tätigkeiten mit Kühlschmierstoffen, DGUV Rule 109-003 (2011) 1–104.

[37] L. Dong, C. Li, F. Zhou, X. Bai, W. Gao, Z. Duan, X. Li, X. Lv, F. Zhang, Temperature of the 45 steel in the minimum quantity lubricant milling with different biolubricants, Int J Adv Manuf Technol 113 (2021) 2779–2790.

[38] T. P. Jeevan, S. R. Jayaram, Tribological Properties and Machining Performance of Vegetable Oil Based Metal Working Fluids — A Review, Modern Mechanical Engineering 8 (2018) 42–65.

[39] O. Damm, M. Bezuidenhout, E. Uheida, L. Dicks, W. Hadasha, D. Hagedorn-Hansen, Yeast-based metalworking fluid for milling of titanium alloy — An example of bio-integration, CIRP J Manuf Sci Technol 34 (2021) 47–60.

[40] E. Benedicto, E. M. Rubio, D. Carou, C. Santacruz, The Role of Surfactant Structure on the Development of a Sustainable and Effective Cutting Fluid for Machining Titanium Alloys, Metals 10 (1388) (2020) 1–14.

[41] M. M. R. Nune, K. P. Chaganti, Performance evaluation of novel developed biodegradable metal working fluid during turning of AISI 420 material, Journal of the Brazilian Society of Mechanical Sciences and Engineering 42 (319).

[42] G. Fromentin, A. Bierla, C. Minfray, G. Poulachon, An experimental study on the effects of lubrication in form tapping, Tribol Int 43 (9) (2010) 1726–1734.

[43] N. C. Ghuge, Influence of Cutting Fluid on Tool Wear and Tool Life during Turning, International Journal of Modern Trends in Engineering & Research 3 (10) (2016) 23–27.

[44] T. Maßmann, Additivmechanismen auf unbeschichteten und beschichteten Oberflächen, in: Wechselwirkung von Additiven mit Metalloberflächen, Expert-Verlag, 2010, Ch. 7, pp. 76–101.

[45] C. L. Ong, X. Jiang, J. Ching, N. Ghaffari, T. Heidelberg, Ashless and non-corrosive disulfide compounds as excellent extreme pressure additives in naphthenic oil, J Mol Liq 351 (118553) (2022) 1–9.

[46] G. Zheng, T. Ding, L. Zheng, T. Ren, The lubrication effectiveness of dialkylpentasul fi de in synthetic ester and, Tribol Int 122 (March) (2018) 76–83.

[47] Z. Yang, B. Guo, Y. Liang, Q. Huang, F. Li, R. Wang, X. Yan, B. Yu, Q. Yu, M. Cai, Performance of oil-soluble ionic liquids as novel lubricant additives, J Mol Liq 363 (119837) (2022) 1–11.

[48] E. Brinksmeier, D. Meyer, A. G. Huesmann-Cordes, C. Herrmann, Metalworking fluids — Mechanisms and performance, CIRP Ann Manuf Technol 64 (2) (2015) 605–628.

[49] J. Schulz, W. Holweger, Wechselwirkung von Additiven mit Metalloberflächen, Expert-Verlag, 2010.

[50] J. Schulz, E. Brinksmeier, D. Meyer, On the Interactions of Additives in Metalworking Fluids with Metal Surfaces, Lubricants 1 (2013) 75–94.

[51] A. G. Huesmann-Cordes, K. Gebert, E. Brinksmeier, J. Schulz, Untersuchung der Wirkmechanismen von Kühlschmierstoff-Additiven an unterschiedlichen Metalloberflächen, in: Sitzung des Fachausschuss 23, Frankfurt, 2013, pp. 1–29.

[52] A. G. Huesmann-Cordes, D. Meyer, J. Schulz, Influence of Additives in Metalworking Fluids on the Wear Resistance of Steels, in: Procedia CIRP CSI, Vol. 13, 2014, pp. 108–113.

[53] H. Wu, S. Yin, L. Wang, Y. Du, Y. Yang, J. Shi, H. Wang, Investigation on the robust adsorption mechanism of alkyl-functional boric acid nanoparticles as high performance green lubricant additives, Tribol Int 157 (106909) (2021) 1–9.

[54] H. Czichos, K.-H. Habig, Tribologie-Handbuch, 3rd Edition, Vieweg+Teubner Verlag, Springer Fachmedien Wiesbaden GmbH 2010, 2010.

[55] W. D. Phillips, Ashless Phosphorus - Containing Lubricating Oil Additives, in: L. R. Rudnick (Ed.), Lubricant Additives, 2nd Edition, CRC Press, 2009, Ch. 3, p. 76.

[56] U. J. Möller, U. Boor, Schmierstoffe im Betrieb, VDI Verlag, Düsseldorf, 1986.

[57] D. Kenbeck, T. F. Bunemann, Organic Friction Modifiers, in: L. R. Rudnick (Ed.), Lubricant Additives, 2nd Edition, CRC Press, 2009, Ch. 7, p. 201.

[58] R. A. McDonald, Zinc Dithiophosphates, in: L. R. Rudnick (Ed.), Lubricant Additives, 2nd Edition, CRC Press, 2009, Ch. 2, p. 58.

[59] T. Rossrucker, A. Fessenbecker, Sulfur Carriers, in: L. R. Rudnick (Ed.), Lubricant Additives, 2nd Edition, CRC Press, 2009, Ch. 9, pp. 252–278.

[60] G. Wen, X. Wen, P. Bai, Y. Meng, L. Ma, Y. Tian, Effect of mixing procedure of oleic acid and BN nanoparticles as additives on lubricant performance of PAO8, Tribol Int 175 (107842) (2022) 1–10.

[61] A. V. Bondarev, A. Fraile, T. Polcar, D. V. Shtansky, Mechanisms of friction and wear reduction by h-BN nanosheet and spherical W nanoparticle additives to base oil: Experimental study and molecular dynamics simulation, Tribol Int 151 (May) (2020) 106493.

[62] Y. Morita, T. Onodera, A. Suzuki, R. Sahnoun, M. Koyama, H. Tsuboi, N. Hatakeyama, A. Endou, H. Takaba, M. Kubo, C. A. Del Carpio, T. Shinyoshi, N. Nishino, A. Suzuki, A. Miyamoto, Development of a new molecular dynamics method for tribochemical reaction and its application to formation dynamics of MoS2tribofilm, Appl Surf Sci 254 (23) (2008) 7618–7621.

[63] Z. Guan, P. Zhang, V. Florian, Z. Wu, D. Zeng, J. Liu, B. Wang, X. Tu, S. Li, W. Li, Preparation and tribological behaviors of magnesium silicate hydroxide-MoS2 nanoparticles as lubricant additive, Wear 492-493 (204237) (2022) 1–14.

[64] Y. Cui, M. Ding, T. Sui, W. Zheng, G. Qiao, S. Yan, X. Liu, Role of nanoparticle materials as water-based lubricant additives for ceramics, Tribol Int 142 (105978) (2020) 1–7.

[65] J. Zhao, T. Gao, Y. Li, Y. He, Y. Shi, Two-dimensional (2D) graphene nanosheets as advanced lubricant additives: A critical review and prospect, Mater Today Commun 29 (March) (2021) 102755.

[66] H. S. Abdel-Hameed, S. M. El-Saeed, N. S. Ahmed, A. M. Nassar, F. El-Kafrawy, A. I. Hashem, Chemical transformation of Jojoba oil and Soybean oil and study of their uses as bio-lubricants, Ind Crops Prod 187 (PA) (2022) 115256.

[67] S. Edla, A. D. Thampi, P. Prasannakumar, S. Rani, Evaluation of physicochemical, tribological and oxidative stability properties of chemically modified rice bran and karanja oils as viable lubricant base stocks for industrial applications, Tribol Int 173 (January) (2022) 107631.

[68] C. T. Lee, B. M. Lee, S. H. Hamdan, W. W. F. Chong, C. T. Chong, H. Zhang, A. W. L. Chen, Trimethylolpropane trioleate as eco-friendly lubricant additive, Engineering Science and Technology, an International Journal 35 (101068).

[69] A. S. A. Sani, S. Baharom, N. A. Mamat, A. S. M. Rozlan, N. Talib, Comparative evaluation of crude Tamanu oil performance as metalworking fluids, Mater Today Proc 48 (2022) 1783–1788.

[70] E. Selbmann, M. Preiß, A. B. Achour, U. Teicher, A. Hänel, S. Ihlenfeldt, Investigation of bio-based cooling lubricants for the machining of aircraft Investigation of 28th cooling lubricants for the machining of aircraft stainless steels stainless steels analyze the functional and physical architecture of existing products for, Procedia CIRP 110 (2022) 47–52.

[71] M. Gul, N. Zulkifli, M. Kalam, H. Masjuki, M. Mujtaba, S. Yousufe, M. N. Bashir, W. Ahmed, M. Yusoff, S. Noor, R. Ahmad, M. T. Hassan, RSM and Artificial Neural Networking based production optimization of sustainable

Cotton bio-lubricant and evaluation of its lubricity tribological properties, Energy Reports 7 (2021) 830–839.

[72] A. Pottirayil, S. V. Kailas, S. K. Biswas, Lubricity of an oil in water emulsion in metal cutting : The effect of hydrophilic / lypophilic balance of emulsifiers, Colloids Surf A Physicochem Eng Asp 384 (1-3) (2011) 323–330.

[73] F. H. de Paula, F. A. de Freitas, D. G. Nunes, S. Iglauer, A. P. Gramatges, R. S. V. Nascimento, E. R. Lachter, Alkyl glyceryl ethers as water-based lubricant additives in mixtures with xanthan gum, Colloids Surf A Physicochem Eng Asp 634 (127881) (2022) 1–8. doi:10.1016/j.colsurfa.2021.127881.

[74] M. Masuko, M. Shibatsuji, M. Yokomizo, S. Aoki, A. Suzuki, On the effort to discriminate the principal function of tribofilm on friction under the boundary lubrication condition, Tribol Int 44 (6) (2011) 702–710.

[75] J. Airey, M. Spencer, R. Greenwood, M. Simmons, The effect of gas turbine lubricant base oil molecular structure on friction, Tribol Int 146 (106052) (2020) 1–11.

[76] B. Lin, A. K. Tieu, H. Zhu, B. Kosasih, O. Novareza, G. Triani, Tribological performance of aqueous copolymer lubricant in loaded contact with Si and coated Ti film, Wear 302 (1-2) (2013) 1010–1016.

[77] K. C. Wickramasinghe, H. Sasahara, M. Usui, Performance evaluation of a sustainable metal working fluid applied to machine Inconel 718 and AISI 304 with minimum quantity lubrication, Journal of Advanced Mechanical Design, Systems, and Manufacturing 15 (4) (2021) 1–13.

[78] M. A. Xavior, M. Adithan, Determining the influence of cutting fluids on tool wear and surface roughness during turning of AISI 304 austenitic stainless steel, J Mater Process Technol 209 (2008) 900–909.

[79] S. A. Lawal, I. A. Choudhury, Y. Nukman, Application of vegetable oil-based metalworking fluids in machining ferrous metals - A review, Int J Mach Tools Manuf 52 (1) (2012) 1–12.

[80] G. Biresaw, G. B. Bantchev, J. Lansing, R. E. Harry-O'kuru, Y. Chen, Sulfurized Methyl Esters of Soya Fatty Acids: Synthesis and Characterization, Tribol Lett 68 (61).

[81] K. S. Siow, L. Britcher, S. Kumar, H. J. Griesser, XPS Study of Sulfur and Phosphorus Compounds with Different Oxidation States, Sains Malaysiana 47 (8) (2018) 1913–1922.

[82] C. Fleming, Investigation into the behaviour of selected boundary regime lubricants when cold forging steel under rolling-sliding conditions, Tribol Int 157 (106771) (2021) 1–15.

[83] S. Bhowmick, M. J. Lukitsch, A. T. Alpas, Tapping of Al-Si alloys with diamond-like carbon coated tools and minimum quantity lubrication, J Mater Process Technol 210 (15) (2010) 2142–2153.

[84] M. N. Najman, M. Kasrai, G. M. Bancroft, Investigating binary oil additive systems containing P and S using X-ray absorption near-edge structure spectroscopy, Wear 257 (1-2) (2004) 32–40.

[85] X. Fu, L. Sun, X. Zhou, J. Li, B. Fan, T. Ren, Tribochemical behaviors of phosphite esters and their combinations with alkyl amines, Appl Surf Sci 357 (2015) 1163–1170.

[86] B. H. Kim, J. C. Jiang, P. B. Aswath, Mechanism of wear at extreme load and boundary conditions with ashless anti-wear additives: Analysis of wear surfaces and wear debris, Wear 270 (3-4) (2011) 181–194.

[87] V. S. Sharma, G. Fromentin, G. Poulachon, R. Brendlen, Investigation of tool geometry effect and penetration strategies on cutting forces during thread milling, Int J Adv Manuf Technol 74 (2014) 963–971.

[88] S. C. Bernat, Hydraulic Fluids for Offshore Applications – the Lubrication Mechanisms of Water-Based Fluids, Ph.D. thesis, NTNU Norwegian University of Science and Technology (2018).

[89] Bruker Corporation, Universal tribological testers (2017).

[90] H. Wittel, D. Muhs, D. Jannasch, J. Voßiek, Roloff/Matek Maschinenelemente, 20th Edition, Vieweg + Teubner, Springer Fachmedien Wiesbaden GmbH, 2011.

[91] Y. Liu, C. L. Jiaa, A. Eltoukhy, S. Clara, Acoustic Emission Study of Lubricant Effect On Proximity Contact Recording, IEEE Trans Magn 3 (5) (1997) 3160–3162.

[92] Rhenus Lub GmbH Co. KG, FluidSafe LubControlSystem (2016) (accessed 07.10.2016) (2016) http://www.rhenuslub.de/en/fluidsafe.html.

[93] Tiefenbach Control Systems GmbH, Prozesssichere Kontrolle und Steuerung wassermischbarer Kühlschmierstoffe, in: Schmierstoffseminar des Verbandes Schmierstoff-Industrie e.V., Cologne, 2016.

[94] Oemeta Chemische Werke GmbH, Oemeta mit Offensive für mehr Nachhaltigkeit, Diamond Business 4 (2022) 70–72.

[95] M. Appleby, F. K. Choy, L. Du, J. Zhe, Oil debris and viscosity monitoring using ultrasonic and capacitance/inductance measurements, Lubrication Science 25 (2013) 507–524.

[96] M. Menta, J. Frayet, B. Grassl, C. Gleyzes, A. Castetbon, M. Potin-Gautier, Development of an alternative analytical methodology to monitor industrial degreasing baths by dynamic light scattering, J Clean Prod 113 (2016) 981–988.

[97] E. Bordatchev, H. Aghayan, J. Yang, Object shape-based optical sensing methodology and system for condition monitoring of contaminated engine lubricants, Opt Lasers Eng 54 (2014) 128–138.

[98] A. L. Demmerling, D. Söffker, Improved examination and test procedure of tapping torque tests according to ASTM D5619 using coated forming taps and water-mixed metalworking fluids, Tribol Int 145 (106151) (2019) 1–11.

[99] U. Heisel, F. Klocke, E. Uhlmann, G. Spur, Handbuch Spanen, Carl Hanser Verlag GmbH Co. KG, 2014.

[100] G. Fromentin, G. Poulachon, A. Moisan, B. Julien, J. Giessler, Precision and surface integrity of threads obtained by form tapping, CIRP Ann Manuf Technol 54 (1) (2005) 519–522.

[101] G. Fromentin, G. Poulachon, A. Moisan, An Experimental and Analytical Method for Investigating Plastic Flow in Form Tapping, International Journal of Forming Processes 9 (4) (2006) 1–16.

[102] L. De Chiffre, W. Belluco, Comparison of Methods for Cutting Fluid Performance Testing, CIRP Ann Manuf Technol 49 (I) (2000) 57–60.

[103] A. Bierla, G. Fromentin, J.-M. Martin, T. L. Mogne, N. Genet, Tribological aspect of lubrication in form tapping of high-strength steel, Lubr Sci 20 (2008) 269–281.

[104] J. F. Landeta, A. F. Valdivielso, L. N. L. De Lacalle, F. Girot, J. M. Pérez Pérez, Wear of Form Taps in Threading of Steel Cold Forged Parts, J Manuf Sci E-T ASME 137.

[105] A. F. Clarens, J. B. Zimmerman, H. R. Landis, K. F. Hayes, S. J. Skerlos, Experimental Comparison of Vegetable and Petroleum Base Oils in Metalworking Fluids Using Tapping Torque Test, Proc JUSFA (2004) 1–6.

[106] S. L. M. Ribeiro Filho, J. T. Vieira, J. A. de Oliveira, É. M. Arruda, L. C. Brandão, Comparison among different vegetable fluids used in minimum quantity lubrication systems in the tapping process of cast aluminum alloy, J Clean Prod 140 (2017) 1255–1262.

[107] S. A. Amiril, E. A. Rahim, Z. Embong, S. Syahrullail, Tribological investigations on the application of oil-miscible ionic liquids additives in modified Jatropha-based metalworking fluid, Tribol Int 120 (2018) 520–534.

[108] T. Norfazillah, S. A. S. Amiril, E. A. Rahim, A. C. G. Saiful, S. Syahrullail, Tribological evaluations of modified RBD palm olein-based lubricants in machining processes, Jurnal Tribologi 19 (July) (2018) 98–106.

[109] T. Rusk, N. Rajagopalan, Evaluation of Aged and Recycled Metalworking Fluids by the Tapping Torque, Lubr Eng 59 (2) (2003) 10–14.

[110] M. Jin, S. Watanabe, S. Miyake, M. Murakawa, Trial fabrication and cutting performance of c-BN-coated taps, Surf Coat Tech 133-134 (2000) 443–447.

[111] M. Piska, P. Sliwkova, A Study of Cutting and Forming Threads With Coated HSS Taps, Journal of Machine Engineering 15 (3) (2015) 65–74.

[112] J. B. Zimmerman, S. Takahashi, K. F. Hayes, S. J. Skerlos, Experimental and Statistical Design Considerations for Economical Evaluation of Metalworking Fluids Using the Tapping Torque Test, Lubr Eng 59 (3) (2003) 18–24.

[113] L. De Chiffre, S. Lassen, K. Pedersen, S. Skade, A Reaming Test for Cutting Fluid Evaluation, J Synth Lubr 11 (1) (1994) 17–34.

[114] D. Axinte, M. Axinte, J. D. T. Tannock, A multicriteria model for cutting fluid evaluation, Proc Inst Mech Eng, Part B: J Eng Manuf 217 (2003) 1341–1353.

[115] D. A. Axinte, L. De Chiffre, Effectiveness and resolution of tests for evaluating the performance of cutting fluids in machining aerospace alloys, CIRP Ann Manuf Technol 57 (2008) 129–132.

[116] A. G. Huesmann-Cordes, D. Meyer, A. Wagner, E. Brinksmeier, Comparison of tribological laboratory tests with practical results from forming and machining processes by the example of sulfur containing metal working fluids (in German), Journal of HTM 71 (4) (2016) 154–162.

[117] R. M. Mullins, P. R. Miller, R. J. Bucko, A Comparison of Matrix and Non-matrix Tapping Torque Test Procedures in the Evaluation of Experimental Cutting Fluids, Lubr Eng 41 (4) (1985) 229–232.

[118] T. H. Webb, E. Holodnik, Statistical Evaluation of the Falex Tapping Torque Test, Lubr Eng 36 (9) (1980) 513–529.

[119] K. Asamene, M. Sundaresan., Analysis of experimentally generated friction related acoustic emission signals, Wear 296 (1-2) (2012) 607–618.

[120] R. Kocich, M. Cagala, J. Crha, P. Kozelsky, Character of Acoustic Emission signal generated during Plastic Deformation, in: Proceedings of the 30th European Conference on Acoustic Emission Testing 7th International Conference on Acoustic Emission, Grenada, Spain, 2012.

[121] A. Hase, H. Mishina, M. Wada, Correlation between features of acoustic emission signals and mechanical wear mechanisms, Wear 292-293 (2012) 144–150.

[122] L. H. A. Maia, A. M. Abrao, W. L. Vasconcelos, W. F. Sales, A. R. Machado, A new approach for detection of wear mechanisms and determination of tool life in turning using acoustic emission, Tribol Int 92 (2015) 519–532.

[123] D. Baccar, D. Söffker, Wear detection by means of wavelet-based acoustic emission analysis, Mech Syst Signal Process 60 (2015) 198–207.

[124] K. Jemielniak, P. J. Arrazola, Application of AE and cutting force signals in tool condition monitoring in micro-milling, CIRP J Manuf Sci Technol 1 (2) (2008) 97–102.

[125] M. Bhuiyan, S. Choudhury, Y. Nukman, Tool condition monitoring using acoustic emission and vibration signature in turning, in: Proceedings of the World Congress on Engineering, Vol. III, London, UK, 2012, pp. 2–6.

[126] S. Kosaraju, V. G. Anne, B. B. Popuri, Online tool condition monitoring in turning titanium (grade 5) using acoustic emission: modeling, Int J Adv Manuf Technol 67 (5-8) (2013) 1947–1954.

[127] A. Srinivasan, D. Dornfeld, R. Bhinge, Integrated vibration and acoustic data fusion for chatter and tool condition classification in milling, International Symposium on Flexible Automation, ISFA 2016 (2016) 263–266.

[128] A. G. Rehorn, J. Jiang, P. E. Orban, State-of-the-art methods and results in tool condition monitoring: a review, Int J Adv Manuf Technol 26 (2005) 693–710.

[129] M. Gómez, A. Hey, C. D'Attelis, J. Ruzzante, Assessment of Cutting Tool Condition by Acoustic Emission, Procedia Materials Science 1 (2012) 321–328.

[130] G. Ferrari, M. P. Gómez, Correlation Between Acoustic Emission, Thrust and Tool Wear in Drilling, Procedia Materials Science 8 (2015) 693–701.

[131] A. Hase, M. Wada, T. Koga, H. Mishina, The relationship between acoustic emission signals and cutting phenomena in turning process, Int J Adv Manuf Technol 70 (5-8) (2014) 947–955.

[132] E. Brinksmeier, D. Meyer, A. G. Huesmann-Cordes, C. Herrmann, Metalworking fluids - Mechanisms and performance, CIRP Ann Manuf Technol 64 (2) (2015) 605–628.

[133] M. Hamel, A. Addali, D. Mba, Monitoring oil film regimes with acoustic emission, Proc Inst Mech Eng, Part J: J Eng Tribol 228 (2) (2014) 223–231.

[134] C. Strablegg, P. Renhart, F. Summer, F. Grün, Methodology , validation signal processing of acoustic emissions for selected lubricated tribological contacts, Mater Today Proc 62 (2022) 2604–2610.

[135] S. Dutta, S. Pal, S. Mukhopadhyay, R. Sen, Application of digital image processing in tool condition monitoring: A review, CIRP J Manuf Sci Technol 6 (2013) 212–232.

[136] Z. Kunpeng, W. Y. San, H. G. Soon, Wavelet analysis of sensor signals for tool condition monitoring : A review and some new results, Int J Mach Tools Manuf 49 (2009) 537–553.

[137] C. H. Lauro, L. C. Brandão, D. Baldo, R. A. Reis, J. P. Davim, Monitoring and processing signal applied in machining processes – A review, Measurement 58 (2014) 73–86.

[138] B. Sick, On-line and indirect tool wear monitoring in turning with artificial neural networks: A review of more than a decade of research, Mech Syst Signal Process 16 (4) (2002) 487–546.

[139] A. González-Laguna, J. Barreiro, A. Fernández-Abia, E. Alegre, V. González-Castro, Design of a TCM system based on vibration signal for metal turning processes, Procedia Eng 132 (2015) 405–412.

[140] SANDVIK Coromant, Wear types (accessed 20.09.2016) (2016) http://www.sandvik.coromant.com/en–gb/knowledge/dr.

[141] Komet Group GmbH, Youtube-Video: Tool and Process Monitoring with ToolScope - Tapping (accessed 15.09.2016) (2016) https://www.youtube.com/watch?v=aS756V9l3Ds.

[142] MCU GmbH, Acoustic Emission (accessed 15.09.2016) (2016) http://www.mcu–gmbh.de/?id=22.

[143] Schwer + Kopka GmbH, Sensors (accessed 15.09.2016) (2016) http://www.schwer–kopka.de/ english/sensors.html.

[144] Nordmann International GmbH, Sensors (accessed 15.09.2016) (2016) http://www.toolmonitoring.com/ sensoren.html.

[145] Hufschmied Zerspanungssysteme GmbH, Akustische Qualitätskontrolle, FORM+Werkzeug 4 (2022) 36–37.

[146] S. Afazov, D. Tdebski, S. Ratchev, J. Segal, S. Liu, Effects of micro-milling conditions on the cutting forces and process stability, J Mater Process Technol 213 (2013) 671–684.

[147] F. Cus, U. Zuperl, Real-Time Cutting Tool Condition Monitoring in Milling, Journal of Mechanical Engineering 57 (2011) 142–150.

[148] E. Kuljanic, M. Ã. Sortino, TWEM, a method based on cutting forces — monitoring tool wear in face milling, Int J Mach Tools Manuf 45 (2005) 29–34.

[149] H. M. Ertunc, K. A. Loparo, E. Ozdemir, H. Ocak, Real Time Monitoring of Tool Wear Using Multiple Modeling Method, in: IEEE Electric Machines and Drives Conference, 2001, pp. 687–691.

[150] M. Nouri, B. K. Fussell, B. L. Ziniti, E. Linder, B. K. Fussel, B. L. Ziniti, E. Linder, Real-time tool wear monitoring in milling using a cutting cindition independent method, Int J Mach Tools Manuf 89 (2015) 1–13.

[151] D. Shi, D. Axinte, N. Gindy, Development of an online machining process monitoring system: a case study of the broaching process, Int J Adv Manuf Technol 34 (2007) 34–46.

[152] H. Wiklund, Bayesian and regression approaches to on-line prediction of residual tool life, Qual Reliab Eng Int 14 (1998) 303–309.

[153] Y. Wu, G. Hong, W. Wong, Prognosis of the probability of failure in tool condition monitoring application-a time series based approach, Int J Adv Manuf Technol 76 (2015) 513–521.

[154] C. Madhusudana, S. Budati, N. Gangadhar, Fault diagnosis studies of face milling cutter using machine learning approach, Journal of Low Frequency Noise, Vibration and Active Control 0 (2016) 1–11.

[155] T. Moriwaki, E. Shamoto, Ultrasonic Elliptical Vibration Cutting, Annals of the CIRP 44 (l) (1995) 31–34.

[156] S. Orhan, A. O. Er, N. Camuscu, E. Aslan, Tool wear evaluation by vibration analysis during end milling of AISI D3 work tool steel with 35 HRC hardness, NDT E Int 40 (2007) 121–126.

[157] K. Rao, B. Murthy, N. M. Rao, Cutting tool condition monitoring by analyzing surface roughness, work piece vibration and volume of metal removed for AISI 1040 steel in boring, Measurement 46 (2013) 4075–4085.

[158] A. Rmili, A. Ouahabi, R. Serra, R. Leroy, An automatic system based on vibratory analysis for cutting tool wear monitoring, Measurement 77 (2016) 117–123.

[159] M. Saimurugan, K. I. Ramachandran, V. Sugumaran, N. R. Sakthivel, Multi component fault diagnosis of rotational mechanical system based on decision tree and support vector machine, Expert Syst Appl 38 (4) (2011) 3819–3826.

[160] K. A. Vikram, C. Ratnam, K. S. Narayana, Vibration diagnosis and prognostics of Turn-milling operations using HSS and carbide end mill cutters, Procedia Technology 23 (2016) 217–224.

[161] S. Dutta, A. Datta, N. D. Chakladar, S. Pal, S. Mukhopadhyay, R. Sen, Detection of tool condition from turned surface images using an accurate grey level co-occurence technique, Precision Engineering 36 (2012) 459–466.

[162] W. König, H.-C. Möhring, Cutting tool condition monitoring using eigenfaces, Prod. Eng. Res. Devel. 16 (2022) 753–768.

[163] D. Lipinski, W. Kacalak, R. Tomkowski, Methodology of Evaluation of Abrasive Tool Wear with the Use of Laser Scanning Microscopy, Scanning 36 (2014) 53–63.

[164] W. Weis, Processing of Optical Sensor Data for Tool Monitoring with Neural Networks, in: Proceedings of WESCON'94, IEEE, Anaheim, CA, 1994.

[165] Y. Zhang, Y. Zhang, H. Tang, L. Wang, Images acquisition of a high-speed boring cutter for tool condition monitoring purposes, Int J Adv Manuf Technol 48 (2010) 455–460.

[166] B. Y. Lee, Y. S. Tarng, Application of the Discrete Wavelet Transform to the Monitoring of Tool Failure in End Milling Using the Spindle Motor Current, Int J Adv Manuf Technol 15 (1999) 238–243.

[167] X. Li, S. K. Tso, J. Wang, Real-Time Tool Condition Monitoring Using Wavelet Transforms and Fuzzy Techniques, IEEE Trans Syst Man Cybern C Appl Rev 30 (3) (2000) 352–357.

[168] D. Brezak, D. Majetic, T. Udiljak, Tool wear estimation using an analytic fuzzy classifier and support vector machines, J Intell Manuf 23 (2012) 797–809.

[169] H. Chelladurai, V. Jain, N. Vyas, Development of a cutting tool condition monitoring system for high speed turning operation by vibration and strain analysis, Int J Adv Manuf Technol 37 (2008) 471–485.

[170] S. Cho, S. Binsaeid, S. Asfour, Design of multisensor fusion-based tool condition monitoring system in end milling, Int J Adv Manuf Technol 46 (2010) 681–694.

[171] K. Jemielniak, T. Urbanski, J. Kossakowska, S. Bombinski, Tool condition monitoring based on numerous signal features, Int J Adv Manuf Technol 59 (2012) 73–81.

[172] S. Karam, P. Centobelli, D. D'Addona, R. Teti, Online prediction of cutting tool life in turning via cognitive decision making, Procedia CIRP 41 (2016) 927–932.

[173] G. K. Pradeep, M. Saimurugan, S. R. Kumar, Tool wear monitoring using the fusion of vibration signals and digital image, Journal of Chemical and Pharmaceutical Sciences 9 (1) (2016) 537–541.

[174] M. Rizal, J. A. Ghani, M. Z. Nuawi, C. H. C. Haron, The Application of I-kaz TM -Based Method for Tool Wear Monitoring using Cutting Force Signal, Procedia Engineering 68 (2013) 461–468.

[175] S. Binsaeid, S. Asfour, S. Cho, A. Onar, Machine ensemble approach for simultaneous detection of transient and gradual abnormalities in end milling using multisensor fusion, J Mater Process Technol 209 (2009) 4728–4738.

[176] H. Gao, D. Li, M. Xu, M. Zhao, X. Shi, H. Huang, Tool Wear Monitoring Based on Novel Evolutionary Artificial Neural Networks, in: Sixth International Conference on Natural Computation, 2010, pp. 1339–1343.

[177] G. Byrne, D. Dornfeld, I. Inasaki, G. Ketteler, W. König, R. Teti, Tool Condition Monitoring - The Status of Research and Industrial Application, CIRP Ann Manuf Technol 44 (2) (1995) 541–567.

[178] G. K. Pradeep, M. Saimurugan, S. R. Kumar, Tool wear monitoring using fusion of vibration signals and digital image, Journal of Chemical and Pharmaceutical Sciences 9 (2016) 537–541.

[179] S. V. Kamarthi, S. R. T. Kumara, P. H. Cohen, Flank Wear Estimation in Turning Through Wavelet Representation of Acoustic Emission Signals, J Manuf Sci 122 (1) (2000) 12–19.

[180] C. Beggan, M. Woulfe, P. Young, G. Byrne, Using Acoustic Emission to Predict Surface Quality, Int J Adv Manuf Technol 15 (10) (1999) 737–742.

[181] M. Kimmelmann, J. Duntschew, I. Schluchter, H.-C. Möhring, Analysis of burr formation mechanisms when drilling CFRP-aluminium Analysis of burr formation when drilling CFRP-aluminium stacks mechanisms using acoustic

emission stacks using acoustic emission, Procedia Manuf 40 (2019) (2019) 64–69.

[182] H.-C. Möhring, M. Kimmelmann, S. Eschelbacher, K. Güzel, C. Gauggel, Process monitoring on drilling fiber-reinforced plastics and aluminum stacks using acoustic emissions aluminum stacks using acoustic emissions Process monitoring on drilling, in: Procedia Manuf, Vol. 18, Elsevier B.V., 2018, pp. 58–67.

[183] S. Arul, L. Vijayaraghavan, S. K. Malhotra, Online monitoring of acoustic emission for quality control in drilling of polymeric composites, J Mater Process Technol 185 (1-3) (2007) 184–190.

[184] A. L. Quadro, J. R. Branco, Analysis of the acoustic emission during drilling test, Surf Coat Technol 94-95 (1997) 691–695.

[185] S. Liu, H. Zhang, C. Li, H. Lu, Y. W. Hu, Fuzzy reliability estimation for cutting tools, Procedia CIRP 15 (2014) 62–67.

[186] I. Marinescu, D. A. Axinte, A critical analysis of effectiveness of acoustic emission signals to detect tool and workpiece malfunctions in milling operations, Int J Mach Tools Manuf 48 (10) (2008) 1148–1160.

[187] I. Marinescu, D. Axinte, A time-frequency acoustic emission-based monitoring technique to identify workpiece surface malfunctions in milling with multiple teeth cutting simultaneously, Int J Mach Tools Manuf 49 (1) (2009) 53–65.

[188] D. A. Dornfeld, Y. Lee, A. Chang, Monitoring of ultraprecision machining processes, Int J Adv Manuf Technol 21 (8) (2003) 571–578.

[189] T. Toutountzakis, C. K. Tan, D. Mba, Application of acoustic emission to seeded gear fault detection, NDT and E International 38 (1) (2005) 27–36.

[190] G. H. Feng, M. Y. Tsai, Y. R. Jeng, A micromachined, high signal-to-noise ratio, acoustic emission sensor and its application to monitor dynamic wear, Sensors and Actuators, A: Physical 188 (2012) 56–65.

[191] T. Skare, Dynamiskt belastade tribologiska system under plastisk formning, del II — analyserade genom akustisk emission, Ph.D. thesis, Lund University (2001).

[192] D. E. Lee, I. Hwang, C. M. Valente, J. F. Oliveira, D. A. Dornfeld, Precision manufacturing process monitoring with acoustic emission, Int J Mach Tools Manuf 46 (2) (2006) 176–188.

[193] T. Jayakumar, C. K. Mukhopadhyay, S. Venugopal, S. L. Mannan, B. Raj, A review of the application of acoustic emission techniques for monitoring forming and grinding processes, J Mater Process Technol 159 (1) (2005) 48–61.

[194] F. Saeidi, S. A. Shevchik, K. Wasmer, Automatic detection of scuffing using acoustic emission, Tribol Int 94 (2016) 112–117.

[195] M. Marian, S. Tremmel, Current Trends and Applications of Machine Learning in Tribology — A Review, Lubricants 9 (86).

[196] Q. Feng, W. Maier, T. Stehle, H.-C. Möhring, Optimization of a clamping concept based on machine learning, Production Engineering 16 (1) (2022) 9–22.

[197] S. Dutta, S. K. Pal, S. Mukhopadhyay, R. Sen, Application of digital image processing in tool condition monitoring : A review, CIRP J Manuf Sci Technol 6 (3) (2013) 212–232.

[198] H.-C. Möhring, P. Wiederkehr, K. Erkorkmaz, Y. Kakinuma, Self-optimizing machining systems, in: CIRP Ann Manuf Technol, Vol. 69, 2020, pp. 740–763.

[199] V. Purushotham, S. Narayanan, S. Prasad, Multi-fault diagnosis of rolling bearing elements using wavelet analysis and hidden Markov model based fault recognition, NDTE International 38 (8) (2005) 654–664.

[200] P. Baruah, R. Chinnam, HMMs for diagnostics and prognos- tics in machining processes, Int J Prod Res 43 (6) (2005) 1275–1293.

[201] A. Bustillo, L. N. López de Lacalle, A. Fernández-Valdivielso, P. Santos, Data-mining modeling for the prediction of wear on forming-taps in the threading of steel components, J Comput Des Eng 3 (4) (2016) 337–348.

[202] J. Sun, M. Rahman, Y. Wong, G. Hong, Multiclassification of tool wear with support vector machine by manufacturing loss consideration, Int J Mach Tools Manuf 44 (11) (2004) 1179–1187.

[203] J. Alves, R. Poppi, Determining the presence of naphthenic and vegetable oils in paraffin-based lubricant oils using near infrared spectroscopy and support vector machines, Anal. Methods 5 (22) (2013) 6457.

[204] L. Breiman, Random Forests, Mach. Learn. 45 (2001) 5–32.

[205] J. Prost, U. Cihak-Bayr, I. A. Neacsu, R. Grundtner, F. Pirker, G. Vorlaufer, Semi-Supervised Classification of the State of Operation in Self-Lubricating Journal Bearings Using a Random, Lubricants 9 (50).

[206] Z. P. Chang, Y. W. Li, N. Fatima, A theoretical survey on Mahalanobis-Taguchi system, Measurement 136 (March 2019) (2019) 501–510.

[207] B. K. Rai, R. B. Chinnam, N. Singh, Prediction of drill-bit breakage from degradation signals using Mahalanobis-Taguchi system analysis Ratna Babu Chinnam and Nanua Singh, Int J Industrial and Systems Engineering 3 (2) (2008) 134–148.

[208] C. Saygin, D. Mohan, J. Sarangapani, Real-time detection of grip length during fastening of bolted joints : a Mahalanobis-Taguchi system (MTS) based approach, J Intell Manuf 21 (2010) 377–392.

[209] R. Rojas, Theorie der neuronalen Netze: Eine systematische Einführung, Springer, Germany, 2013.

[210] B. Sick, On-line and indirect tool wear monitoring in turning with Artificial Neural Networks: a review of more than a decade of research, Mech Syst Signal Process 16 (2002) 487–546.

[211] B. Sick, Fusion of Hard and Soft Computing Techniques in Indirect, Online Tool Wear Monitoring, IEEE Trans Syst Man Cybern C Appl Rev 32 (2) (2002) 80–91.

[212] H. Sadegh, A. Najafabadi, A. Mehdi, Classification of acoustic emission signals generated from journal bearing at different lubrication conditions based on wavelet analysis in combination with artificial neural network and genetic algorithm, Tribol Int 95 (2016) 426–434.

[213] S. M. Jafari, H. Mehdigholi, M. Behzad, Valve Fault Diagnosis in Internal Combustion Engines Using Acoustic Emission and Artificial Neural Network, Shock and Vibration 2014 (823514) (2014) 9.

[214] Y. Lecun, L. Bottou, Y. Bengio, H. P., Gradient-based Learning Applied to Document Regonition, Proceedings of the IEEE 86 (1998) 2278–2324.

[215] A. Krizhevsky, I. Sutskever, G. E. Hinton, ImageNet Classification with Deep Convolutional Neural Networks, in: Proceedings of the 25th international conference on neural information processing systems, Nevada, USA, 2012, pp. 1097–1105.

[216] P. P. Shinde, S. Shah, A Review of Machine Learning and Deep Learning Applications, in: Fourth International Conference on Computing Communication Control and Automation (ICCUBEA), 2018, pp. 1–6.

[217] R. Yamashita, M. Nishio, R. Kinh, G. Do, K. Togashi, R. K. G. Do, K. Togashi, Convolutional neural networks: an overview and application in radiology, Insights into Imaging 9 (2018) 611–629.

[218] A. Klofat, Die wichtigsten Typen neuronaler Netze für Deep Learning, BigData Insider (accessed 10.11.2022) (2022) https://www.bigdata–insider.de/die–wichtigsten–typ.

[219] J. Brownlee, How do convolutional layers work in deep learning neural networks. (accessed 15.05.2021) (2021) www.machinelearningmastery.com/convolutionallayers.

[220] S. H. S. Basha, S. R. Dubey, V. Pulabaigari, S. Mukherje, Impact of fully connected layers on performance of convolutional neural networks for image classification, Neurocomputing 378 (2020) 112–119.

[221] F. König, C. Sous, A. Ouald Chaib, G. Jacobs, Machine learning based anomaly detection and classification of acoustic emission events for wear monitoring in sliding bearing systems, Tribol Int 155 (December 2020) (2021) 106811.

[222] A. Prosvirin, J. Y. Kim, J. Kim, Bearing Fault Diagnosis Based on Convolutional Neural Networks with Kurtogram Representation of Acoustic Emission Signals, in: International Conference on Computer Science and its Applications, Cute, CSA, 2017, pp. 21–26.

[223] X. Wang, D. Mao, X. Lic, Bearing fault diagnosis based on vibro-acoustic data fusion and 1D-CNN network, Measurement 173 (108518).

[224] S. Shevchik, C. Kenel, C. Leinenbach, K. Wasmer, Acoustic emission for in situ quality monitoring in additive manufacturing using spectral convolutional neural networks, Addit Manuf 21 (2018) 598–604.

[225] H.-C. Möhring, S. Eschelbacher, P. Georgi, Machine learning approaches for real-time monitoring and evaluation of surface roughness using a sensory milling tool, in: Procedia CIRP, Vol. 102, Elsevier B.V., 2021, pp. 264–269.

[226] X.-C. Cao, B.-Q. Chen, B. Yao, W.-P. Heb, Combining translation-invariant wavelet frames and convolutional neural network for intelligent tool wear state identification, Computers in Industry 106 (April 2019) (2019) 71–84.

[227] Q. Deng, J. Wang, D. Söffker, Prediction of human driver behaviors based on an improved HMM approach, in: 2018 IEEE Intelligent Vehicles Symposium, Changshu, Suzhou, China, 2018, pp. 2066–2071.

[228] Q. Deng, Improved machine learning approaches for individualized human assistance, supervision, and behavior prediction, Ph.D. thesis, University Duisburg-Essen (2020).

[229] A. Hase, Acoustic Emissions during Tribological Processes, in: International Tribology Conference, Japanese Society of Tribologists, Tokyo, 2015, pp. 210–211.

[230] D. Strombergsson, P. Marklund, E. Edin, F. Zeman, Acoustic emission monitoring of a mechanochemical surface finishing process, Tribol Int 112 (March) (2017) 129–136.

[231] S. Poddar, N. Tandon, Detection of particle contamination in journal bearing using acoustic emission and vibration monitoring techniques, Tribol Int 134 (December 2018) (2019) 154–164.

[232] J. Miettinen, P. Andersson, Acoustic emission of rolling bearings lubricated with contaminated grease, Tribol Int 33 (2000) 777–787.

[233] N. Wei, F. Gu, T. Wang, G. Li, Y. Xu, L. Yang, A. Ball, Characterisation of Acoustic Emissions for the Frictional Effect in Engines using Wavelets based Multi-resolution Analysis, in: Proceedings of the 21st International Conference on Automation and Computing, IEEE, 2015.

[234] N. Wei, F. Gu, G. Li, T. Wang, A. Ball, Characterising the Friction and Wear Be- Tween the Piston Ring and Cylinder Liner Based on Acoustic Emission Analysis, in: 21st International Congress on Sound and Vibration, 13th-17th July, Beijing, China, 2014.

[235] H. Towsyfyan, P. Raharjo, F. Gu, A. Ball, Characterization of Acoustic Emissions from Journal Bearings for Fault Detection, in: NDT, 10th-12th September, Telford, UK, 2013.

[236] A. Towsyfyan, Hossein, Wei, Nasha, Raharjo, Parno, Gu, Fengshou and Ball, Identification of lubrication Regimes in Mechanical Seals using Acoustic Emission for Condition Monitoring, in: The 54th Annual Conference of The British Institute of Non Destructive Testing BINDT, 8th-10th September, Telford, UK, 2015.

[237] A. Moshkovich, V. Perfilyev, I. Lapsker, Y. Feldman, L. Rapoport, Study of the transition from EHL to BL regions under friction of Ag and Ni. I. Analysis of acoustic emission, Tribol Int 113 (July 2016) (2017) 189–196.

[238] ILCO Chemikalien GmbH, ILCO Prospekt.pdf (accessed 13.07.2022) (2022) https://ilco–chemie.de/content/produkte/96–ester/.

[239] S. A. Umoren, M. M. Solomon, V. S. Saji, Polyglycols, in: Polymeric Materials in Corrosion Inhibition, Elsevier Inc., 2022, Ch. 14, pp. 325–340.

[240] ASTM Committee D5619, Standard Test Method for Comparing Metal Removal Fluids Using the Tapping Torque Test Machine (2011).

[241] T. Engbert, T. Heymann, D. Biermann, A. Zabel, Flow drilling and thread forming of continuously reinforced aluminium extrusions, Proc Inst Mech Eng, Part B: J Eng Manuf 225 (3) (2011) 398–407.

[242] I. C. Pereira, M. B. da Silva, Study of the internal thread process with cut and form taps according to secondary characteristics of the process, Int J Adv Manuf Technol 93 (5-8) (2017) 2357–2368.

[243] A. O. De Carvalho, L. C. Brandão, T. H. Panzera, C. H. Lauro, Analysis of form threads using fluteless taps in cast magnesium alloy (AM60), J Mater Process Technol 212 (8) (2012) 1753–1760.

[244] M. Otto, Chemometrics: statistics and computer application in analytical chemistry, 3rd Edition, Wiley-VCH, Weinheim, 2017.

[245] J. C. Goswami, Fundamentals of Wavelets, John Wiley and Sons, Ltd, 2011.

[246] D. Frick, A. Gadatsch, J. Kaufmann, B. Lankes, C. Quix, A. Schmidt, U. Schmitz (Eds.), Data Science, 1st Edition, Springer Vieweg Wiesbaden, 2021.

[247] W. Roundi, A. E. Mahi, A. E. Gharad, J. L. Rebiere, Acoustic emission monitoring of damage progression in Glass/Epoxy composites during static and fatigue tensile tests, Applied Acoustics 132 (2018) 124–134.

[248] M. Saeedifar, M. A. Najafabadi, D. Zarouchas, H. H. Toudeshky, M. Jalalvand, Clustering of interlaminar and intralaminar damages in laminated composites under indentation loading using acoustic emission, Composites Part B: Engineering 144 (2018) 206–219.

[249] W. Zhou, W.-Z. Zhao, Y.-N. Zhang, Z.-J. Ding, Cluster analysis of acoustic emission signals and deformation measurement for delaminated glass fiber epoxy composites, Composite Structures 195 (349-358).

[250] Q. Huang, Y. Cui, L. B. Tjernberg, G. Ab, Wind turbine health assessment framework based on power analysis using machine learning method, in: 2019 IEEE PES Innovative Smart Grid Technologies Europe (ISGT-Europe), 2019.

[251] C. Wang, Z. Bao, P. Zhang, W. Ming, M. Chen, Tool wear evaluation under minimum quantity lubrication by clustering energy of acoustic emission burst signals, Measurement 138 (2019) 256–265.

[252] A. Tharwat, Classification assessment methods, Applied Computing and Informatics 17 (1) (2021) 168–192.

[253] R. V. Dinter, C. Catal, B. Tekinerdogan, A Multi-Channel Convolutional Neural Network approach to automate the citation screening process, Appl Soft Comput 112 (2021) 107765.

[254] G. Montavon, G. Orr, K.-R. Müller, Neural networks: tricks of the trade, 7700th Edition, Springer, Germany, 2012.

[255] S. H. Haji, A. M. Abdulazeez, Comparison of optimization techniques based on gradient descent algorithm: a review, PalArch's Journal of Archaeology of Egypt / Egyptology 18 (4) (2021) 2715–2743.

[256] F. Jochmann, Classification of Acoustic Emission-based industry and CWRU benchmark datasets affected by variable operating conditions using Convolutional Neural Network (CNN), Master Thesis, Chair of Dynamics and Control, University Duisburg-Essen (2021) 3–25.

[257] M. Taylor, P. Stone, Transfer Learning for Reinforcement Learning Domains: A Survey, J Mach Learn Res 10 (2009) 1633–1685.

[258] J. Hollingsworth, M. Ratz, P. Tanedo, D. Whiteson, Efficient sampling of constrained high-dimensional theoretical spaces with machine learning, Eur Phys J C 81 (2021) 1–9.

[259] G. Vanwinckelen, H. Blockeel, On Estimating Model Accuracy with Repeated Cross-Validation, in: Proceedings of the 21st Belgian-Dutch conference on machine learning, 2012, pp. 39–44.

Publications

This thesis is based on the results and development steps presented in the following previously published contributions.

Journal articles

- Demmerling, A. L., Wei, X. and Söffker, D. (2022). 'Extended tapping torque test to differentiate metalworking fluids.' *Tribology International* 175, 107819.

- Demmerling, A.L. and Söffker, D. (2019). 'Improved examination and test procedure of tapping torque tests according to ASTM D5619 using coated forming taps and water-mixed metalworking fluids'. *Tribology International* 145, 106151.

Conference papers

- Wei, X., Jochmann, F., Demmerling, A. L. and Söffker, D. (2022). 'Application of Transfer Learning in metalworking fluid distinction.' *International Design Engineering Technical Conferences and Computers and Information in Engineering Conference*, American Society of Mechanical Engineers, Vol. 86212.

- Wei, X., Demmerling, A. L. and Söffker, D. (2021). 'Metalworking Fluid Classification Based on Acoustic Emission Signals and Convolutional Neural Network.' *Proceedings of the 6th European Conference Prognostics and Health Management Society*, 471-476.

- Wirtz, S. F., Demmerling, A. L. and Söffker, D. (2017). 'In-situ wear monitoring: An experimental investigation of Acoustic Emission during thread forming.' *Proceedings of Structural Health Monitoring*, USA, Stanford, 1198-1205.

- Demmerling, A. L. and Söffker, D. (2016). 'Condition monitoring: A review on real-time measurement techniques for tool condition monitoring and analysis of metalworking fluids.' *AKIDA - The Maintenance, Monitoring and Control Conference*, Germany, Aachen, 191-208.

During the time of research the following journal paper were published in addition. However, the content of this paper is not directly related to the content of this thesis. Additionally, in the context of research projects at the Chair of Dynamics and Control, the following student thesis has been supervised by Anna Lena Demmerling and Univ.-Prof. Dr.-Ing. Dirk Söffker. Development steps and results of the research project and the student thesis are integrated with each other and hence are also part of this thesis.

Journal article, student thesis, and US patent

- Demmerling, A. L., Schlindwein, H. J., Geier, S., Mahrholz, T. (2017). 'Investigation of interactions of CFRP with processing fluids', *Lightweight Design* 10, 10-15.
- Jochmann, F. 'Classification of Acoustic Emission-based industry and CWRU benchmark datasets affected by variable operating conditions using Convolutional Neural Network (CNN)'. Master Thesis, University Duisburg-Essen, 2021.
- Demmerling, A. L., Schlindwein, H. J., Hediger, T., Quotschalla, U. (2022/4/12). 'Coolant for composite materials'. US Patent 11,299,691, 2022

DOI: 10.17185/duepublico/78741
URN: urn:nbn:de:hbz:465-20230803-162734-9